NASA TN D-1806

TECHNICAL NOTE

D-1806

INVESTIGATION OF PROPELLER–POWER-PLANT AUTOPRECESSION BOUNDARIES FOR A DYNAMIC-AEROELASTIC MODEL OF A FOUR-ENGINE TURBOPROP TRANSPORT AIRPLANE

By Frank T. Abbott, Jr., H. Neale Kelly,
and Kenneth D. Hampton

Langley Research Center
Langley Station, Hampton, Va.

NATIONAL AERONAUTICS AND SPACE ADMINISTRATION
WASHINGTON

August 1963

NATIONAL AERONAUTICS AND SPACE ADMINISTRATION

TECHNICAL NOTE D-1806

INVESTIGATION OF PROPELLER—POWER-PLANT AUTOPRECESSION BOUNDARIES FOR A DYNAMIC-AEROELASTIC MODEL OF A FOUR-ENGINE TURBOPROP TRANSPORT AIRPLANE*

By Frank T. Abbott, Jr., H. Neale Kelly,
and Kenneth D. Hampton

SUMMARY

A flexibly mounted aircraft engine may under certain conditions experience a self-excited whirling instability involving a coupling between the gyroscopic and aerodynamic forces acting on the propeller, and the inertial, elastic, and damping forces contributed by the power plant, nacelle, and wing. This phenomenon has been called autoprecession, or whirl instability. An experimental investigation was made in the Langley transonic dynamics tunnel at Mach numbers below 0.3 to study some of the pertinent parameters influencing the phenomenon. These parameters included propeller rotational speed, stiffness of the power-plant assembly in the pitch and yaw planes and the ratio of pitch stiffness to yaw stiffness, structural damping of the power-plant assembly in the pitch and yaw planes, simulated fuel load in the wings, and the location and number of autoprecessing power-plant assemblies. A large dynamic-aeroelastic model of a four-engine turboprop transport airplane mounted on a vertical rod in a manner which provided several limited body degrees of freedom was used in the investigation.

It was found that the boundary for autoprecession decreased markedly with reduction of power-plant stiffness and/or damping, and to a lesser degree decreased with reduction of simulated fuel load in the wings. Increasing propeller rotational speed generally lowered the autoprecession boundary. This effect was more pronounced as the stiffness was increased. An inboard power plant was found to be more susceptible to autoprecession than an outboard one. Combinations in which two or more power plants had the same level of reduced stiffness resulted in autoprecession boundaries considerably lower than that of a single power plant with the same level of reduced stiffness.

INTRODUCTION

Under certain conditions the use of flexible engine mounts, such as are commonly used on aircraft to isolate engine vibrations, can lead to a self-excited

*The information presented herein was previously given limited distribution.

whirling instability of the propeller—power-plant installation. This phenomenon, described briefly in reference 1, involves a coupling of the gyroscopic and aerodynamic forces acting on the propeller, and the inertial, elastic, and damping forces contributed by the power plant, nacelle, and wing. The resulting motion is a wobbling of the plane of rotation of the spinning propeller. When this motion is self-sustaining, it is called autoprecession.

Experience has indicated that this phenomenon has not been a critical design condition for reciprocating engine installations. However, recent configurations with greatly increased power, changed geometry, and softer mounts, have brought about renewed interest in the whirl instability or autoprecession phenomenon. Elementary studies of this phenomenon are reported in references 2 to 5.

Concurrent with the analytic studies of reference 2, a low-speed, experimental investigation was made in the Langley transonic dynamics tunnel with a large dynamic-aeroelastic model of a four-engine turboprop transport airplane. The model was mounted on a vertical rod by means of a sliding pivot arrangement which allowed body freedoms in vertical translation, pitch, and yaw. The mounting also allowed freedom with slight spring restraint for small motions in roll, side translation, and fore and aft translation. The model was aerodynamically trimmed so that it was "flying" (supporting its own weight) during each run as the tunnel velocity was gradually increased to the point of autoprecession. The tests consisted of studies of the effects of variations in power-plant mounting stiffness and structural damping, propeller rotational speed, and wing fuel loading on the dynamic pressure for autoprecession. The present report presents data from these tests, along with the physical characteristics of the model, for use in comparison with analytical studies.

SYMBOLS

b	chord of propeller-blade element, ft
f	frequency, cps
g	structural damping coefficient, $\frac{1}{\pi s} \log \frac{x_n}{x_{n+s}}$, where x_n is the amplitude of the oscillation at the nth cycle and x_{n+s} the amplitude s cycles later ($s = 1,2,3, \ldots$)
h	blade-section maximum thickness, ft
M	free-stream Mach number
N	propeller rotational speed, rpm
q	free-stream dynamic pressure, lb/sq ft
R	propeller tip radius, ft

r radius to any blade element, ft

S stiffness, $\frac{\text{in-lb}}{\text{radian}}$

S_{rms} root-mean-square stiffness, $\sqrt{\frac{S_\theta^2 + S_\psi^2}{2}}$, $\frac{\text{in-lb}}{\text{radian}}$

V free-stream velocity, ft/sec

β propeller-blade angle at 0.75 radius, deg

ρ free-stream air density, slugs/cu ft

Subscripts:

a autoprecession

θ propeller-axis pitch rotation

ψ propeller-axis yaw rotation

TUNNEL

The model was tested in the Langley transonic dynamics tunnel, shown in figures 1 and 2, which is a return-flow, variable-pressure, slotted-throat tunnel having a test section 16 feet square (with cropped corners). Although pressure was held relatively constant during the present investigation, the tunnel is capable of operation at stagnation pressures from near vacuum to slightly above atmospheric. The axial velocity distribution is uniform to within about ±0.5 percent in the region in which the model was mounted, for the velocity range employed in the present investigation. Some random-type roughness of the flow was evident in the flying of the model, but the degree of roughness is unknown since turbulence measurements have not been made at this time in the velocity range of this investigation.

Figure 2 shows the tunnel control room and the platform from which the model was controlled. Both the control room and the test-section wall are provided with large windows for close, unobstructed viewing of the model.

MODEL

General Considerations

In order to simulate the boundary conditions for instabilities involving unsymmetrical phenomena, a full-span model with body freedoms was used. During the tests, the model was flown with sufficient lift to support its own weight,

and trim was maintained by remotely adjusting the horizontal stabilizer. Details of the mounting will be discussed in a subsequent section of this paper.

The general structure of the model followed conventional practice and will be described in the section entitled "Design and Construction." Several assumptions were necessary, however, in designing the simulated nacelle—power-plant installation to avoid undue complexity. It was assumed that the stiffness parameters most pertinent to the investigation were the rotational stiffnesses in pitch and yaw at the propeller hub. The design, therefore, was arranged to permit independent variation of these stiffnesses so that the effects of stiffness ratio, as well as the level of stiffness, might be studied. No attempt was made to duplicate the load paths or exact geometry of a practical installation. Mass and inertia properties, however, were designed to simulate one type of power plant.

Another assumption, which appeared to be justified by an analytical investigation (ref. 2), was that the effects of power on the autoprecession boundary are small. The propellers were designed to freely windmill rather than to deliver thrust from a power source.

Design and Construction

Model dimensions are shown in figure 3, and the assembled model is shown mounted in the tunnel in figure 4.

Wing.- The wing, shown in figure 5, was constructed with a heat-treated, welded aluminum beam which varied in cross section. The airfoil contour was formed by balsa pods attached to the wing beam. The gaps between pods were sealed with flexible, foam-plastic strips. Ailerons and flaps were not simulated. The weight of each pod was adjusted to give a representative mass distribution of a wing with the fuel tanks empty. Lead weights as shown in figures 5 and 6 were fastened to the wing beam to obtain mass distributions simulating a range of fuel configurations.

Model power plants and propellers.- The propeller—power-plant assembly was represented by a rotating propeller and simulated power plant as shown in figures 7 and 8. A single beam was used to provide a representative value of nacelle structural stiffness. Angular stiffness over a range in both pitch and yaw was obtained through the use of ball-bearing gimbals and cantilever springs extending from the gimbals to adjustable clamps attached to the nacelle beam. Pitch and yaw stiffnesses of the simulated power-plant assembly could be varied by changing the position of the string clamps and, at higher stiffnesses, by the addition of a booster spring. Structural damping in pitch and yaw was obtained by wedging strips of foam rubber between the respective springs and the beams to which they were clamped. Mass and inertia properties of a turboprop engine and reduction gear were simulated by the gimbal-mounted propeller, bearing housing, and a lead weight (simulating the engine mass) attached to the housing in a manner simulating a typical full-scale engine installation.

Power plants that were expected to precess during a run were provided with mechanical stops to limit the motion of the simulated power-plant assembly while

precessing. In addition, the power plants were provided with a device to stop precession. This device consisted of a cable attached to the simulated engine which would be pulled taut by a remotely operated solenoid.

The model had four-blade, 20.25-inch-diameter, aluminum-alloy propellers. (See fig. 8.) Design details of the NACA 16-series airfoil blades, which were used in the present investigation, are given in figure 9. The propellers were attached to ball-bearing-mounted shafts and were allowed to windmill in the moving airstream. Rotational speed was varied by adjustment of blade angle before each run. The direction of rotation of all four propellers was clockwise, when viewed from the rear.

Fuselage.- The fuselage was constructed of a load-carrying aluminum tube with balsa segments to form the outer edge. Lead weights distributed along the tube (fig. 10) were used to obtain the desired mass and center-of-gravity characteristics.

Empennage.- The empennage, shown in figure 11, was constructed of load-carrying aluminum box beams with balsa coverings. A remotely operated, all-movable horizontal tail was used for longitudinal trim. The vertical tail was nonmovable. A small fixed rudder tab was used during most runs to improve roll and yaw trim. The small aerodynamic oscillator shown on the tip of the horizontal tail was not attached during most of this investigation.

Shakers.- Propeller precession at subcritical speeds was excited during all but a few test runs by means of an electrically driven eccentric weight shaker in one of the power-plant assemblies. The shaker formed part of the simulated engine mass as shown in figure 8. Aerodynamic oscillators were used to excite precession in several tests. The oscillators were low-aspect-ratio vanes mounted at the tips of the horizontal tail as shown in figure 11. Each vane had a rectangular planform with a chord of 4 inches and a span of 3 inches and had a thickness of about 11 percent of the chord. They were constructed of lightweight balsa and silk in order to add very little mass or inertia. The vanes were driven through an amplitude of about $\pm 5^{\circ}$ by an electric motor at frequencies which could be varied remotely from about 1 to 25 cps.

Physical Properties

Stiffness.- Bending and torsional deflections of the model wing are presented in figure 12 as slopes of the deflection curves of the wing beam due to the application of a concentrated load or due to moments near the wing tips. Measurements were obtained from the outputs of calibrated accelerometers located at seven stations on the center line (elastic axis) of the wing beam. (See fig. 5.) The accelerometers were sensitive to static angular position, and outputs were read with a self-balancing potentiometer. Linearity and repeatability of the calibrations of the accelerometers indicate probable errors less than 1 or 2 percent in the measurement of the slopes.

Bending and torsional angular deflections of the horizontal and vertical stabilizers were measured by means of calibrated accelerometers in the same manner

as for the wing. Measured model deflections for the horizontal and vertical stabilizers are presented in figures 13 and 14.

Bending and torsional deflections of the fuselage were also measured by using a calibrated accelerometer. Deflections in terms of angular changes in the local slope with load are shown in figure 15.

The stiffnesses of the simulated power-plant assembly were measured before each test after a change in setting of the pitch or yaw springs had been made. (See table I.) For these measurements the nacelle beam, with the simulated power plant attached, was removed from the wing and clamped to a rigid support, and the propeller was replaced by a loading fixture. Angular deflections of the propeller shaft due to applied moments in pitch and yaw were measured, relative to the point of attachment of the nacelle beam to the wing beam, by means of the calibrated accelerometer or by use of an optical system. Load-deflection curves were usually nearly linear except for configurations showing high damping. For these conditions average values of the slopes of the load-deflection curves are presented. The maximum errors in stiffness measurements are thought to be within ±10 percent of the values given in table I. Most of the values, however, especially those for configurations having relatively low damping, are considerably more accurate.

Vertical and lateral displacements of each propeller hub due to applied loads on the hubs, measured relative to the point of attachment of the nacelle beam to the wing beam, were measured before testing the model. These measurements were made with the pitch and yaw springs set at average values of rotational stiffness of about $9.1 \times 10^3 \frac{\text{in-lb}}{\text{radian}}$ and $6.1 \times 10^3 \frac{\text{in-lb}}{\text{radian}}$, respectively. Average vertical and lateral spring rates for the above conditions were 297 lb/in. and 172 lb/in., respectively.

Weight and inertia.- The weight, static unbalance, and moment of inertia of each segment of the wing (fig. 5), without simulated fuel, are listed in table II. Moments of inertia were measured by means of a calibrated torsion pendulum and are given about the wing-beam center line.

Table III lists the weights, center-of-gravity locations, and moments of inertia about the wing-beam center line of the lead blocks used to simulate the various fuel loadings tested. Gross weights of the model with the various simulated fuel loadings are as follows:

Fuel, percent full	Gross weight, lb
0	266.3
32	288.7
64	311.0
100	336.1

Fuel loadings were distributed to correspond to assumed steady flight attitudes for level flight, climb, roll, and dive.

Weights of the model horizontal and vertical stabilizers were 4.67 and 4.47 pounds, respectively. Weights and center-of-gravity locations for the fuselage segments are given in table IV. Fuselage moments of inertia were not measured. Table V lists weights and chordwise center-of-gravity locations of the propellers and various parts of the nacelles and simulated power plants.

Moments of inertia of a propeller were measured by swinging the propeller as a compound pendulum about an axis parallel to the axis about which the moments of inertia are desired. Values for this propeller are as follows:

Reference axis	Moment of inertia, lb-in.^{2}
Axis of propeller rotation	41.4
Axis through center of gravity and perpendicular to axis of propeller rotation	20.1

Natural frequencies and damping.- Vibration measurements of the complete model for each of the fuel configurations tested were made prior to the wind-tunnel tests. The model was vibrated through a range of frequencies by a pair of electromagnetic shakers applied to the wings (usually near the tips) or by one shaker applied near the nose of the fuselage as shown schematically in figure 16. Node lines were determined by using a lightweight probe which was moved around on the model surface. Electrical signals from the probe proportional to amplitude of motion were applied to the vertical axis of an oscilloscope, and signals from the shaker control were applied to the horizontal axis. By observing the amplitude and orientation of the resulting Lissajous figures, qualitative measurements were made of the model motion and the node lines were determined.

Node lines and frequencies for each of the configurations tested are presented in figures 17 to 20. Unfortunately, however, three different model suspension systems were used during the measurements (fig. 16), and the data for the different systems are not comparable. The symmetrical and antisymmetrical modes for the configuration with 0-percent fuel loading and the symmetrical modes for the configuration with a simulated 100-percent fuel loading were obtained with the model mounted on three cantilever springs located at points corresponding to a typical tricycle landing gear. (See fig. 16(a).) The antisymmetrical modes for the configuration with a 100-percent fuel loading were obtained with the model suspended from two flexible cables. (See fig. 16(b).) Node lines and frequencies for the configurations having 32-percent and 64-percent fuel loadings were obtained with the model suspended by two long, soft coil springs attached to the fuselage tube. (See fig. 16(c).) Results obtained with the coil-spring mount are believed to be more nearly representative of the properties of the model "flying" in the tunnel.

Attempts were made to measure damping with the power plants installed on the wing. Such measurements were not satisfactory, however, because of severe beats in the motion. Therefore, in this report, all damping and natural frequencies for

the power plants were obtained with the power-plant assemblies removed from the wing and clamped to a rigid support as shown in figure 8. Presumably, the damping of the system when the power plants are mounted on the wing would be higher than the values measured with the assembly clamped to the rigid support.

In making the measurements the propeller spinner was given a small displacement in pitch or yaw and released. The response of the pitch- or yaw-spring strain gages to the subsequent decaying oscillation was recorded. The resulting time history was used to determine the frequency and damping. Frequency was determined by counting cycles during a known time interval. The damping was obtained from the logarithmic decrement of the amplitude of the oscillation and expressed as the structural damping coefficient.

Structural damping coefficients and frequencies for the various configurations tested are given in table I. For configurations in which beats were not present in the decaying-oscillation records, the damping coefficients were generally repeatable within 0.001 to 0.003. For some configurations, however, damping values deviated by larger amounts because of slight beating; the extent of these deviations is shown in the following table:

Point (table I)	Nacelle	Deviations of measurements	
		g_θ	g_ψ
770	4	0.005	0.004
922	4	.007	.012
1,232	3	-----	.008
	4	-----	.011
1,287	1	-----	.008
	4	.007	-----

Mounting System

The model mount used in the wind-tunnel tests is of the type described in reference 6. It consisted of a vertical 3/8-inch-diameter rod attached between the floor and ceiling of the test section as shown schematically in figure 21. Guy wires were attached to the rod above and below the limits of model travel, as shown in figure 4, to reduce lateral flexibility. The rod passed through the gimbals near the center of gravity of the model. The gimbals allowed the model freedom in pitch and yaw; freedom in vertical translation was obtained by the gimbals sliding on rollers on the rod. Bending of the rod and slight free play between the gimbal and the rod allowed limited roll motion, side translation, and fore and aft translation. Concentric tubes surrounding the 3/8-inch-diameter rod served as stops which limited the vertical translation of the model to about 10 inches above and below the tunnel center line. Hydraulic shock absorbers between the tubes and the floor and ceiling of the test section reduced the acceleration of the model at the limits of the vertical travel.

Instrumentation

Instrumentation was used primarily to determine frequencies and mode shapes rather than for quantitative analysis of stresses. Instrumentation included 60 channels of wire strain gages and accelerometers shown schematically in figure 22. Strain gages sensitive to bending and torsion deflections were mounted at six positions on the wing: at the root, inboard and outboard of the inboard power plant, inboard and outboard of the outboard power plant, and at the tip. Each simulated power plant had strain gages sensitive to pitch and yaw deflections mounted on the nacelle beam, and on the pitch spring and yaw spring. Accelerometers at the root of each wing and on the fuselage measured body motion. Bending and torsion strain gages were mounted on the fuselage center-line tube. Strain gages were also installed on the horizontal and vertical stabilizers.

The strain-gage and accelerometer signals were fed into recording oscillographs. Pitch- and yaw-spring signals and wing bending and torsion signals from one station of each wing were also monitored continuously during each run on direct-writing recorders and on oscilloscopes. Remote-reading tachometer generators connected to the propeller shafts were used to determine propeller rotational speeds.

TESTS

Scope

The variables investigated were restricted to those considered to have the most important effect on the behavior of the wing—power-plant combination. The variables considered were the following:

(a) Propeller rotational speed
(b) Stiffness of the power-plant assembly in the pitch and yaw planes
(c) Ratio of pitch stiffness to yaw stiffness of the power-plant assembly
(d) Structural damping of the power-plant assembly in the pitch and yaw planes
(e) Simulated fuel load in the wings
(f) Location and/or number of autoprecessing power-plant assemblies

Procedure

Each run was begun with the model on the lower stop. When the tunnel airspeed reached the flying speed of the model, an operator on a platform alongside the test section (fig. 21) trimmed the model to take off and fly at approximately the center of the test section. As the airspeed was varied, the operator changed the horizontal-stabilizer incidence to maintain trimmed flight near the center of the test section. Vertical surging motions of the model during the test were

restrained and damped manually by a second operator also stationed on the platform. Cables attached to the gimbals were conducted out through the floor and ceiling of the test section to this operator, who provided the force necessary to restrain the model. Some difficulty was encountered in flying the model as a result of rolling oscillations (similar to Dutch roll) at about 1 cps at the higher flying speeds. Lack of a roll-control device also proved to be a handicap at the higher speeds. These model flying difficulties limited the dynamic pressure to which it seemed safe to fly the model to values below 133.3 lb/sq ft.

The use of windmilling propellers and the lack of a remote propeller pitch control required that tests of each configuration be made at a number of propeller pitch settings in order that the autoprecession dynamic pressure could be obtained at a desired propeller rotational speed. Boundaries defining the start of autoprecession, if within the range of tunnel velocities at which the model could be flown, were established for each configuration by gradually increasing the tunnel airspeed until sustained autoprecession oscillations of nearly constant amplitude were observed on the model and on oscilloscope and oscillograph displays of signals from strain gages on the power-plant mounting system. The electrically driven shaker was operated periodically as the tunnel velocity was increased to excite precession so that estimates of the damping could be made from records of the decay of the oscillations when the shaker was stopped. Figure 23 shows a representative sampling of the variation of the damping and frequency of the precession mode as determined from short records taken at subcritical speeds for several typical configurations. It will be noted that an extrapolation of these data to zero damping shows no inconsistency with the point of autoprecession picked by the observer. In general, the observer's selection, by virtue of a longer sampling time, is believed to be the more reliable point and has been used throughout the report.

Another method of exciting autoprecession was tried on a few runs. This consisted of the use of small aerodynamic oscillators mounted on the horizontal tail, as shown in figure 11, and tuned to the precession frequency.

RESULTS AND DISCUSSION

Test data, most of which were obtained with a wing mass distribution simulating a configuration having a 64-percent fuel load during level flight, are presented in table I. Boundaries denoting the start of autoprecession as a function of airstream dynamic pressure and propeller rotational speed are presented in figures 24 to 29. In general, cross plots obtained from these boundaries have been used to illustrate the effects of the different variables investigated on the dynamic pressure for autoprecession. It should be noted that the variation in dynamic pressure for autoprecession reflects primarily the effects of changes in velocity since the density was held relatively constant throughout the tests at 0.00237 slug/cu ft ± 3 percent. In plotting the boundaries as a function of dynamic pressure it is not meant to imply that the phenomenon is not separately a function of density and velocity. The effects of density variation are treated in the analytical work of references 2 to 4.

During the majority of the tests, a pitch stiffness of about $9.1 \times 10^3 \frac{\text{in-lb}}{\text{radian}}$ and a yaw stiffness of about $6.1 \times 10^3 \frac{\text{in-lb}}{\text{radian}}$, which gave a root-mean-square stiffness of $7.8 \times 10^3 \frac{\text{in-lb}}{\text{radian}}$ and a stiffness ratio of 1.5, were maintained in three of the power-plant assemblies. These stiffnesses are used as a base for the discussion and will be referred to as "reference stiffness." Similarly, 3,240 rpm is arbitrarily referred to as "reference propeller rotational speed."

Outboard Power Plant

The majority of the tests were run with power plant 4 (right outboard) at stiffnesses less than the reference values. Damping coefficients were also less than those of the other three power plants for most of the tests.

Propeller rotational speed.- The effects of variation of gyroscopic moment, studied by varying the propeller rotational speed, on the dynamic pressure for autoprecession when all propellers are operating at the same speed are illustrated by the autoprecession boundaries for power plant 4 presented in figure 24. For these data the stiffness and damping of power-plant mount 4 were adjusted to give a ratio of pitch stiffness to yaw stiffness of 1.0 and an average damping coefficient of 0.014; the remaining power plants were set for reference stiffness and an average damping of about 0.04. As shown, the curves have a general family characteristic and are typical of the autoprecession boundaries usually encountered during this test regardless of the position or number of power plants involved. In general, overspeeding of the propellers (i.e., rotational speeds greater than 3,240 rpm) lowered the dynamic pressure for autoprecession. As indicated by the slopes of the boundaries near reference propeller rotational speed, the detrimental effect of propeller overspeeding was more pronounced at the higher stiffnesses (fig. 24) but was little changed by damping. (See, for example, fig. 26.) Similar trends for other configurations are shown in figures 25, and 27 to 29.

Stiffness.- As discussed in reference 2, systems having different relative pitch and yaw stiffnesses are sometimes correlated by use of an effective stiffness parameter defined as the root-mean-square stiffness S_{rms}. This parameter, together with the stiffness ratio S_θ/S_ψ, is used in the present report to define or compare the various power-plant stiffness configurations. The effect of reduced stiffness in an outboard power-plant installation on the dynamic pressure for autoprecession at a stiffness ratio of 1.0 and reference propeller rotational speed is illustrated by figure 30 which is a cross plot of the data in figure 24. Power plants 1, 2, and 3 are set at reference stiffness and an average damping coefficient of about 0.04. Figure 30 shows that the dynamic pressure for autoprecession is lowered with a reduction in stiffness.

Some additional data showing the effects of stiffness were obtained at a stiffness ratio of 1.5. Autoprecession boundaries for these configurations are presented in figure 25. Insufficient data were obtained to show the effects of

stiffness at reference propeller rotational speed. Figure 31, which was cross-plotted from figures 24 and 25, shows the effects of stiffness on the dynamic pressure for autoprecession at 140 percent of the reference propeller rotational speed for stiffness ratios of 1.5 and 1.0. From the figure, it appears that at the higher stiffnesses a configuration with a stiffness ratio of 1.5 would be more susceptible to autoprecession than a configuration with the same stiffness but having a stiffness ratio of 1.0.

Structural damping.- From figure 32(a) it can be seen that the dynamic pressure for autoprecession is very sensitive to small changes in damping. The effects of structural damping on the dynamic pressure for autoprecession were investigated at root-mean-square stiffnesses of $3.2 \times 10^3 \frac{\text{in-lb}}{\text{radian}}$ and $4.0 \times 10^3 \frac{\text{in-lb}}{\text{radian}}$ at a stiffness ratio of 1.0 and $3.6 \times 10^3 \frac{\text{in-lb}}{\text{radian}}$ at stiffness ratios of 0.55 and 1.81. Plots of the basic data for these configurations are presented in figures 26 and 27. The indicated values of damping employed in the figures are averages of the values measured in the pitch and yaw degrees of freedom. The ratio of the damping in pitch to damping in yaw varied somewhat in the investigation as indicated in table I, and no attempt was made to systematically vary this ratio during these experimental tests. The effects of varying the ratio of damping in pitch to damping in yaw have, however, been investigated analytically in references 2 and 4.

Cross plots of the data in figure 27 showing the effects of damping on the dynamic pressure for autoprecession at reference propeller rotational speed are presented in figure 32(b). The large effects on the dynamic pressure for autoprecession of small changes in structural damping are readily apparent in this figure. For example, in figure 32(a), at a stiffness of $4.0 \times 10^3 \frac{\text{in-lb}}{\text{radian}}$, an increase in the structural damping coefficient of 0.02 increased the dynamic pressure for autoprecession about 60 lb/sq ft.

Fuel loadings.- Data obtained at a constant propeller-blade angle with wing mass distributions simulating configurations having 0-, 32-, 64-, and 100-percent fuel loads are listed in table I. These data, adjusted to reference propeller rotational speed, are presented in figure 33. The data were adjusted by adding to the values given in the table the increments in dynamic pressure that corresponding changes in propeller rotational speed would produce in the autoprecession boundary for a configuration with a 64-percent fuel load and a root-mean-square stiffness of $4.0 \times 10^3 \frac{\text{in-lb}}{\text{radian}}$. (See fig. 24.)

The results shown in figure 33 indicate a decrease in dynamic pressure for autoprecession from 79 lb/sq ft to 41.5 lb/sq ft as the fuel loading is reduced from 100 to 0 percent. Neither the climb nor the rolling attitude with a 64-percent fuel load lowered the dynamic pressure for autoprecession. For the configuration with a 64-percent fuel load, however, additional data obtained at a different stiffness $\left(3.9 \times 10^3 \frac{\text{in-lb}}{\text{radian}}\right)$ and not presented in the figure (see data points 430 and 436 in table I) indicate that at reference propeller

rotational speed, the autoprecession dynamic pressure for the configuration representing the dive attitude would be slightly lower than that for the level-flight configuration.

Inboard Power Plant

The variation of dynamic pressure for autoprecession with reduced stiffness for an outboard power plant (fig. 30) is reproduced in figure 34. Also shown are the data for an inboard power plant at reduced stiffness, which were taken from figure 28 and superimposed. It is evident in the figure that the inboard power plant is much more susceptible to autoprecession than the outboard power plant.

Power-Plant Combinations

It appeared to be of interest to find the effects of simultaneous reductions in stiffness in more than one power plant. The effects of reduced stiffness with several combinations are illustrated in figure 35. In the figure, data for the model with power plants 3 and 4 and power plants 1 and 4 at reduced stiffness, obtained from the basic data of figure 28, are superimposed on the curves for a single outboard power plant. It is evident that simultaneous reduction in stiffness of two power plants significantly reduced the dynamic pressure for autoprecession below that of a single power plant having a corresponding stiffness. Figure 35(b) indicates that the dynamic pressure for autoprecession was lower for the configuration having reduced stiffness in two power plants on the same side of the wing than it was for the two outboard power plants.

At dynamic pressures well below the autoprecession dynamic pressure, the behavior of the configurations with more than one power-plant assembly at reduced stiffness was characterized by a tendency for cyclic variations in the amplitude of precession of the two propellers, with the amplitude of precession a maximum for one while the other was a minimum. Whenever two power plants on the same wing were involved, the inboard power plant always precessed first; autoprecession of the outboard power plant occurred at 2 to 8 lb/sq ft higher dynamic pressure.

Somewhat limited data are used in figure 36 to indicate autoprecession boundaries for the model with all power plants at reference stiffness but with various combinations of damping. The boundaries indicate that as the damping was reduced on additional power plants, more could respond and influence the motion. The single point labeled "no precession" for the configuration having an average structural damping coefficient of about 0.04 shows that with the addition of a relatively small amount of structural damping in all power plants, the autoprecession boundary was beyond the test range.

The complexity of working with multiple power-plant assemblies was such that in some cases it was difficult to predict or explain the behavior of the system. As an example, because of the sensitivity of the autoprecession boundary to variations in propeller rotational speed when all the propellers were running at the

same speed, some tests were made to determine the effects of a single inboard propeller overspeeding with the remaining propellers near reference speed. For these tests all power plants were set for reference stiffness and low damping. The data of figure 37 show that overspeed initially decreased the dynamic pressure for autoprecession; however, at still higher propeller rotational speeds the dynamic pressure for autoprecession was increased. No increase of similar magnitude was encountered during tests with all propellers operating at the same speed. In the region in which autoprecession would be expected if all propellers were operating at the same speed, severe intermittent autoprecession was encountered as indicated by the dashed lines in the figure.

Autoprecession Mode and Frequencies

In all cases in which the direction of the precession motion was checked, it was found to be opposite in sense to the rotation of the propeller; that is, autoprecession occurred in the retrograde mode.

Figure 38 illustrates the effects of several different variables on the autoprecession frequency. At a stiffness of $4.0 \times 10^3 \frac{\text{in-lb}}{\text{radian}}$, autoprecession frequency decreased by 0.6 to 1.9 cps, depending upon the configuration, as the propeller rotational speed increased from 80 to 140 percent of the reference value. Decreases of similar magnitudes were noted at other stiffnesses.

At reference propeller rotational speed and for a fixed stiffness, outboard power plants, inboard power plants, and inboard-outboard power-plant combinations autoprecessed at progressively higher frequencies. As would be expected, the autoprecession frequency increased with increased stiffness (fig. 38(b)), but changed very little with variations in damping (fig. 38(a)).

Forced Precession

When the small aerodynamic oscillators, which were installed on the horizontal tail as shown in figure 11, were tuned to the precession frequency, the oscillators produced negligibly small disturbances to the motion of the model but induced propeller precession at dynamic pressures well below the autoprecession boundary. At reference stiffness, but with low structural damping, forced precession amplitudes of the same magnitude as those at autoprecession were encountered at a dynamic pressure 60 lb/sq ft below the autoprecession point.

Wing Response to Autoprecession

Some qualitative trends regarding wing response to autoprecession have been established from a review of the data. These trends are illustrated in figure 39 by the results of a power-spectral-density analysis of a wing strain gage. The points at which the data were obtained are not presented in table I, but are typical of those presented. The data were obtained at the autoprecession dynamic pressure of 56 lb/sq ft and at 2 lb/sq ft below the autoprecession point. As

shown by the concentration of power near the autoprecession frequency, the predominant motion of the wing is seen to occur at the same frequency as that of the autoprecession motion. It is also evident from the figure that an increase in amplitude of the precession motion is accompanied by an increase in amplitude of the wing motion. The results obtained with the power-plant motion restrained by the snubber indicate decisively that when the autoprecession stopped, the wing motion stopped, even at the same dynamic pressure.

CONCLUSIONS

The conclusions concerning the precession phenomenon and the autoprecession boundary at which the propeller—power-plant assembly is neutrally stable, at Mach numbers below 0.3, are as follows:

1. Reduction of stiffness in a power plant lowers the dynamic pressure at which the boundary for autoprecession occurs.

2. At the higher stiffnesses investigated, a configuration with a stiffness ratio of 1.5 is more susceptible to autoprecession than a configuration with the same stiffness but having a stiffness ratio of 1.0.

3. The dynamic pressure for autoprecession is very sensitive to changes in damping; small reductions in structural damping caused large reductions in the dynamic pressure for autoprecession.

4. An inboard power plant is more susceptible to autoprecession than an outboard power plant. The autoprecession boundary is considerably lower for configurations with two or more power plants simultaneously having about the same reduced level of stiffness than it is for configurations in which the stiffness is reduced to this level in only one power plant.

5. Overspeeding of the propellers lowers the dynamic pressure for autoprecession. The detrimental effect of propeller overspeeding is more pronounced at the higher stiffnesses, but is little changed by damping.

6. Reduction of the fuel loading lowers the dynamic pressure for autoprecession.

7. Propeller precession motion is accompanied at about the same frequency by wing response in bending and torsion, and an increase in amplitude of the precession motion is accompanied by an increase in amplitude of the wing motion.

Langley Research Center,
National Aeronautics and Space Administration,
Langley Station, Hampton, Va., April 22, 1963.

REFERENCES

1. Taylor, E. S., and Browne, K. A.: Vibration Isolation of Aircraft Power Plants. Jour. Aero. Sci., vol. 6, no. 2, Dec. 1938, pp. 43-49.

2. Reed, Wilmer H., III, and Bland, Samuel R.: An Analytical Treatment of Aircraft Propeller Precession Instability. NASA TN D-659, 1961.

3. Houbolt, John C., and Reed, Wilmer H., III: Propeller-Nacelle Whirl Flutter. Jour. Aerospace Sci., vol. 29, no. 3, Mar. 1962, pp. 333-346.

4. Sewall, John L.: An Analytical Trend Study of Propeller Whirl Instability. NASA TN D-996, 1962.

5. Bland, Samuel R., and Bennett, Robert M.: Wind-Tunnel Measurement of Propeller Whirl-Flutter Speeds and Static-Stability Derivatives and Comparison With Theory. NASA TN D-1807, 1963.

6. Kinnaman, E. Berkeley: Flutter Analysis of Complex Airplanes by Experimental Methods. Jour. Aero. Sci., vol. 19, no. 9, Sept. 1952, pp. 577-584.

TABLE I.- TEST DATA

Data point		770	788	762	783	778	832	821	814	825	807	1129	1135	1114	1116	1073
Power plant autoprecessing		4	→													
q, lb/sq ft		48.1	43.7	34.3	32.4	32.2	106.5	84.7	75.4	58.6	71.9	37.3	44.1	40.9	35.2	89.3
M		.18	.17	.15	.14	.15	.26	.23	.22	.20	.22	.16	.17	.16	.15	.24
V, ft/sec		202	192	170	165	169	300	268	252	223	246	178	193	186	172	274
ρ, slugs/cu ft		2,368 $\times 10^{-6}$	2,371 $\times 10^{-6}$	2,368 $\times 10^{-6}$	2,368 $\times 10^{-6}$	2,269 $\times 10^{-6}$	2,369 $\times 10^{-6}$	2,368 $\times 10^{-6}$	2,370 $\times 10^{-6}$	2,367 $\times 10^{-6}$	2,273 $\times 10^{-6}$	2,361 $\times 10^{-6}$	2,368 $\times 10^{-6}$	2,375 $\times 10^{-6}$	2,370 $\times 10^{-6}$	2,374 $\times 10^{-6}$
Fuel load[a], percent		64L	→													
f_a, cps		7.43	7.30	7.05	6.10	6.00	7.08	7.05	7.02	6.38	6.60	6.76	7.49	7.11	6.83	6.76
Power plant 1	β, deg	46	43	35	43	25	58	52	48	35	43	33	44	41	35	55
	N, rpm	2,700	-----	3,390	2,730	4,950	2,520	2,850	3,150	4,410	-----	-----	-----	-----	-----	-----
	S_θ, in-lb/radian	9,291														
	S_ψ, in-lb/radian	6,112														
	S_{rms}, in-lb/radian	7,864														
	S_θ/S_ψ	1.52														
	f_θ, cps	19.69										19.30				
	f_ψ, cps	14.95										14.70				
	g_θ	.038										.023				
	g_ψ	.029										.045				
Power plant 2	β, deg	46	43	35	43	25	58	52	48	35	43	33	44	41	35	55
	N, rpm	2,700	2,910	3,330	2,490	4,860	2,490	2,820	3,000	4,410	3,630	3,750	2,820	3,000	3,450	2,610
	S_θ, in-lb/radian	9,144														
	S_ψ, in-lb/radian	6,161														
	S_{rms}, in-lb/radian	7,797														
	S_θ/S_ψ	1.48														
	f_θ, cps	19.94										21.05				
	f_ψ, cps	17.34										17.43				
	g_θ	.030										.036				
	g_ψ	.051										.064				
Power plant 3	β, deg	46	43	35	43	25	58	52	48	35	43	33	44	41	35	55
	N, rpm	-----	-----	-----	-----	-----	-----	-----	-----	-----	-----	3,780	2,790	2,970	3,420	2,610
	S_θ, in-lb/radian	9,340										9,046				
	S_ψ, in-lb/radian	6,210										6,064				
	S_{rms}, in-lb/radian	7,931										7,701				
	S_θ/S_ψ	1.51										1.49				
	f_θ, cps	20.00										21.72				
	f_ψ, cps	18.00										17.34				
	g_θ	.032										.036				
	g_ψ	.034										.053				
Power plant 4	β, deg	46	43	35	25	25	58	52	48	35	43	33	44	41	35	55
	N, rpm	2,670	2,850	3,330	4,710	4,860	2,520	2,850	3,060	4,380	3,600	3,750	2,790	2,970	3,450	2,610
	S_θ, in-lb/radian	3,262										4,147		2,465		
	S_ψ, in-lb/radian	3,174										2,743		4,450		
	S_{rms}, in-lb/radian	3,218										3,516		3,597		
	S_θ/S_ψ	1.03										1.51		.55		
	f_θ, cps	10.19					10.29					11.72		8.73		8.92
	f_ψ, cps	10.89					11.37					9.81		12.60		12.60
	g_θ	.015					.030				.039	.012		.011		.026
	g_ψ	.010					.034					.008		.010		.012

[a]Symbols indicating flight conditions: level, L; diving, D; rolling, R; climbing, C.

TABLE I.- TEST DATA - Continued

Data point		1060	1069	1065	1082	1106	1096	1337	1332	1340	1353	1347	1357	1391	1397
Power plant autoprecessing		4	→												
q, lb/sq ft		59.1	48.4	42.5	45.6	117.1	92.6	44.3	29.5	29.0	49.7	43.3	39.6	74.5	54.1
M		.20	.18	.17	.17	.27	.24	.17	.14	.14	.18	.17	.16	.22	.19
V, ft/sec		223	202	189	196	314	280	193	158	157	205	191	183	251	214
ρ, slugs/cu ft		2,373 x10⁻⁶	2,366 x10⁻⁶	2,370 x10⁻⁶	2,372 x10⁻⁶	2,376 x10⁻⁶	2,372 x10⁻⁶	2,367 x10⁻⁶	2,358 x10⁻⁶	2,368 x10⁻⁶	2,370 x10⁻⁶	2,366 x10⁻⁶	2,368 x10⁻⁶	2,365 x10⁻⁶	2,368 x10⁻⁶
Fuel load[a], percent		64L	→												
f_a, cps		7.30	6.89	6.60	5.78	6.79	6.67	7.68	7.21	6.29	7.59	7.08	6.92	7.30	6.79
Power plant 1	β, deg	47	41	34	26	51	45	52	38	28	49.5	41	35	52	40
	N, rpm	-----	-----	-----	-----	-----	-----	2,040	2,910	4,050	2,490	3,150	3,690	2,760	3,570
	S_θ, in-lb/radian	9,291						9,242							
	S_ψ, in-lb/radian	6,112						6,161							
	S_{rms}, in-lb/radian	7,864	→					7,854	→						
	S_θ/S_ψ	1.52						1.50							
	f_θ, cps	19.30						18.64							
	f_ψ, cps	14.70						15.53							
	g_θ	.023						.034							
	g_ψ	.045						.055							
Power plant 2	β, deg	47	41	34	26	51	45	52	38	28	49.5	41	35	52	40
	N, rpm	2,880	3,270	3,930	5,430	3,450	3,840	-----	-----	-----	2,430	-----	3,630	2,730	3,630
	S_θ, in-lb/radian	9,144													
	S_ψ, in-lb/radian	6,161													
	S_{rms}, in-lb/radian	7,797	→												
	S_θ/S_ψ	1.48													
	f_θ, cps	21.05													
	f_ψ, cps	17.43													
	g_θ	.036													
	g_ψ	.064													
Power plant 3	β, deg	47	41	34	26	51	45	52	38	28	49.5	41	35	52	40
	N, rpm	2,880	3,270	3,930	5,370	3,450	3,780	2,010	2,880	3,990	2,430	3,060	3,600	2,700	3,540
	S_θ, in-lb/radian	9,046						9,144							
	S_ψ, in-lb/radian	6,064						6,259							
	S_{rms}, in-lb/radian	7,701	→					7,836	→						
	S_θ/S_ψ	1.49						1.46							
	f_θ, cps	21.72						20.19							
	f_ψ, cps	17.34						16.32							
	g_θ	.036						.012							
	g_ψ	.053						.010							
Power plant 4	β, deg	47	41	34	26	51	45	52	38	28	49.5	41	35	52	40
	N, rpm	2,880	3,270	3,920	5,370	3,450	3,840	2,040	2,880	3,990	2,430	3,060	3,600	2,730	3,570
	S_θ, in-lb/radian	2,465						4,450						4,479	→
	S_ψ, in-lb/radian	4,450	→					2,465	→					2,474	
	S_{rms}, in-lb/radian	3,597						3,597						3,618	
	S_θ/S_ψ	.55						1.80						1.81	
	f_θ, cps	8.92				9.65	→	12.07			12.38	→		12.29	
	f_ψ, cps	12.60	→			13.02		9.02	→		9.59		→	9.59	
	g_θ	.026				.041		.016			.022			.027	
	g_ψ	.012				.030		.013			.016			.027	

[a]Symbols indicating flight conditions: level, L; diving, D; rolling, R; climbing, C.

TABLE I.- TEST DATA - Continued

Data point		1365	1383	424	430	436	892	879	884	888	897	900	922	929	913
Power plant autoprecessing		4	→												
q, lb/sq ft		85.4	66.5	47.8	67.5	65.5	77.8	63.0	45.6	39.7	39.6	42.2	122.9	91.5	74.5
M		.24	.21	.18	.21	.21	.22	.20	.17	.16	.16	.16	.28	.24	.22
V, ft/sec		269	237	201	239	235	256	230	196	183	183	189	320	278	251
ρ, slugs/cu ft		2,360 x10^{-6}	2,370 x10^{-6}	2,366 x10^{-6}	2,368 x10^{-6}	2,370 x10^{-6}	2,369 x10^{-6}	2,375 x10^{-6}	2,368 x10^{-6}	2,367 x10^{-6}	2,371 x10^{-6}	2,373 x10^{-6}	2,398 x10^{-6}	2,370 x10^{-6}	2,368 x10^{-6}
Fuel load[a], percent		64L	→		→	64D	64L	→							
f_a, cps		7.14	7.11	8.0	7.62	7.68	7.72	7.62	7.49	7.24	6.86	6.54	7.62	7.27	7.18
Power plant 1	β, deg	52	46	43	46	→	49	43	35	29	26	25	51	44	39
	N, rpm	2,940	3,210	-----	-----	-----	3,120	3,450	3,960	4,410	5,070	5,430	3,510	4,020	4,350
	S_θ, in-lb/radian	9,242		9,291											
	S_ψ, in-lb/radian	6,161		6,112											
	S_{rms}, in-lb/radian	7,854		7,864											
	S_θ/S_ψ	1.50	→	1.52											
	f_θ, cps	18.64		20.99			19.69								
	f_ψ, cps	15.53		16.54	→		14.95								
	g_θ	.034		.014			.038								
	g_ψ	.055		.015			.029								
Power plant 2	β, deg	52	46	43	46	→	49	40	35	29	26	25	51	44	39
	N, rpm	2,910	3,180	3,000	3,150	3,120	3,060	3,420	3,930	4,380	5,100	5,400	3,480	3,900	4,320
	S_θ, in-lb/radian	9,144		9,242			9,144								
	S_ψ, in-lb/radian	6,161	→	6.161			6,161								
	S_{rms}, in-lb/radian	7,797		7,854			7,797								
	S_θ/S_ψ	1.48		1.50	→		1.48								
	f_θ, cps	21.05		18.89			21.05								
	f_ψ, cps	17.43	→	15.46			19.75								
	g_θ	.036		.015			.051								
	g_ψ	.064		.009			.106								
Power plant 3	β, deg	52	46	43	46	→	49	43	35	29	26	25	51	44	39
	N, rpm	2,850	3,180	-----	-----	-----	-----	-----	-----	-----	-----	-----	-----	-----	-----
	S_θ, in-lb/radian	9,144		9,340											
	S_ψ, in-lb/radian	6,259		6,210											
	S_{rms}, in-lb/radian	7,836	→	7,931											
	S_θ/S_ψ	1.46		1.50											
	f_θ, cps	20.19		19.15			20.00								
	f_ψ, cps	16.32		15.05	→		18.00								
	g_θ	.012		.021			.032								
	g_ψ	.010		.020			.034								
Power plant 4	β, deg	52	46	43	46	→	49	43	35	29	26	25	51	44	39
	N, rpm	2,820	3,180	3,030	3,150	3,090	3,090	3,390	3,900	4,320	5,010	5,400	3,510	3,960	4,320
	S_θ, in-lb/radian	4,450	4,479	4,750	2,738		3,961								
	S_ψ, in-lb/radian	2,465	2,474	3,120	4,743		3,951								
	S_{rms}, in-lb/radian	3,597	3,618	4,020	3,873		3,956								
	S_θ/S_ψ	1.80	1.81	1.52	.58	→	1.00								
	f_θ	12.57	12.45	12.15	10.32		11.21						12.29		
	f_ψ	9.78	9.75	10.33	12.67		11.91					→	11.75		
	g_θ	.025	.028	.016	.023		.018						.043		
	g_ψ	.036	.038	.011	.007		.009						.040		

[a]Symbols indicating flight conditions: level, L; diving, D; rolling, R; climbing, C.

TABLE I.- TEST DATA - Continued

Data point		936	942	949	648	656	612	621	629	641	867	859	1143
Power plant autoprecessing .		4	→										
q, lb/sq ft		69.7	64.6	66.9	56.3	61.9	68.9	70.8	68.7	71.9	123.8	102.0	118.0
M		.21	.20	.21	.19	.20	.21	.21	.21	.22	.28	.26	.28
V, ft/sec		243	234	238	218	228	241	245	241	247	321	293	315
ρ, slugs/cu ft		2,370 $\times 10^{-6}$	2,369 $\times 10^{-6}$	2,372 $\times 10^{-6}$	2,367 $\times 10^{-6}$	2,373 $\times 10^{-6}$	2,373 $\times 10^{-6}$	2,368 $\times 10^{-6}$	2,371 $\times 10^{-6}$	2,363 $\times 10^{-6}$	2,403 $\times 10^{-6}$	2,375 $\times 10^{-6}$	2,378 $\times 10^{-6}$
Fuel load[a], percent		64L	→		0	32L	64L	64R	64C	100L	64L	→	
f_a, cps		7.21	7.21	6.60	8.10	7.62	7.68	7.49	7.62	7.49	7.65	7.65	9.68
Power plant 1	β, deg	35	33	30	45	→					48	43	44
	N, rpm	4,710	5,010	5,460	-----	-----	-----	-----	-----	-----	3,990	4,320	-----
	S_θ, $\frac{\text{in-lb}}{\text{radian}}$	9,291											
	S_ψ, $\frac{\text{in-lb}}{\text{radian}}$	6,112	→										
	S_{rms}, $\frac{\text{in-lb}}{\text{radian}}$ . . .	7,864											
	S_θ/S_ψ	1.52											
	f_θ, cps	19.69			19.30						19.69		19.30
	f_ψ, cps	14.95	→		13.91	→				→	14.95	→	14.70
	g_θ	.038			.016						.038		.023
	g_ψ	.029			.029						.029		.045
Power plant 2	β, deg	35	33	30	45	→					48	43	44
	N, rpm	4,620	5,010	5,400	3,030	3,150	3,330	3,390	3,300	3,390	3,930	4,260	4,470
	S_θ, $\frac{\text{in-lb}}{\text{radian}}$	9,144											
	S_ψ, $\frac{\text{in-lb}}{\text{radian}}$	6,161	→										
	S_{rms}, $\frac{\text{in-lb}}{\text{radian}}$ . . .	7,797											
	S_θ/S_ψ	1.48											
	f_θ, cps	21.05			19.34						20.00		21.05
	f_ψ, cps	19.75	→		15.91	→				→	19.75	→	17.43
	g_θ	.051			-----						.051		.036
	g_ψ	.106			-----						.106		.064
Power plant 3	β, deg	35	33	30	45	→					48	43	44
	N, rpm	-----	-----	-----	-----	-----	-----	-----	-----	-----	-----	-----	4,440
	S_θ, $\frac{\text{in-lb}}{\text{radian}}$	9,340											9,046
	S_ψ, $\frac{\text{in-lb}}{\text{radian}}$	6,210	→										5,868
	S_{rms}, $\frac{\text{in-lb}}{\text{radian}}$ . . .	7,931											7,625
	S_θ/S_ψ	1.50											1.48
	f_θ, cps	20.00			19.34						20.00		21.72
	f_ψ, cps	18.00	→		15.97	→				→	18.00	→	17.34
	g_θ	.032			-----						.032		.036
	g_ψ	.034			-----						.034		.053
Power plant 4	β, deg	35	33	30	45	→					48	43	44
	N, rpm	4,680	4,980	5,430	3,030	3,150	3,300	3,390	3,300	3,360	3,930	4,260	4,440
	S_θ, $\frac{\text{in-lb}}{\text{radian}}$	3,961			4,147						4,743		6,553
	S_ψ, $\frac{\text{in-lb}}{\text{radian}}$	3,951	→		4,112	→				→	4,719	→	4,352
	S_{rms}, $\frac{\text{in-lb}}{\text{radian}}$ . . .	3,956			4,130						4,731		5,562
	S_θ/S_ψ	1.00			1.01						1.01		1.51
	f_θ, cps	12.29			11.24						12.41		14.83
	f_ψ, cps	11.75			11.87						13.27		12.41
	g_θ	.043			.021						.022		.015
	g_ψ	.040			.008						.010		.009

[a]Symbols indicating flight conditions: level, L; diving, D; rolling, R; climbing, C.

TABLE I.- TEST DATA - Continued

Data point		1149	1027	1035	1033	1012	995	1043	989	1002	1182	1170	1161	1175	1191
Power plant autoprecessing		4	3	→	→	3, 4	←	←	←	←	←	←	←	←	3
q, lb/sq ft		110.9	77.6	47.0	34.6	42.4	33.1	33.5	30.4	30.3	88.4	59.5	49.3	39.7	82.6
M		.27	.22	.18	.15	.17	.15	.15	.14	.14	.24	.20	.18	.16	.23
V, ft/sec		304	256	199	171	189	167	168	160	160	274	224	204	183	264
ρ, slugs/cu ft		2,299 $\times 10^{-6}$	2,376 $\times 10^{-6}$	2,368 $\times 10^{-6}$	2,369 $\times 10^{-6}$	2,369 $\times 10^{-6}$	2,367 $\times 10^{-6}$	2,373 $\times 10^{-6}$	2,386 $\times 10^{-6}$	2,366 $\times 10^{-6}$	2,365 $\times 10^{-6}$	2,368 $\times 10^{-6}$	2,367 $\times 10^{-6}$	2,370 $\times 10^{-6}$	2,370 $\times 10^{-6}$
Fuel load[a], percent		64L	→	→	→	→	←	←	←	←	←	←	←	←	→
f_a, cps		7.49	8.51	8.41	7.56	9.75	9.78	9.59	8.89	7.49	10.99	10.80	10.32	8.92	10.03
Power plant 1	β, deg	40	55	40	27	55	47	47	35	27	58	48	40	28	45
	N, rpm	-----	2,430	3,390	4,620	1,860	2,160	2,220	3,210	4,080	2,310	-----	-----	4,710	3,660
	S_θ, in-lb/radian	9,291	↓	↓	↓	↓	↓	↓	↓	↓	↓	↓	↓	↓	↓
	S_ψ, in-lb/radian	6,112	↓	↓	↓	↓	↓	↓	↓	↓	↓	↓	↓	↓	↓
	S_{rms}, in-lb/radian	7,864	↓	↓	↓	↓	↓	↓	↓	↓	↓	↓	↓	↓	↓
	S_θ/S_ψ	1.52	↓	↓	↓	↓	↓	↓	↓	↓	↓	↓	↓	↓	↓
	f_θ, cps	19.30	18.92	↓	↓	↓	↓	↓	↓	↓	19.27	↓	↓	↓	↓
	f_ψ, cps	14.70	14.32	↓	↓	↓	↓	↓	↓	↓	14.70	↓	↓	↓	↓
	g_θ	.023	.019	↓	↓	↓	↓	↓	↓	↓	.023	↓	↓	↓	↓
	g_ψ	.045	.014	↓	↓	↓	↓	↓	↓	↓	.046	↓	↓	↓	↓
Power plant 2	β, deg	40	55	40	27	55	47	47	35	27	58	48	40	28	45
	N, rpm	4,920	2,400	3,330	4,620	1,830	2,160	2,220	3,180	4,140	2,280	2,790	3,390	4,650	3,660
	S_θ, in-lb/radian	9,144	↓	↓	↓	↓	↓	↓	↓	↓	↓	↓	↓	↓	↓
	S_ψ, in-lb/radian	6,161	↓	↓	↓	↓	↓	↓	↓	↓	↓	↓	↓	↓	↓
	S_{rms}, in-lb/radian	7,797	↓	↓	↓	↓	↓	↓	↓	↓	↓	↓	↓	↓	↓
	S_θ/S_ψ	1.48	↓	↓	↓	↓	↓	↓	↓	↓	↓	↓	↓	↓	↓
	f_θ, cps	21.05	18.67	↓	↓	↓	↓	↓	↓	↓	↓	↓	21.05	↓	↓
	f_ψ, cps	17.43	15.53	↓	↓	↓	↓	↓	↓	↓	↓	↓	17.43	↓	↓
	g_θ	.036	.014	↓	↓	↓	↓	↓	↓	↓	↓	↓	.036	↓	↓
	g_ψ	.064	.011	↓	↓	↓	↓	↓	↓	↓	↓	↓	.064	↓	↓
Power plant 3	β, deg	45	55	40	27	55	47	47	35	27	58	48	40	28	45
	N, rpm	4,950	2,370	3,300	4,590	1,830	2,160	2,190	3,150	4,320	2,250	2,790	3,390	4,620	3,600
	S_θ, in-lb/radian	9,046	4,000	3,971	↓	4,000	↓	↓	↓	↓	6,553	↓	↓	↓	↓
	S_ψ, in-lb/radian	5,868	3,946	3,941	↓	3,946	↓	↓	↓	↓	4,342	↓	↓	↓	↓
	S_{rms}, in-lb/radian	7,625	3,973	3,956	↓	3,973	↓	↓	↓	↓	5,558	↓	↓	↓	↓
	S_θ/S_ψ	1.48	1.01	1.01	→	1.01	→	→	→	→	1.51	→	→	→	→
	f_θ, cps	21.72	12.06	11.59	↓	12.07	↓	↓	↓	↓	15.62	↓	↓	↓	↓
	f_ψ, cps	17.34	12.70	11.81	↓	12.70	↓	↓	↓	↓	13.30	↓	↓	↓	↓
	g_θ	.036	.017	.015	↓	.017	↓	↓	↓	↓	.013	↓	↓	↓	↓
	g_ψ	.053	.010	.015	↓	.010	↓	↓	↓	↓	.008	↓	↓	↓	↓
Power plant 4	β, deg	40	55	40	27	55	47	47	35	27	58	48	40	28	85
	N, rpm	4,920	2,400	3,360	4,590	1,830	2,160	2,190	3,180	4,290	2,280	2,820	3,420	4,650	-----
	S_θ, in-lb/radian	6,553	9,487	↓	↓	3,961	↓	4,020	3,961	↓	6,553	↓	↓	↓	
	S_ψ, in-lb/radian	4,352	6,210	↓	↓	3,951	↓	4,010	3,951	↓	4,352	↓	↓	↓	
	S_{rms}, in-lb/radian	5,562	8,018	↓	↓	3,956	↓	4,015	3,956	↓	5,562	↓	↓	↓	
	S_θ/S_ψ	1.51	1.53	→	→	1.00	→	1.00	1.00	→	1.51	→	→	→	
	f_θ, cps	14.83	19.53	↓	↓	11.46	↓	11.65	11.46	↓	14.86	↓	↓	↓	
	f_ψ, cps	12.41	16.03	↓	↓	12.00	↓	12.80	12.00	↓	12.41	↓	↓	↓	
	g_θ	.015	.021	↓	↓	.020	↓	.015	.020	↓	.015	↓	↓	↓	
	g_ψ	.009	.012	↓	↓	.014	↓	.011	.014	↓	.010	↓	↓	↓	

[a]Symbols indicating flight conditions: level, *L*; diving, *D*; rolling, *R*; climbing, *C*.

TABLE I.- TEST DATA - Continued

Data point		1199	1232	1215	1225	1265	1252	451	462	468	481	492	498	505	477
Power plant autoprecessing		None	3, 4	→	→	1, 4	→	None	2	→	→	→	→	→	→
q, lb/sq ft		114.0	66.6	88.1	116.2	128.0	79.1	104.5	112.6	112.0	90.3	87.7	82.1	88.1	117.5
M		.27	.21	.24	.27	.29	.23	.26	.27	.27	.24	.24	.23	.24	.28
V, ft/sec		310	237	273	311	329	258	297	308	308	275	272	264	272	314
ρ, slugs/cu ft		2,372 $\times 10^{-6}$	2,371 $\times 10^{-6}$	2,362 $\times 10^{-6}$	2,396 $\times 10^{-6}$	2,371 $\times 10^{-6}$	2,369 $\times 10^{-6}$	2,372 $\times 10^{-6}$	2,370 $\times 10^{-6}$	2,369 $\times 10^{-6}$	2,388 $\times 10^{-6}$	2,371 $\times 10^{-6}$	2,365 $\times 10^{-6}$	2,378 $\times 10^{-6}$	2,381 $\times 10^{-6}$
Fuel load[a], percent		64L	→	→	→	→	→	→	→	→	→	→	→	→	→
f_a, cps		-----	9.49	10.16	10.70	8.99	8.00	-----	12.29	12.38	11.78	11.78	11.56	10.95	10.41
Power plant 1	β, deg	45	34	45	55	52	36	52	→	→	→	49.5	48	→	52
	N, rpm	4,200	4,890	3,810	2,850	3,510	4,950	-----	-----	-----	-----	-----	-----	-----	-----
	S_θ, in-lb/radian	9,291	→	→	→	6,553	→	9,291	→	→	→	→	→	→	→
	S_ψ, in-lb/radian	6,112	→	→	→	4,342	→	6,112	→	→	→	→	→	→	→
	S_{rms}, in-lb/radian	7,864	→	→	→	5,558	→	7,864	→	→	→	→	→	→	→
	S_θ/S_ψ	1.52	→	→	→	1.51	→	1.52	→	→	→	→	→	→	→
	f_θ, cps	19.27	19.30	→	→	14.86	→	19.30	→	→	→	→	→	→	→
	f_ψ, cps	14.70	14.51	→	→	12.13	→	13.91	→	→	→	→	→	→	→
	g_θ	.023	.029	→	→	.020	→	.016	→	→	→	→	→	→	→
	g_ψ	.046	.043	→	→	.015	→	.029	→	→	→	→	→	→	→
Power plant 2	β, deg	45	34	45	55	52	36	52	→	→	43	→	40	38.5	37
	N, rpm	4,200	4,830	3,780	2,820	3,420	4,860	3,120	3,210	3,210	4,020	4,020	4,290	4,740	5,610
	S_θ, in-lb/radian	9,144	→	→	→	→	→	9,242	→	→	→	→	→	→	→
	S_ψ, in-lb/radian	6,161	→	→	→	→	→	6,161	→	→	→	→	→	→	→
	S_{rms}, in-lb/radian	7,797	→	→	→	→	→	7,854	→	→	→	→	→	→	→
	S_θ/S_ψ	1.48	→	→	→	→	→	1.50	→	→	→	→	→	→	→
	f_θ, cps	21.05	→	→	→	→	→	18.57	→	→	→	→	→	→	→
	f_ψ, cps	17.43	→	→	→	→	→	15.34	→	→	→	→	→	→	→
	g_θ	.036	→	→	→	→	→	.016	→	→	→	→	→	→	→
	g_ψ	.064	→	→	→	→	→	.009	→	→	→	→	→	→	→
Power plant 3	β, deg	85	34	45	55	52	36	52	→	→	→	49.5	48	→	52
	N, rpm	-----	4,800	3,720	2,880	3,420	4,860	-----	-----	-----	-----	-----	-----	-----	-----
	S_θ, in-lb/radian	6,553	→	→	→	9,144	→	9,340	→	→	→	→	→	→	→
	S_ψ, in-lb/radian	4,342	→	→	→	6,259	→	6,210	→	→	→	→	→	→	→
	S_{rms}, in-lb/radian	5,558	→	→	→	7,836	→	7,931	→	→	→	→	→	→	→
	S_θ/S_ψ	1.51	→	→	→	1.46	→	1.51	→	→	→	→	→	→	→
	f_θ, cps	15.62	16.13	→	→	20.19	→	19.15	→	→	→	→	→	→	→
	f_ψ, cps	13.30	13.81	→	→	16.32	→	15.75	→	→	→	→	→	→	→
	g_θ	.013	.025	→	→	.012	→	.021	→	→	→	→	→	→	→
	g_ψ	.008	.040	→	→	.010	→	.020	→	→	→	→	→	→	→
Power plant 4	β, deg	45	34	45	55	52	36	37	52	→	→	49.5	48	→	52
	N, rpm	4,200	4,830	3,750	2,910	3,450	4,860	5,340	3,270	3,270	2,940	3,180	3,240	3,300	3,330
	S_θ, in-lb/radian	6,553	→	→	→	→	→	9,095	→	→	→	→	→	→	→
	S_ψ, in-lb/radian	4,352	→	→	→	→	→	6,064	→	→	→	→	→	→	→
	S_{rms}, in-lb/radian	5,562	→	→	→	→	→	7,730	→	→	→	→	→	→	→
	S_θ/S_ψ	1.51	→	→	→	→	→	1.50	→	→	→	→	→	→	→
	f_θ, cps	14.86	15.43	→	→	→	→	18.07	→	→	→	→	→	→	→
	f_ψ, cps	12.41	13.27	→	→	→	→	14.99	→	→	→	→	→	→	→
	g_θ	.015	.023	→	→	→	→	.023	→	→	→	→	→	→	→
	g_ψ	.010	.036	→	→	→	→	.009	→	→	→	→	→	→	→

[a]Symbols indicating flight conditions: level, L; diving, D; rolling, R; climbing, C.

TABLE I.- TEST DATA - Concluded

Data point		1287	1314	1281	1295	1305	1515	1430	1496	1502	747
Power plant autoprecessing .		None	3	None	→	3	None	2, 3	None	2, 3	None
q, lb/sq ft		110.7	133.3	107.8	105.5	105.1	123.5	93.4	74.9	68.4	112.5
M		.27	.29	.26	.26	.26	.28	.25	.22	.21	.27
V, ft/sec		306	336	301	298	298	323	281	252	241	308
ρ, slugs/cu ft		2,369 $\times 10^{-6}$	2,367 $\times 10^{-6}$	2,375 $\times 10^{-6}$	2,378 $\times 10^{-6}$	2,369 $\times 10^{-6}$	2,371 $\times 10^{-6}$	2,371 $\times 10^{-6}$	2,366 $\times 10^{-6}$	2,366 $\times 10^{-6}$	2,368 $\times 10^{-6}$
Fuel load[a], percent		64L	→								→
f_a, cps		-----	12.00	-----	-----	11.49	-----	11.56	-----	10.54	-----
Power plant 1	β, deg	48	→	45	48	40	54	40	37	30	52
	N, rpm	3,720	4,110	4,170	3,660	4,920	3,120	4,620	4,560	5,730	-----
	S_θ, $\frac{\text{in-lb}}{\text{radian}}$	9,242					9,242	9,242			9,291
	S_ψ, $\frac{\text{in-lb}}{\text{radian}}$	6,161					6,259	6,161			6,112
	S_{rms}, $\frac{\text{in-lb}}{\text{radian}}$ . . .	7,854					7,893	7,854			7,864
	S_θ/S_ψ	1.50				→	1.48	1.50			1.52
	f_θ, cps	18.64					18.86				20.51
	f_ψ, cps	15.53					15.81				15.21
	g_θ	.034					.027				.042
	g_ψ	.055					.022				-----
Power plant 2	β, deg	48	→	45	48	40	54	40	37	30	52
	N, rpm	3,720	4,080	4,140	3,630	4,860	3,090	4,680	4,470	5,730	3,150
	S_θ, $\frac{\text{in-lb}}{\text{radian}}$	9,144									9,242
	S_ψ, $\frac{\text{in-lb}}{\text{radian}}$	6,161									6,161
	S_{rms}, $\frac{\text{in-lb}}{\text{radian}}$ . . .	7,797									7,854
	S_θ/S_ψ	1.48									1.50
	f_θ, cps	21.05					18.00				19.97
	f_ψ, cps	17.43					14.99				17.56
	g_θ	.036				→	.016			→	.034
	g_ψ	.064					.013				.054
Power plant 3	β, deg	48	→	45	40	→	54	40	34	30	52
	N, rpm	3,690	4,020	4,080	4,740	4,830	3,090	4,560	4,500	5,730	-----
	S_θ, $\frac{\text{in-lb}}{\text{radian}}$	9,144									9,340
	S_ψ, $\frac{\text{in-lb}}{\text{radian}}$	6,259									6,210
	S_{rms}, $\frac{\text{in-lb}}{\text{radian}}$ . . .	7,836									7,931
	S_θ/S_ψ	1.46									1.51
	f_θ, cps	20.26						20.00			20.03
	f_ψ, cps	16.38						16.19			18.16
	g_θ	.012						.015			.034
	g_ψ	.010						.011			.040
Power plant 4	β, deg	48	→	45	48	40	54	40	37	30	52
	N, rpm	3,720	4,080	4,140	3,630	4,860	3,120	4,650	4,470	5,640	3,210
	S_θ, $\frac{\text{in-lb}}{\text{radian}}$	9,242					8,998	9,242	8,998		118,534
	S_ψ, $\frac{\text{in-lb}}{\text{radian}}$	6,259					6,112	6,259	6,112		83,912
	S_{rms}, $\frac{\text{in-lb}}{\text{radian}}$ . . .	7,893					7,691	7,893	7,691		102,693
	S_θ/S_ψ	1.47				→	1.47	1.48	1.47	→	1.40
	f_θ, cps	19.78					-----	19.37	-----		19.59
	f_ψ, cps	15.56					-----	14.61	-----		16.64
	g_θ	.016					-----	.043	-----		.044
	g_ψ	.011					-----	.038	-----		.040

[a]Symbols indicating flight conditions: level, L; diving, D; rolling, R; climbing, C.

TABLE II.- WING-SEGMENT WEIGHT, INERTIA, AND BALANCE DATA

[Zero-fuel-loading condition]

Wing station, in.	Weight, lb	Moment of inertia about wing-beam center line, lb-in.^{2}	Unbalance about wing-beam center line, in-lb
Left wing			
8.169 to 13.245	2.021	101.8	-2.12
13.245 to 18.321	1.391	52.9	1.07
18.321 to 23.397	1.852	77.28	.726
23.397 to 28.473	1.579	58.24	-.471
28.473 to 33.549	1.272	43.05	-1.10
33.549 to 38.625	1.047	34.57	-.639
38.625 to 44.875	1.123	34.03	1.03
44.875 to 51.315	1.350	35.17	0
51.315 to 56.391	.735	10.80	-.603
56.391 to 61.467	.594	8.11	-.542
61.467 to 66.543	.526	6.45	-.582
66.543 to 71.619	.451	4.75	-1.126
71.619 to 74.25	.223	2.02	-.264
Right wing			
8.169 to 13.245	2.007	104.22	-2.1
13.245 to 18.321	1.386	57.17	.547
18.321 to 23.397	1.835	87.21	1.407
23.397 to 28.473	1.571	58.24	-.326
28.473 to 33.549	1.281	43.43	-1.22
33.549 to 38.625	1.041	33.09	-.79
38.625 to 44.875	1.128	31.60	0
44.875 to 51.315	1.297	35.77	-.238
51.315 to 56.391	.706	11.70	-1.48
56.391 to 61.467	.604	8.38	-.76
61.467 to 66.543	.634	6.66	-1.21
66.543 to 71.619	.441	4.03	-.94
71.619 to 74.25	.227	1.96	-.23

TABLE III.- SIMULATED FUEL WEIGHT AND INERTIA DATA

Wing station, in.	Weight forward of wing-beam center line, lb	Distance c.g. of weight forward of wing-beam center line, in.	Weight rearward of wing-beam center line, lb	Distance c.g. of weight rearward of wing-beam center line, in.	Moment of inertia about wing-beam center line, lb-in.^{2}	Total weight, lb
Simulated 100-percent, level-flight fuel loading						
10.71	3.98	3.98	3.98	3.98	133.8	7.96
13.25	2.96	3.81	2.96	3.81	91.0	5.92
15.78	2.54	3.67	2.54	3.67	72.6	5.08
18.32	2.26	3.53	2.26	3.53	59.6	4.52
21.41	3.42	3.35	3.42	3.35	79.0	6.64
25.70	2.91	3.14	2.91	3.14	60.7	5.82
28.47	1.49	2.98	1.49	2.98	28.1	2.98
31.01	1.67	2.86	1.67	2.86	28.9	3.34
33.55	1.58	2.73	1.58	2.73	25.0	3.16
36.09	1.48	2.60	1.48	2.60	21.3	2.96
38.62	1.35	2.47	1.35	2.47	17.4	2.70
41.10	1.20	2.33	1.20	2.33	13.8	2.40
43.38	1.16	2.17	1.16	2.17	11.8	2.32
46.41	.94	1.99	.94	1.99	8.2	1.88
48.80	1.03	1.93	1.03	1.93	8.1	2.06
51.32	.85	1.86	.85	1.86	6.2	1.70
53.85	.78	1.80	.78	1.80	5.3	1.56
56.39	.69	1.74	.69	1.74	4.5	1.38
58.93	.62	1.72	.62	1.72	3.9	1.24
61.47	.54	1.70	.54	1.70	3.3	1.08
64.01	.49	1.71	.49	1.71	3.0	.98
66.54	.44	1.71	.44	1.71	2.7	.88
70.80	.64	1.70	.64	1.70	3.9	1.28
Simulated 64-percent, level-flight fuel loading						
10.71	3.52	4.25	3.52	4.25	134.6	7.04
13.25	1.93	4.06	1.93	4.06	67.4	3.86
15.78	1.59	3.93	1.59	3.93	51.6	3.18
18.32	1.18	3.76	1.18	3.76	35.4	2.36
21.41	1.38	3.57	1.38	3.57	37.4	2.76
25.70	.44	3.35	.44	3.35	10.5	.88
28.47	1.49	2.98	1.49	2.98	28.1	2.98
31.01	1.67	2.86	1.67	2.86	28.9	3.34
33.55	1.58	2.73	1.58	2.73	25.0	3.16
36.09	1.45	2.60	1.45	2.60	20.8	2.90
38.62	1.30	2.47	1.30	2.47	16.8	2.60
41.10	1.06	2.33	1.06	2.33	12.2	2.12
43.38	1.03	2.19	1.03	2.19	10.4	2.06
46.41	.89	2.03	.89	2.03	7.8	1.78
48.80	.68	1.93	.68	1.93	5.4	1.36
51.32	.52	1.85	.52	1.85	3.8	1.04
53.85	.37	1.80	.37	1.80	2.5	.74
56.39	.29	1.74	.29	1.74	1.9	.58
Simulated 32-percent, level-flight fuel loading						
10.71	2.64	4.04	2.64	4.04	91.4	5.28
13.25	1.32	3.87	1.32	3.87	41.8	2.64
15.78	.98	3.73	.98	3.73	28.9	1.96
18.32	.66	3.58	.66	3.58	17.9	1.32
28.47	.94	3.07	.94	3.07	18.8	1.88
31.01	1.00	2.94	1.00	2.94	18.4	2.00
33.55	.89	2.81	.89	2.81	14.9	1.78
36.09	.76	2.68	.76	2.68	11.6	1.52
38.62	.64	2.54	.64	2.54	8.8	1.28
41.10	.59	2.40	.59	2.40	6.0	1.18
43.38	.42	2.25	.42	2.25	4.5	.84
46.41	.30	2.09	.30	2.09	2.8	.60
48.80	.18	1.99	.18	1.99	1.5	.36

TABLE III.- SIMULATED FUEL WEIGHT AND INERTIA DATA - Concluded

Wing station, in.	Weight forward of wing-beam center line, lb	Distance c.g. of weight forward of wing-beam center line, in.	Weight rearward of wing-beam center line, lb	Distance c.g. of weight rearward of wing-beam center line, in.	Moment of inertia about wing-beam center line, lb-in.^{2}	Total weight, lb
Simulated 64-percent, climb fuel loading						
10.71	0	0	3.98	3.98	66.9	3.98
13.25	2.96	3.81	2.96	3.81	91.0	5.92
15.78	0	0	2.54	3.67	36.3	2.54
18.32	2.26	3.53	2.26	3.53	59.6	4.52
21.41	1.38	3.35	3.42	3.35	58.2	4.80
25.70	.44	3.14	2.91	3.14	35.6	3.35
28.47	0	0	1.49	2.98	14.1	1.49
31.01	1.67	2.86	1.67	2.86	28.9	3.34
33.55	0	0	1.58	2.73	12.5	1.58
36.09	1.48	2.60	1.48	2.60	21.3	2.96
38.62	0	0	1.35	2.47	8.7	1.35
41.10	1.20	2.33	1.20	2.33	13.8	2.40
43.38	0	0	1.16	2.17	5.9	1.16
46.41	.94	1.99	.94	1.99	8.2	1.88
48.80	0	0	1.03	1.93	4.1	1.03
51.32	0	0	.85	1.86	3.1	.85
53.85	0	0	.78	1.80	2.7	.78
56.39	0	0	.69	1.74	2.3	.69
58.93	0	0	.62	1.72	2.0	.62
Simulated 64-percent, rolling fuel loading						
10.71	0	0	0	0	0	0
13.25	2.96	3.81	2.96	3.81	91.0	5.92
15.78	2.54	3.67	2.54	3.67	72.6	5.08
18.32	2.26	3.53	2.26	3.53	59.6	4.52
21.41	1.38	3.35	1.38	3.35	0	2.76
25.70	2.91	3.14	2.91	3.14	60.7	5.82
28.47	0	0	0	0	0	0
31.01	0	0	0	0	0	0
33.55	0	0	0	0	0	0
36.09	0	0	0	0	0	0
38.62	1.35	2.47	1.35	2.47	17.4	2.70
41.10	1.20	2.33	1.20	2.33	13.8	2.40
43.38	1.16	2.17	1.16	2.17	11.8	2.32
46.41	.94	1.99	.94	1.99	8.2	1.88
48.80	1.03	1.93	1.03	1.93	8.1	2.06
51.32	.85	1.86	.85	1.86	6.2	1.70
53.85	.78	1.80	.78	1.80	5.3	1.56
56.39	.69	1.74	.69	1.74	4.5	1.38
58.93	.62	1.72	.62	1.72	3.9	1.24
61.47	.54	1.70	.54	1.70	3.3	1.08
64.01	.49	1.71	.49	1.71	3.0	.98
66.54	.44	1.71	.44	1.71	2.7	.88
70.80	.64	1.70	.64	1.70	3.9	1.28
Simulated 64-percent, dive fuel loading						
10.71	3.98	3.98	0	0	66.9	3.98
13.25	2.96	3.81	2.96	3.81	91.0	5.92
15.78	2.54	3.67	0	0	36.3	2.54
18.32	2.26	3.53	2.26	3.53	59.6	4.52
21.41	3.42	3.35	1.38	3.35	58.2	4.80
25.70	2.91	3.14	.44	3.14	35.6	3.35
28.47	1.49	2.98	0	0	14.1	1.49
31.01	1.67	2.86	1.67	2.86	28.9	3.34
33.55	1.58	2.73	0	0	12.5	1.58
36.09	1.48	2.60	1.48	2.60	21.3	2.96
38.62	1.35	2.47	0	0	8.7	1.35
41.10	1.20	2.33	1.20	2.33	13.8	2.40
43.38	1.16	2.17	0	0	5.9	1.16
46.41	.94	1.99	.94	1.99	8.2	1.88
48.80	1.03	1.93	0	0	4.1	1.03
51.32	.85	1.86	0	0	3.1	.85
53.85	.78	1.80	0	0	2.7	.78
56.39	.69	1.74	0	0	2.3	.69
58.93	.62	1.72	0	0	2.0	.62

TABLE IV.- FUSELAGE-SEGMENT WEIGHT AND CENTER-OF-GRAVITY LOCATION

Fuselage station, in.	Weight, lb	Fuselage station (c.g. location), in.
5.25 to 27.25	18.02	16.56
27.25 to 46.18	4.72	36.71
46.18 to 65.10	4.70	55.64
65.10 to 95.85	26.48	80.65
95.85 to 112.62	4.27	103.23
112.62 to 129.25	5.68	120.60
129.25 to 147.69	7.32	140.20
147.69 to 162.06	.93	152.15

TABLE V.- POWER-PLANT WEIGHTS AND CENTER-OF-GRAVITY LOCATIONS

	Power plant 1		Power plant 2		Power plant 3		Power plant 4	
	Weight, lb	Fuselage station (c.g. location), in.	Weight, lb	Fuselage station (c.g. location), in.	Weight, lb	Fuselage station (c.g. location), in.	Weight, lb	Fuselage station (c.g. location), in.
Nacelle and bracket	1.66	69.82	2.63	71.02	2.05	71.41	1.61	70.19
Motor mount beam	1.87	69.40	3.08	69.74	3.17	70.17	1.90	69.42
Sliding clamp	.31	65.22	.31	64.11	.31	64.11	.31	65.22
Bolts	.08	77.00	.08	76.00	.08	76.00	.08	77.00
Landing gear			2.41	72.60	2.90	71.70		
Propeller	3.18	53.85	3.18	52.74	3.18	52.74	3.18	53.85
Gearbox and motor mass	6.52	61.70	6.71	61.20	6.71	61.20	6.52	61.70
Total	13.62	62.40	18.40	64.17	18.89	64.25	13.60	62.40

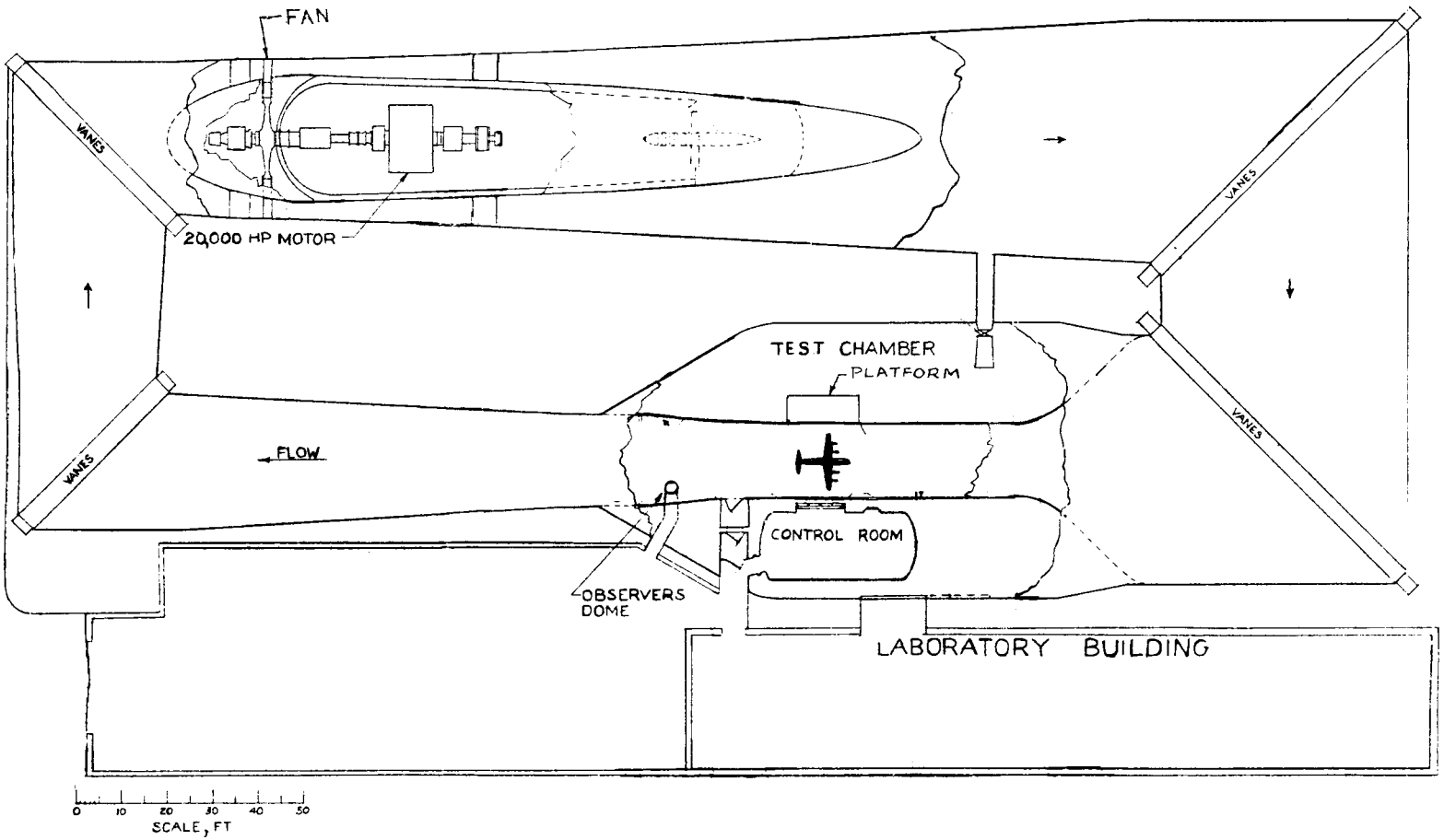

Figure 1.- General arrangement of Langley transonic dynamics tunnel.

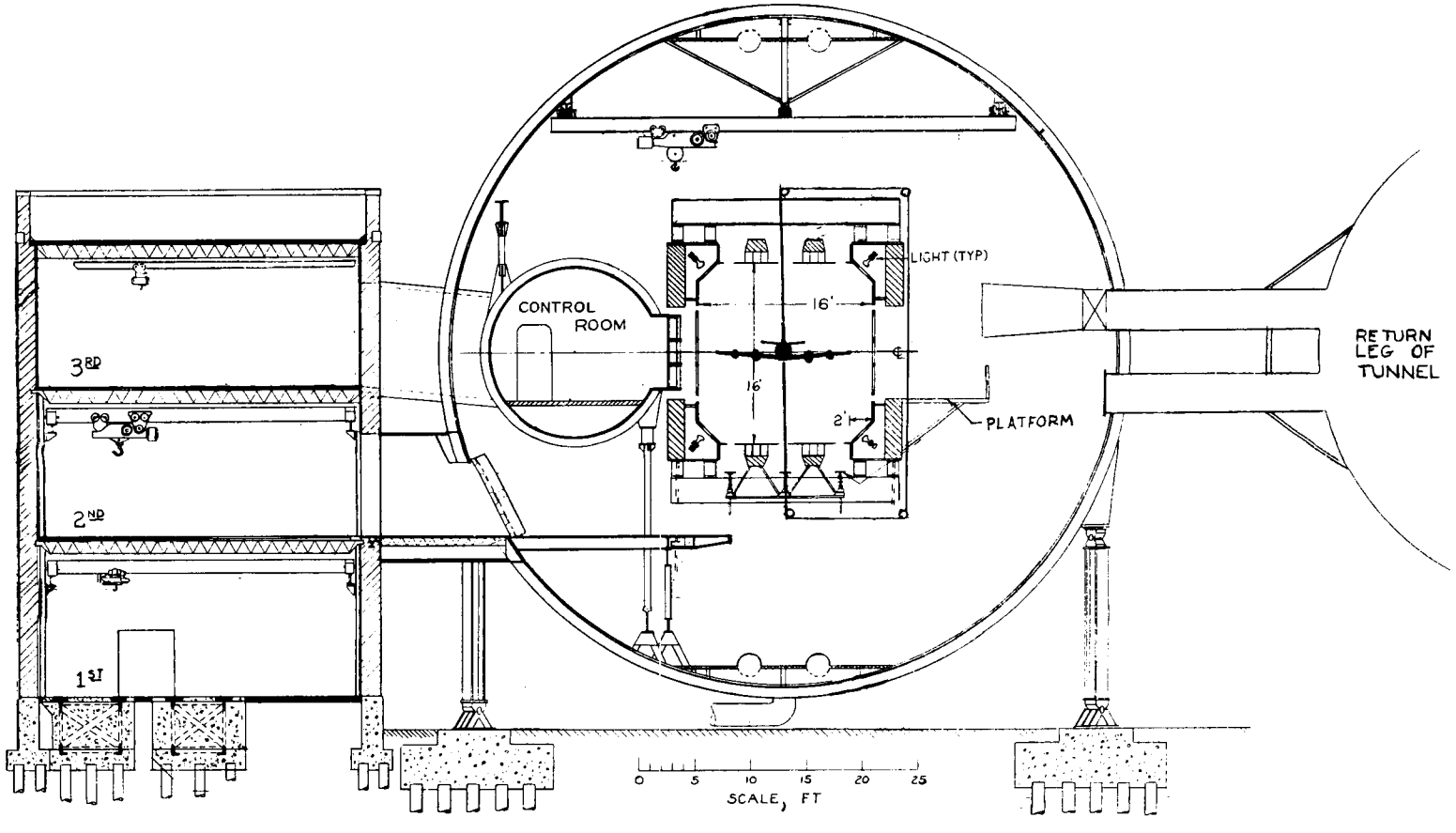

Figure 2.- Cross section through laboratory building, test chamber, control room, and test section of Langley transonic dynamics tunnel.

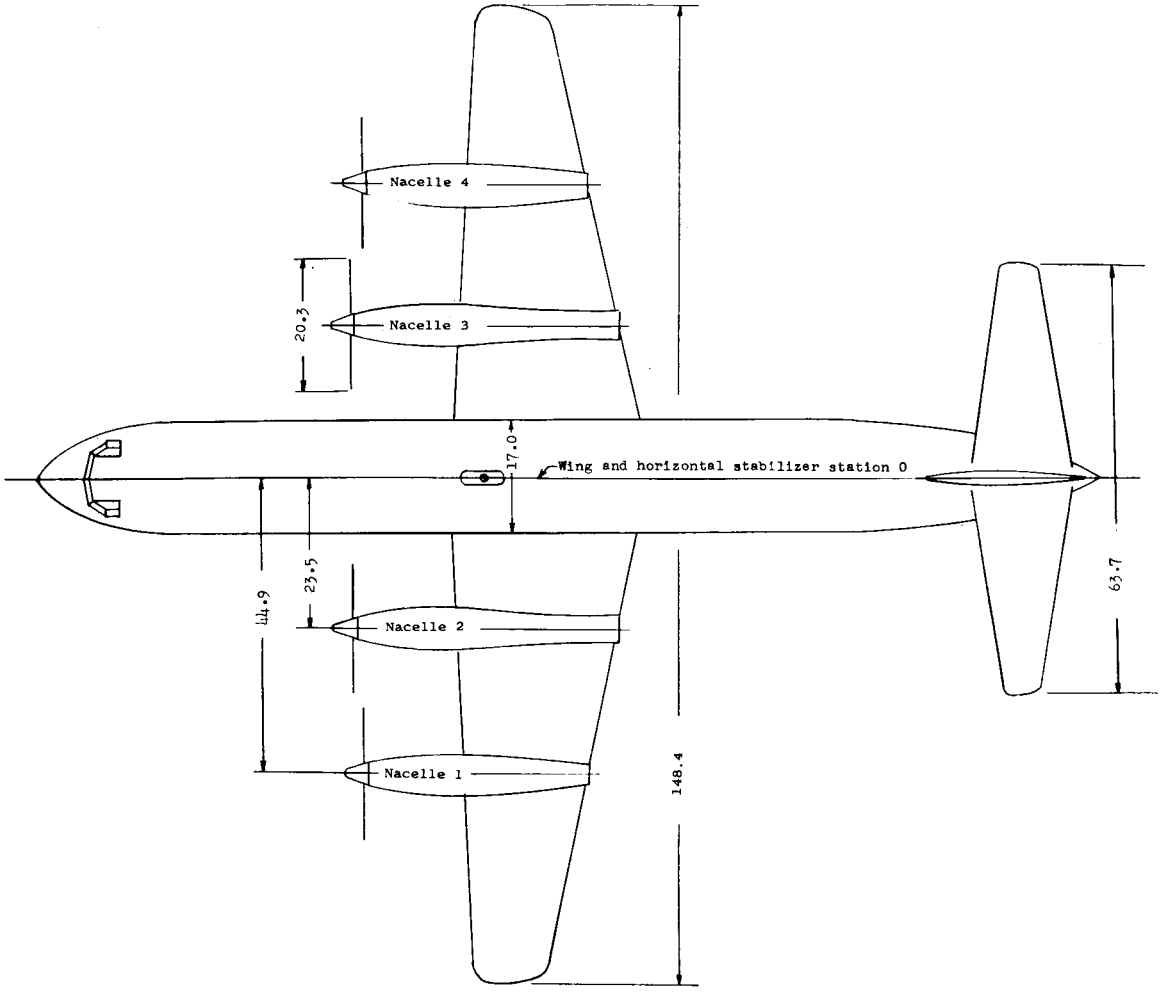

Wing area, sq ft	20.32
Wing mean aerodynamic chord, in.	21.09
Wing aspect ratio	7.5

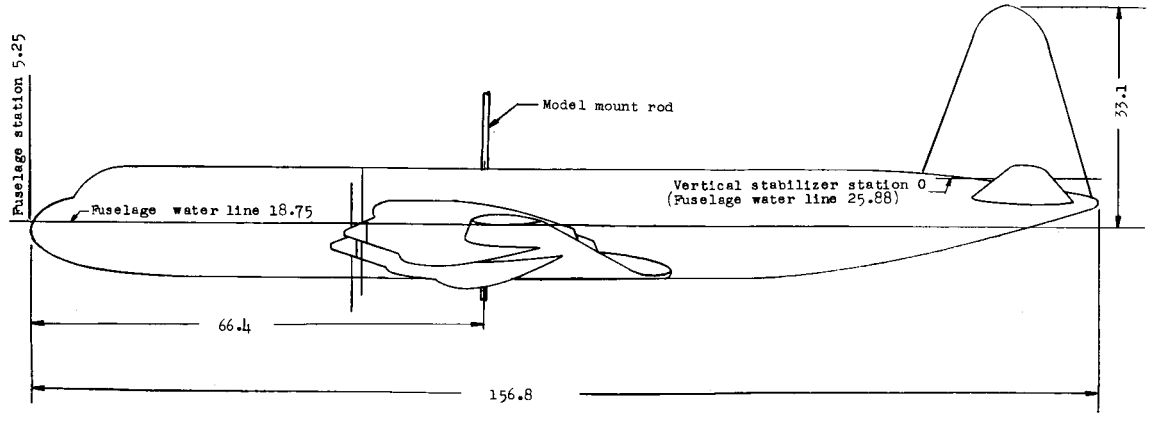

Figure 3.- Two-view drawing of model used in investigation. All dimensions are in inches.

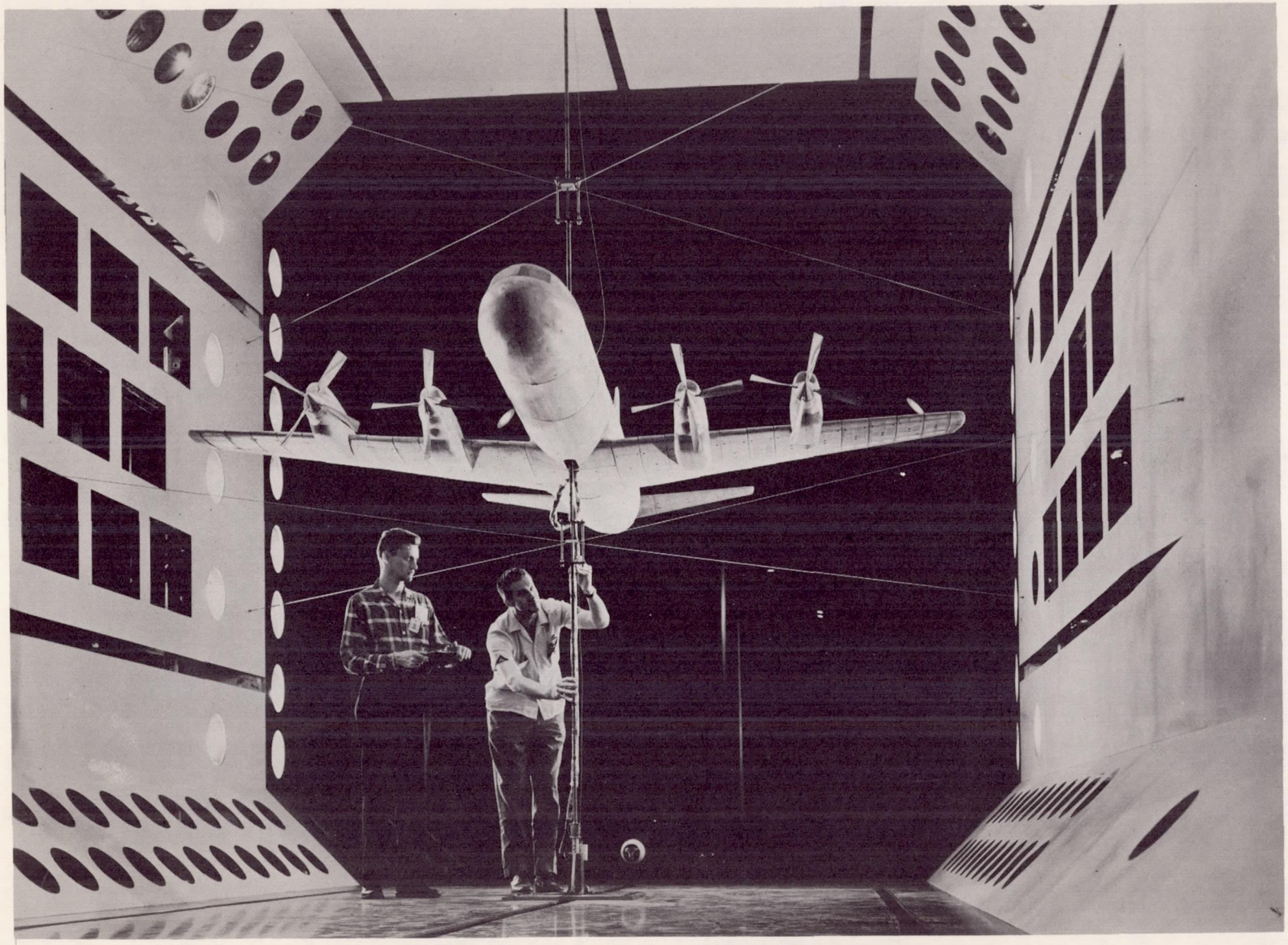

Figure 4.- Photograph of model mounted in test section of Langley transonic dynamics tunnel. L-60-2562

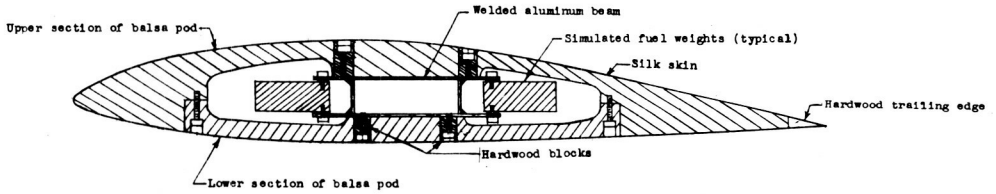

(a) Typical section through wing.

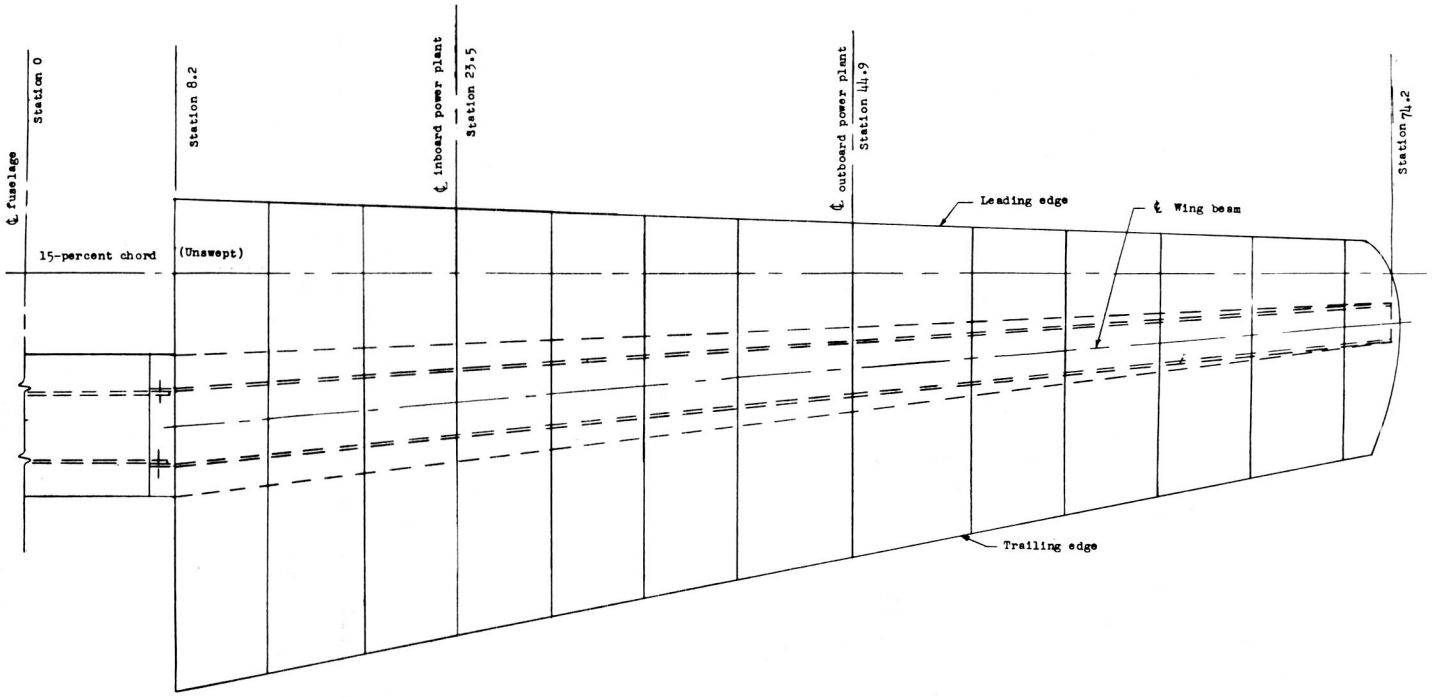

(b) Plan view.

Figure 5.- Diagram of wing showing location of spar and balsa pods. Wing stations in inches measured from center line of fuselage.

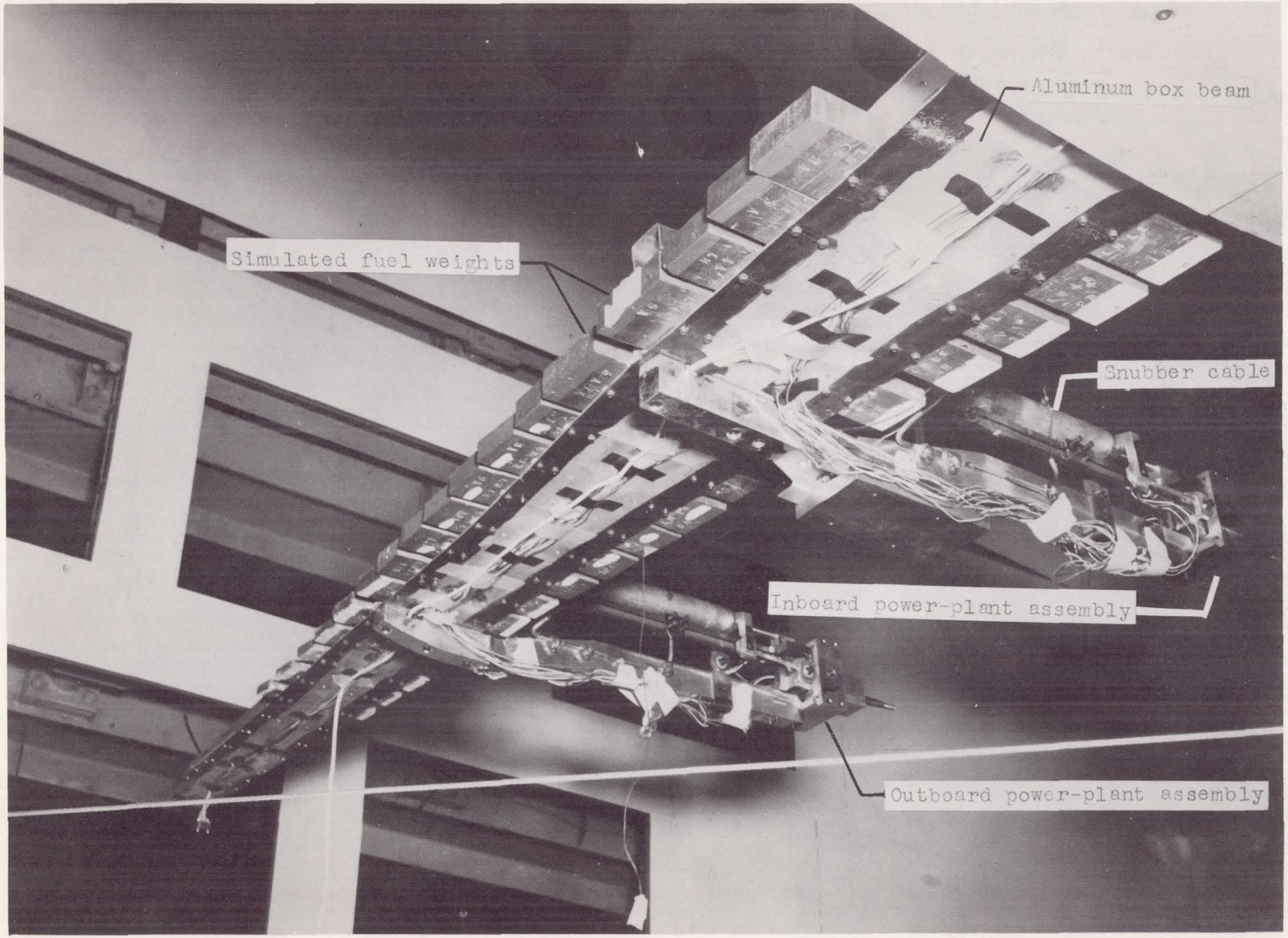

Figure 6.- Photograph of left wing with balsa pods removed. L-60-4776.1

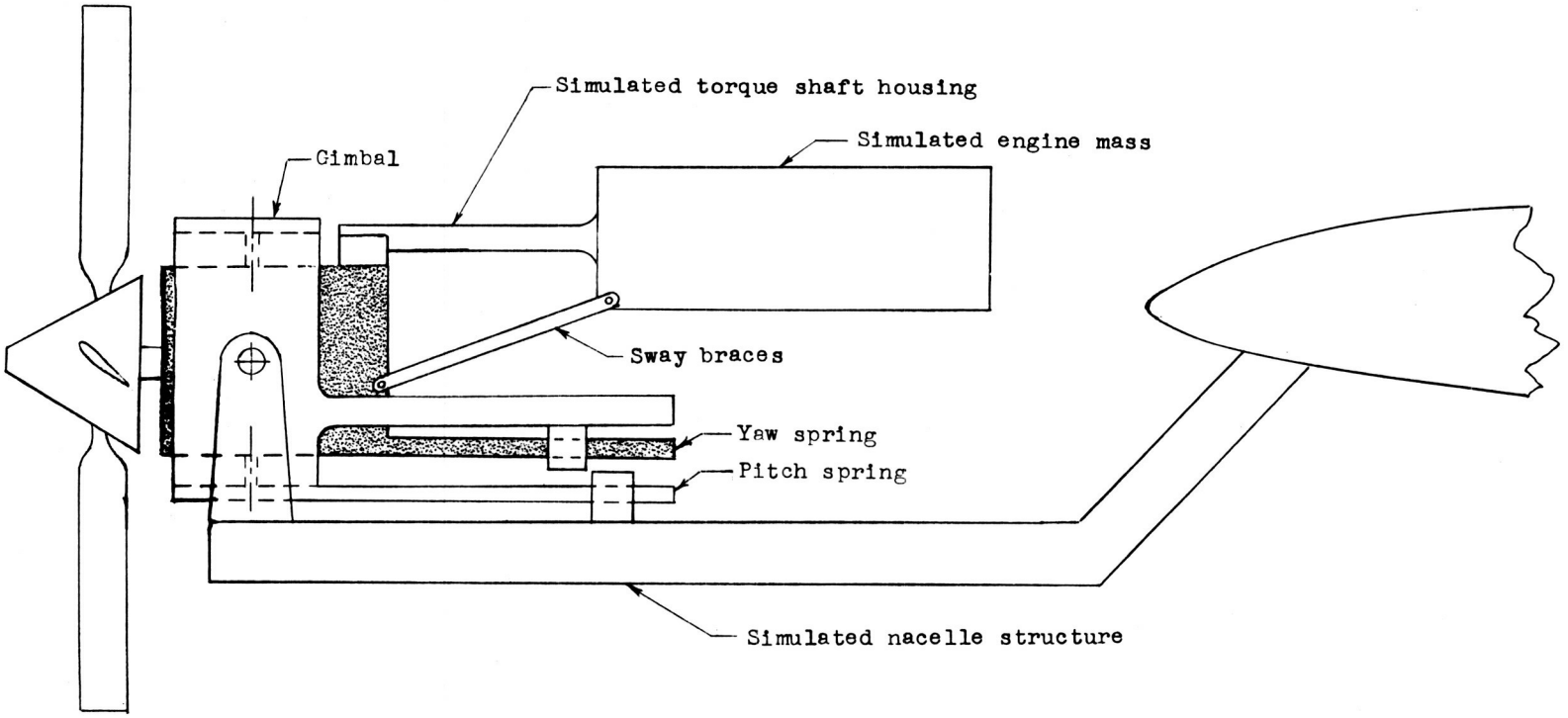

Figure 7.- Schematic representation of power-plant installation.

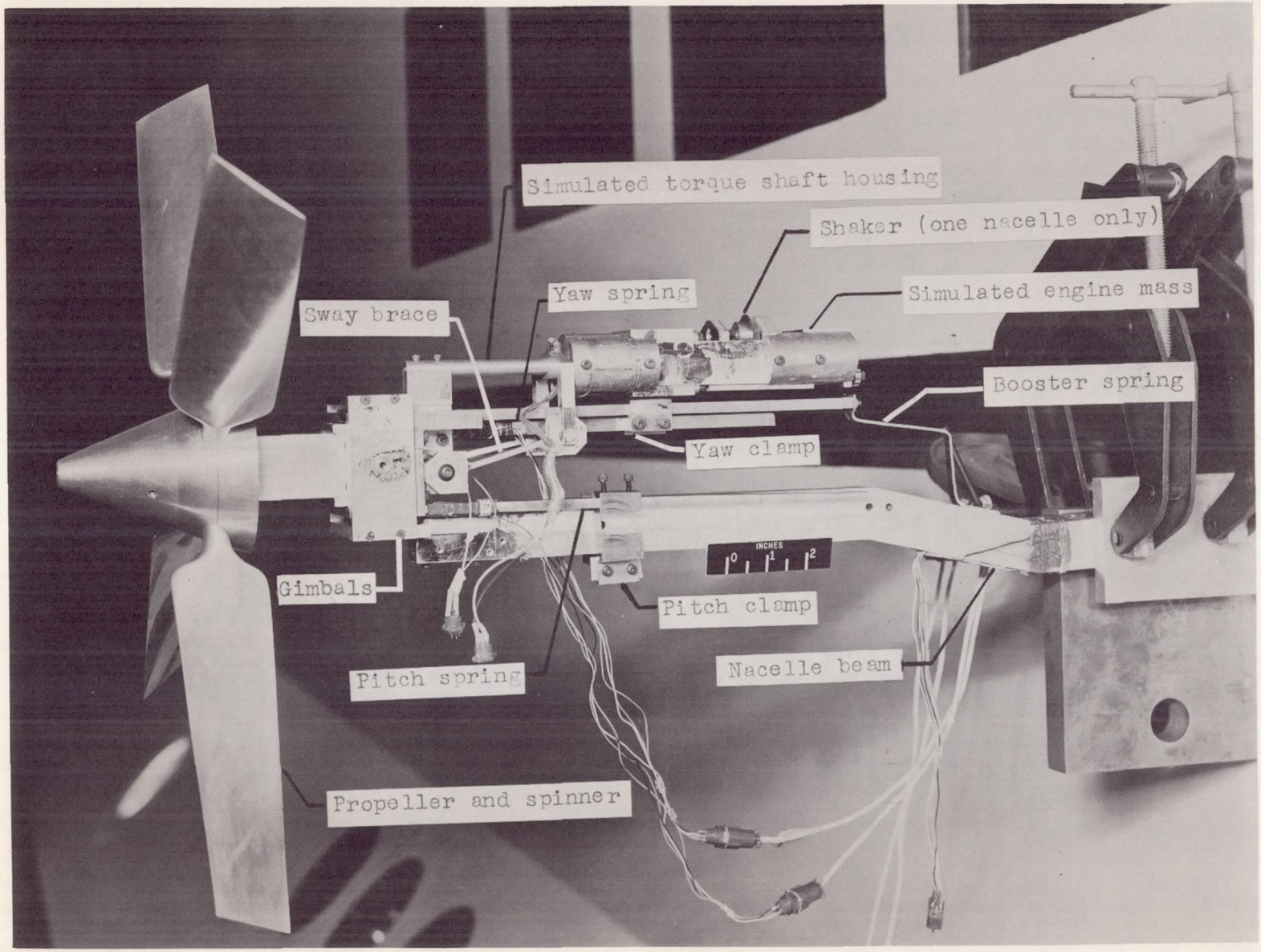

Figure 8.- Simulated-power-plant and propeller assembly. L-60-3977.1

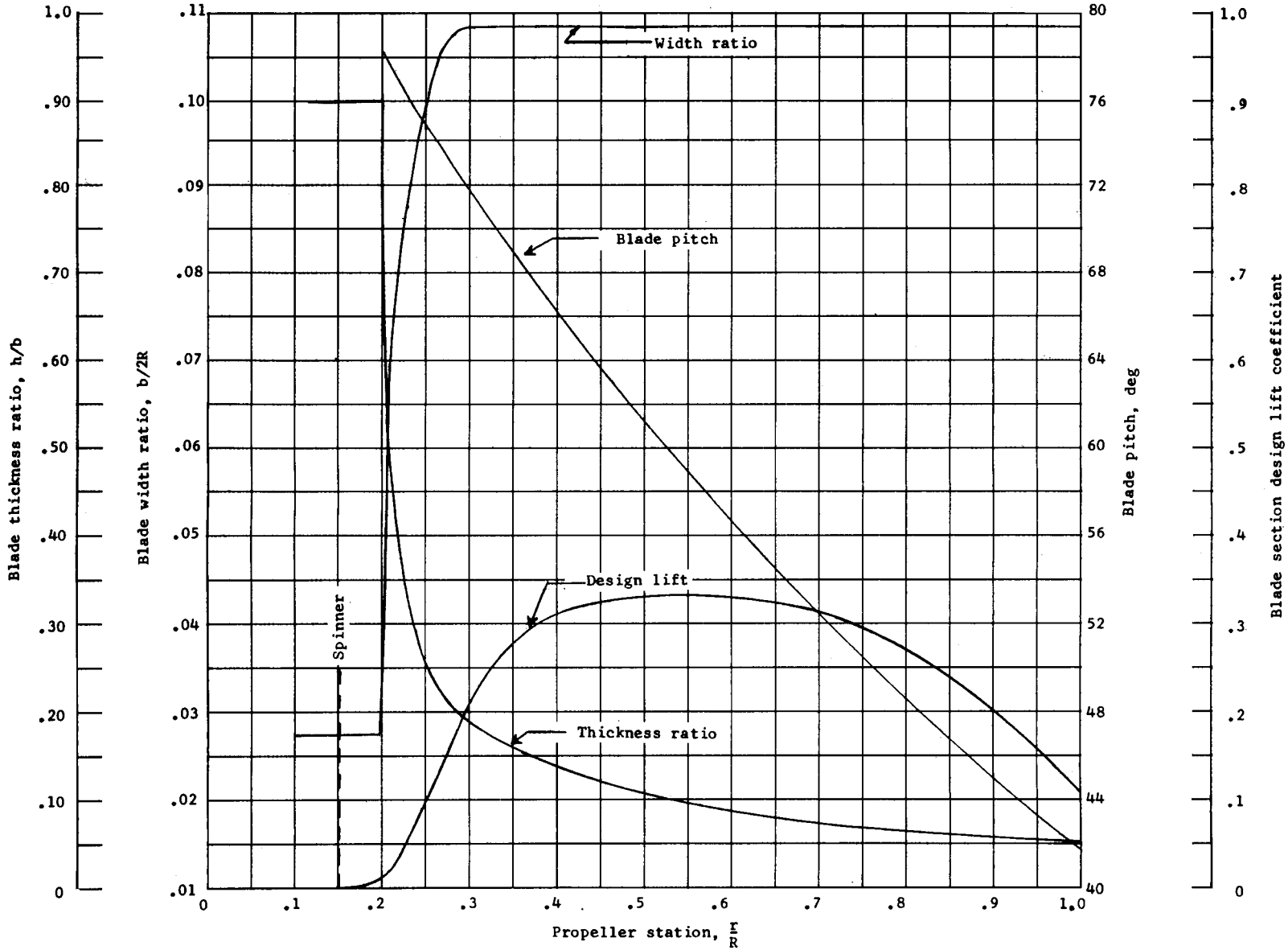

Figure 9.- Design characteristics of the NACA 16-series airfoil blades.

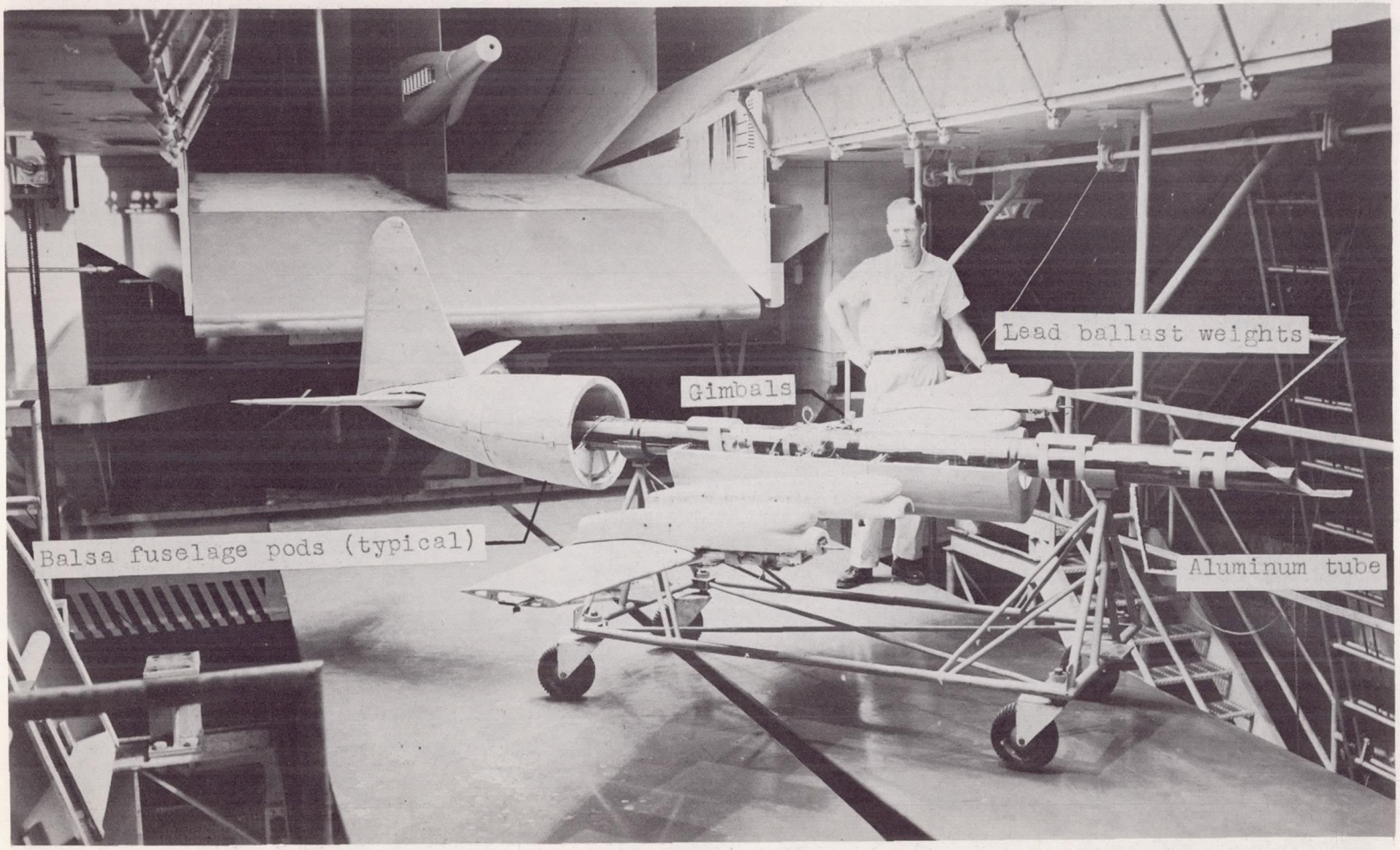

Figure 10.- Photograph of model with part of fuselage pods removed. L-60-3500.1

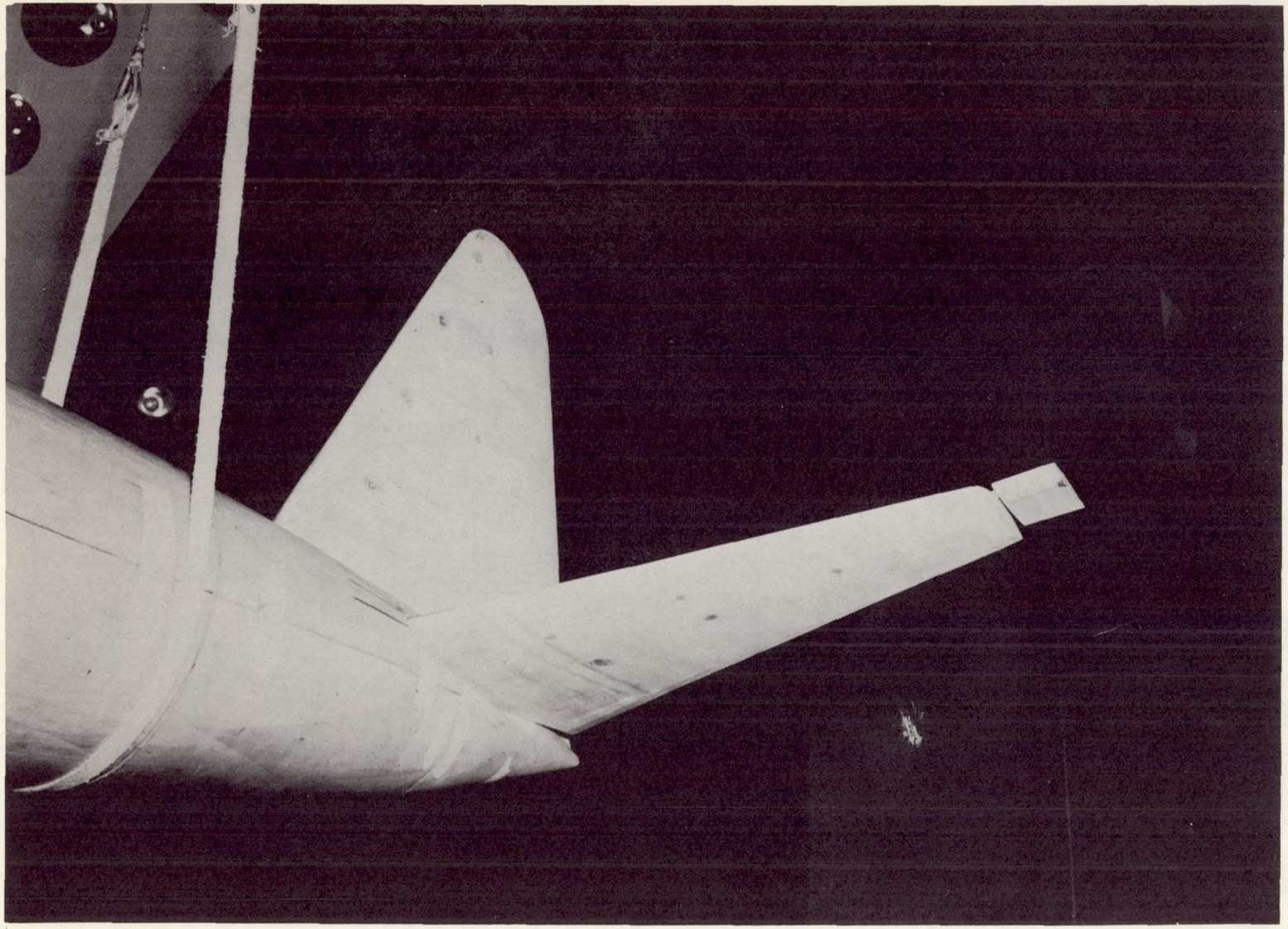

Figure 11.- Photograph of aerodynamic oscillator mounted on horizontal tail. L-60-4792

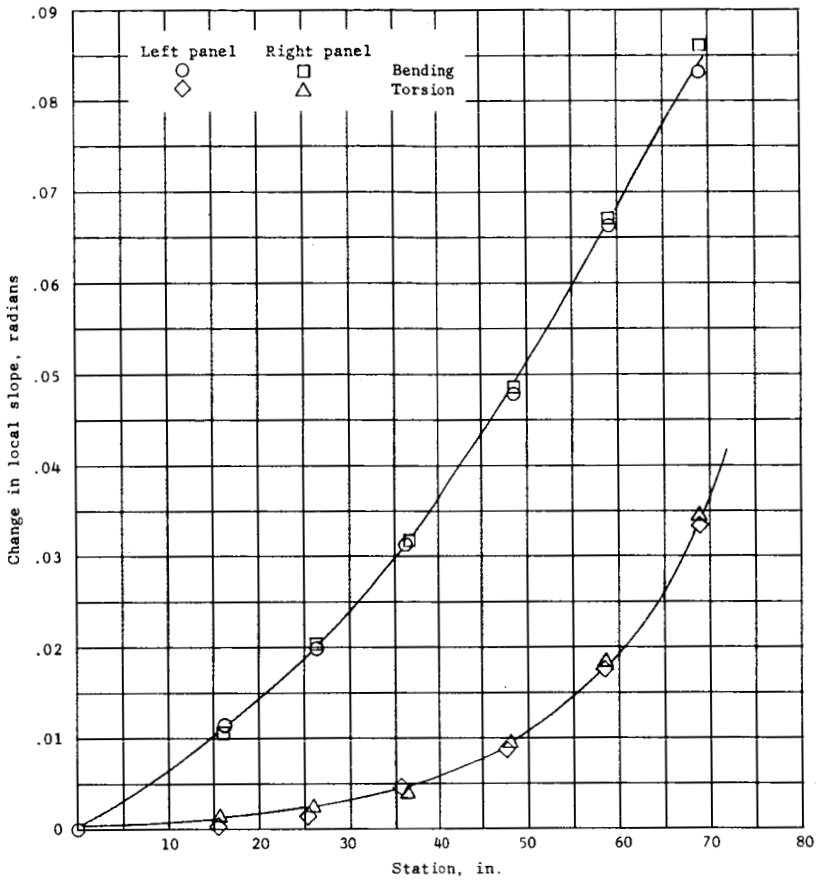

Figure 12.- Slopes of wing-deflection curves. Loaded at station 73.38; bending load, 50 pounds; torsion load, 250 in-lb.

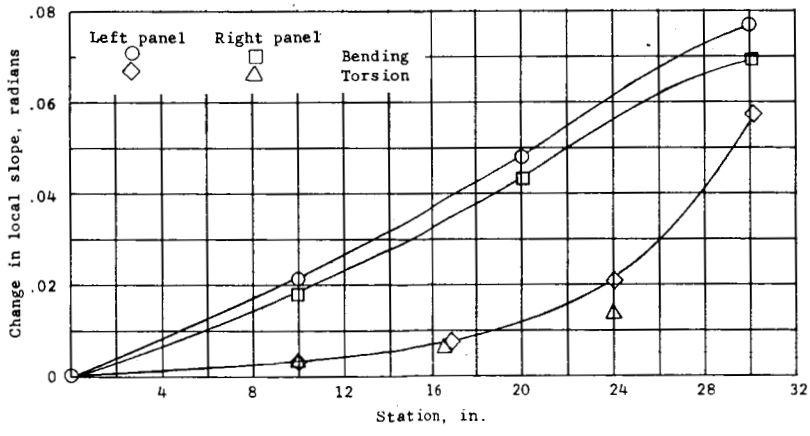

Figure 13.- Slopes of horizontal-stabilizer-deflection curves. Loaded at station 31.44; bending load, 25 pounds; torsion load, 100 in-lb.

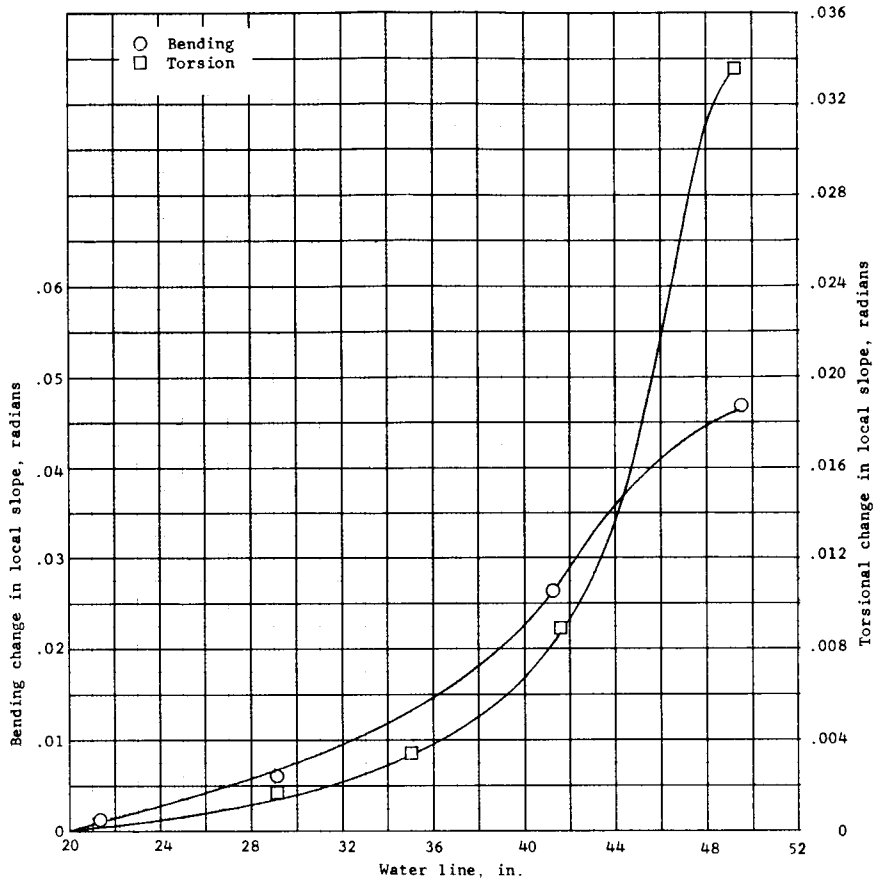

Figure 14.- Slopes of vertical-stabilizer-deflection curves. Loaded at station 50.52; bending load, 25 pounds; torsion load, 100 in-lb.

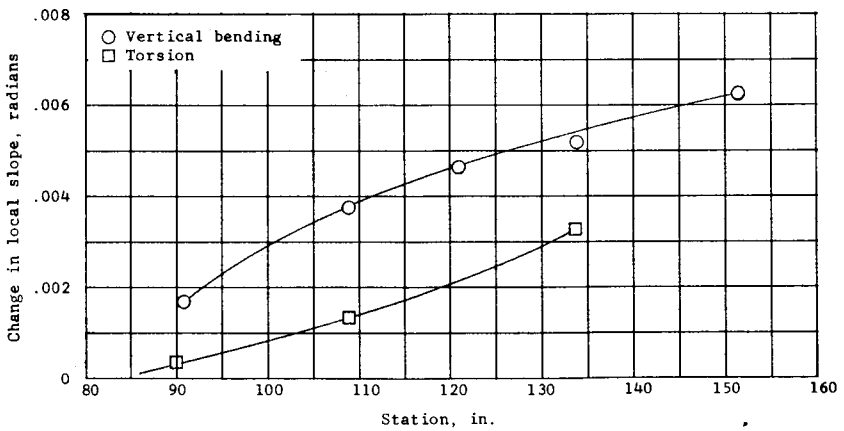

Figure 15.- Slopes of fuselage-deflection curves. Loaded at station 151.53; vertical bending load, 100 pounds; torsion load, 1,572 in-lb.

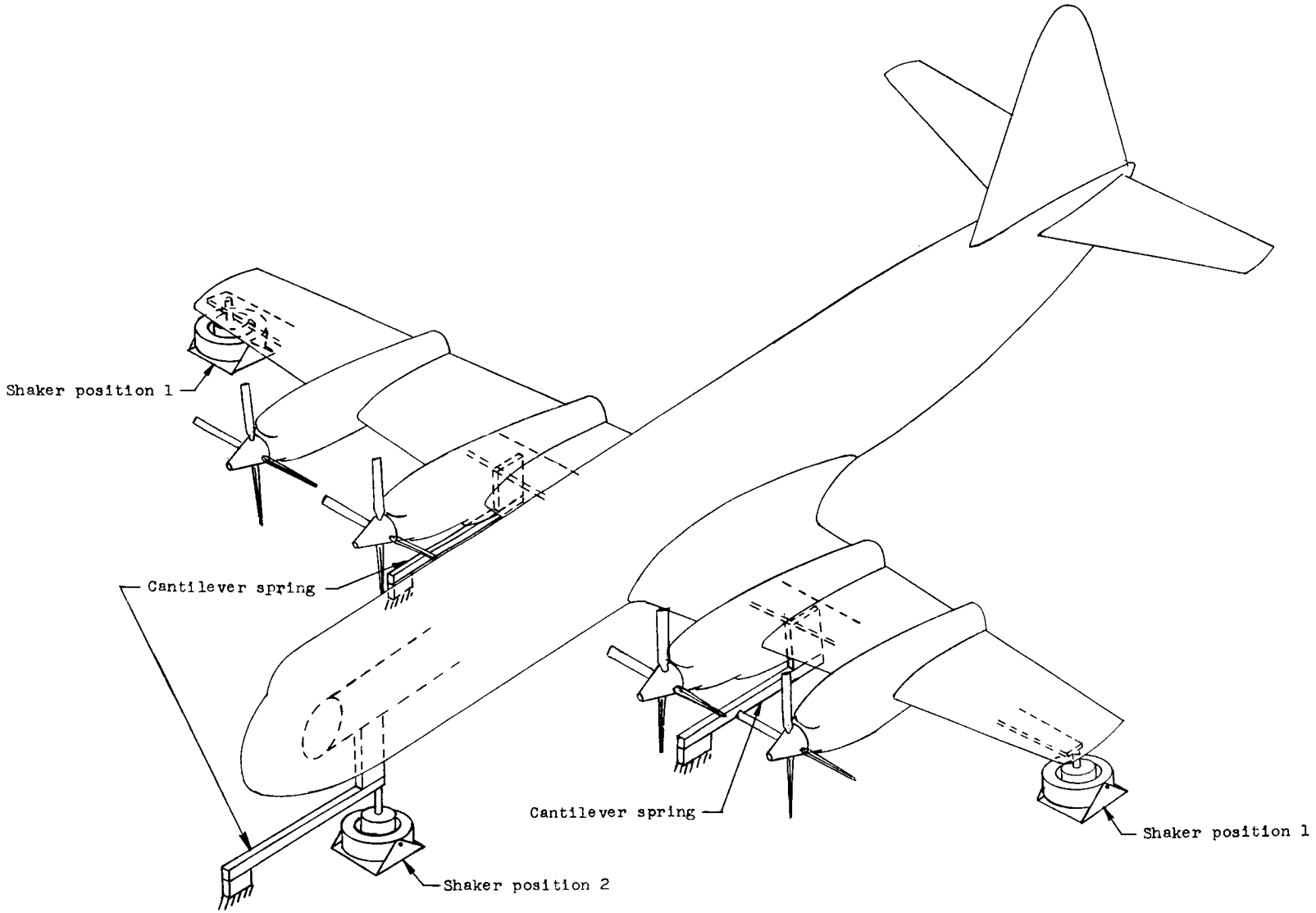

(a) Suspension configuration 1.

Figure 16.- Suspension configurations for shake tests.

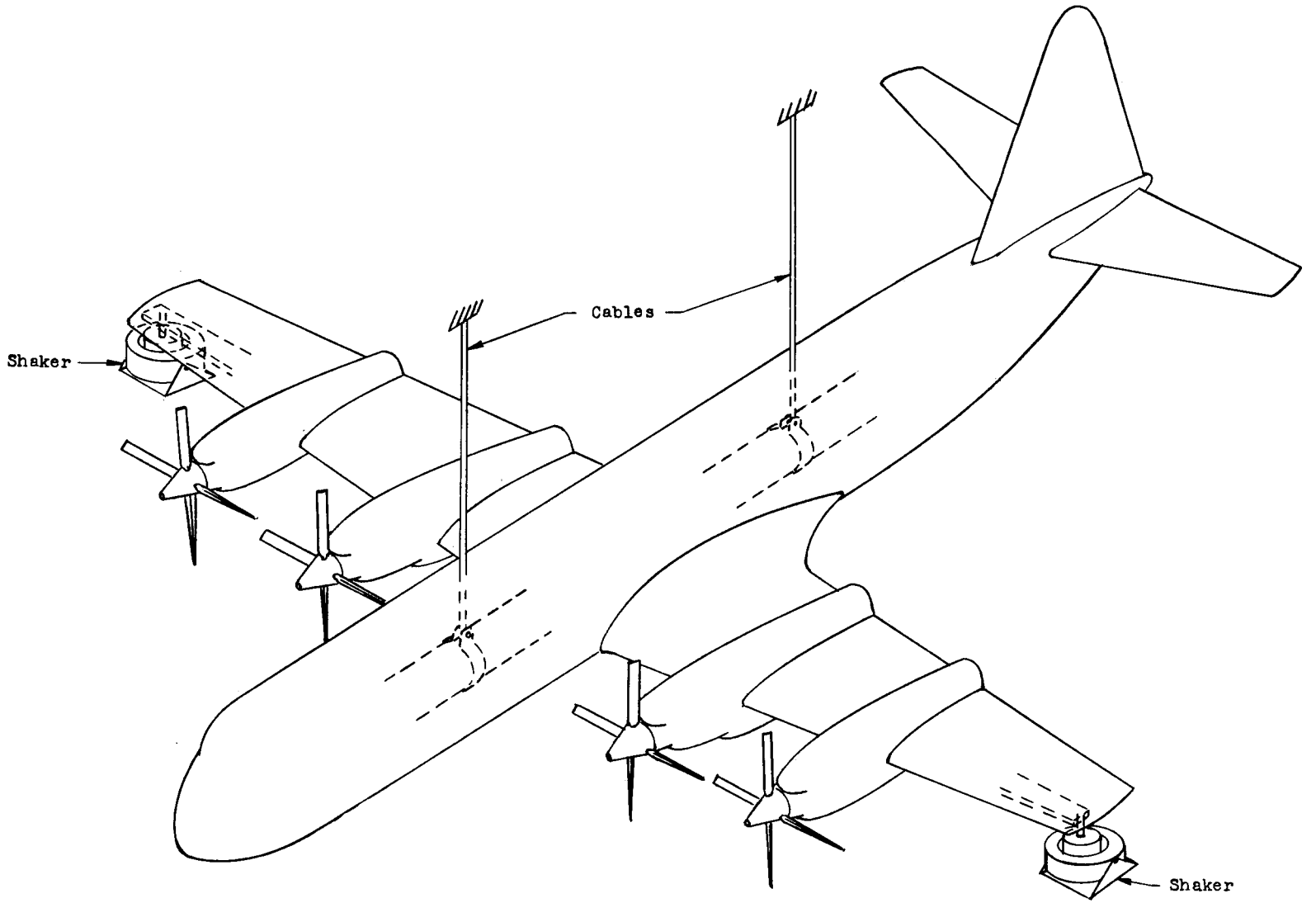

(b) Suspension configuration 2.

Figure 16.- Continued.

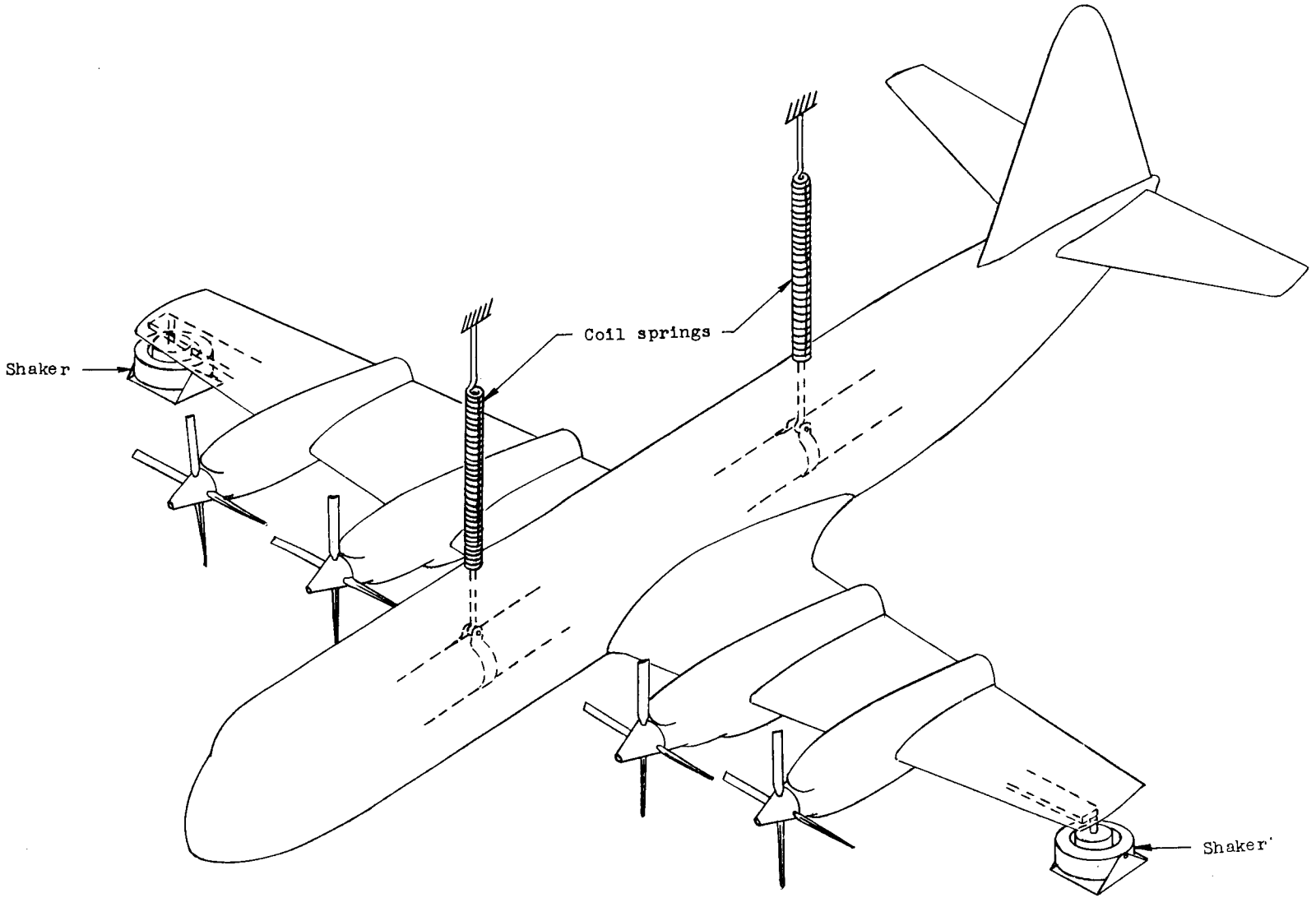

(c) Suspension configuration 3.

Figure 16.- Concluded.

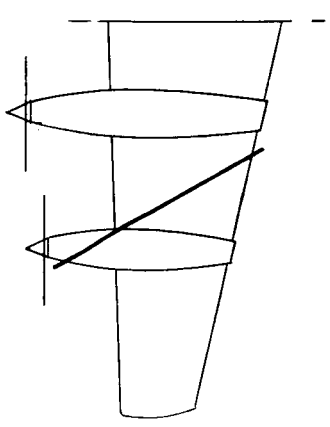

f = 10.0

Wing bending out of phase with fuselage pitch and plunge

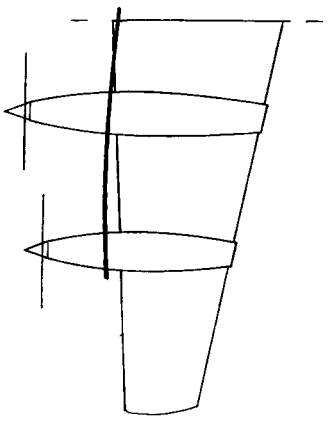

f = 12.6

Wing torsion

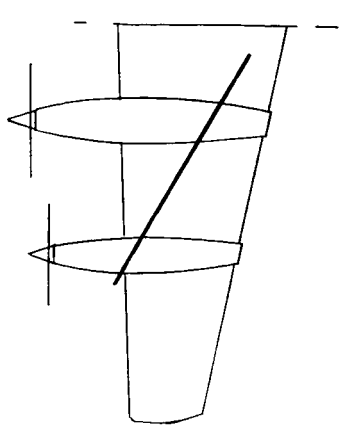

f = 16.2

Wing fore and aft bending with nacelle pitching in phase when viewed from above

Symmetric modes

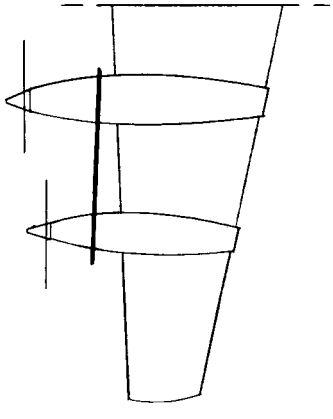

f = 11.2

Wing torsion

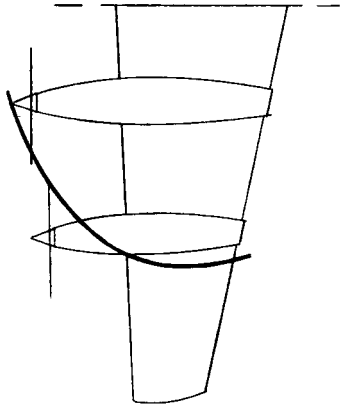

f = 25.3

Wing bending with inboard nacelle pitch

Antisymmetric modes

Figure 17.- Mode shapes and frequencies of model with 0-percent fuel load.

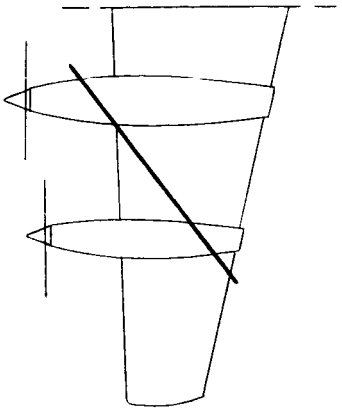

f = 7.6

Wing bending;
pitch node at the tail;
outboard nacelle pitch

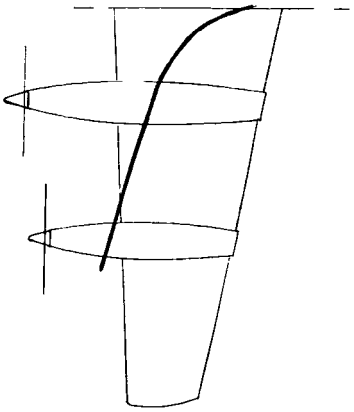

f = 12.0

Wing torsion

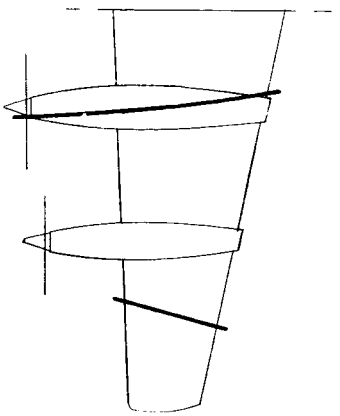

f = 28.3

2nd wing bending

Symmetric modes

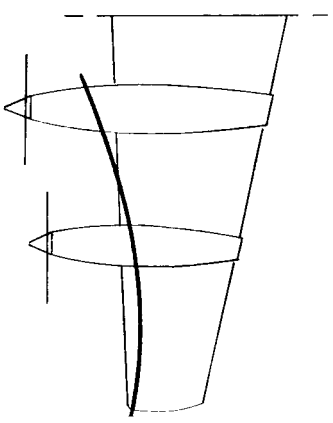

f = 9.9

Wing torsion

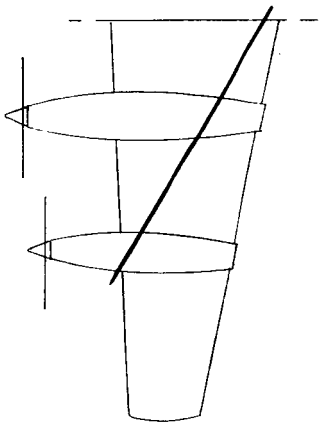

f = 13.4

Wing bending with
fuselage lateral bending
and torsion

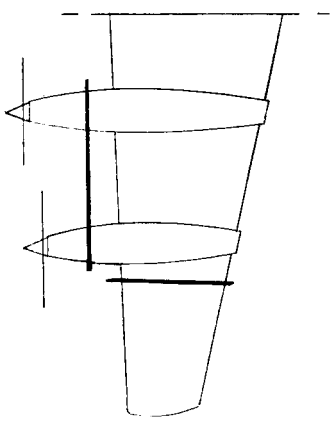

f = 21.2

Wing bending with
all nacelles pitching;
empennage roll

Antisymmetric modes

Figure 18.- Mode shapes and frequencies of model with 32-percent fuel load.

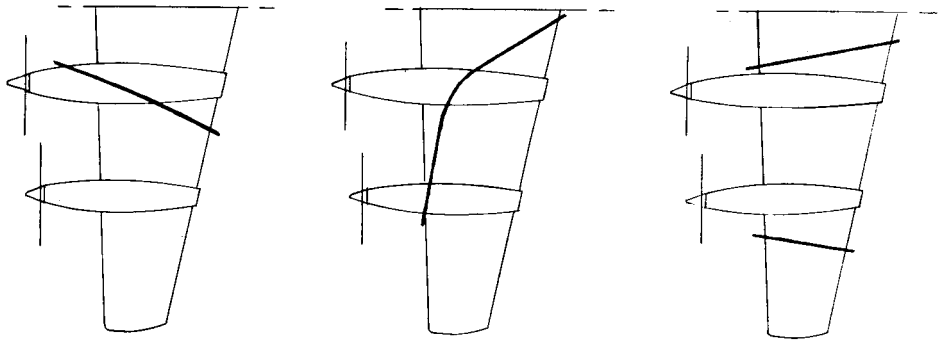

f = 7.1
Wing bending

f = 10.8
Wing torsion

f = 25.5
Wing bending out of phase with fuselage pitch and plunge; outboard nacelle pitch

Symmetric modes

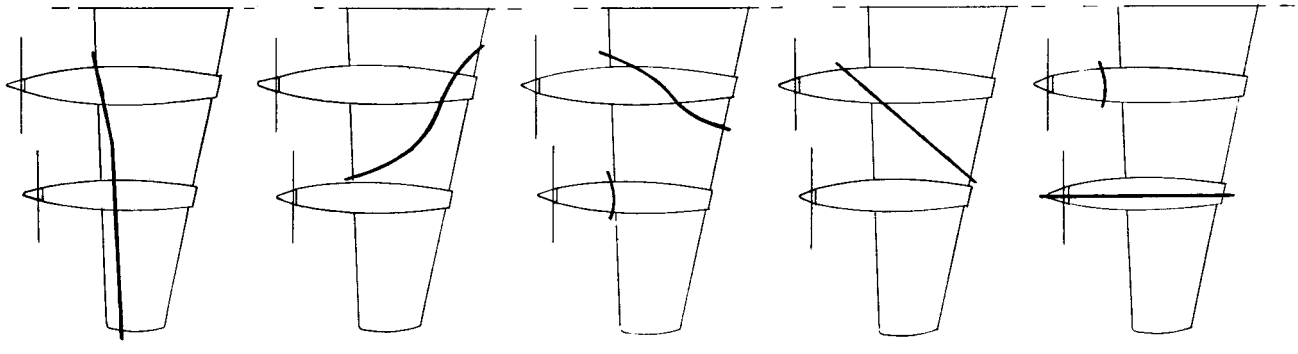

f = 9.2
Wing torsion

f = 12.9
Wing bending with fuselage lateral bending

f = 16.3
Wing bending with fuselage lateral bending; nacelles yawing

f = 22.6
Wing bending with stabilizer bending

f = 24.4

Antisymmetric modes

(a) Level-flight fuel configuration.

Figure 19.- Mode shapes and frequencies of model with 64-percent fuel load.

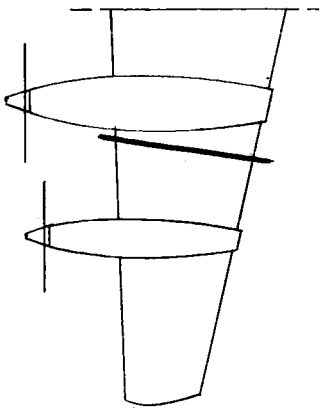

f = 6.3

Wing bending out of phase with fuselage plunge

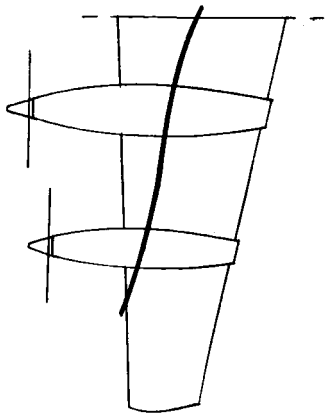

f = 9.5

Wing torsion

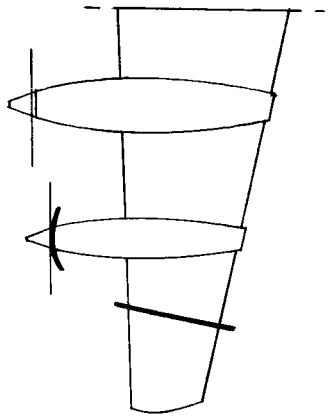

f = 23.7

2nd wing bending

Symmetric modes

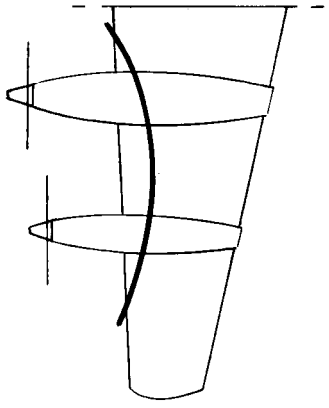

f = 9.1

Wing torsion

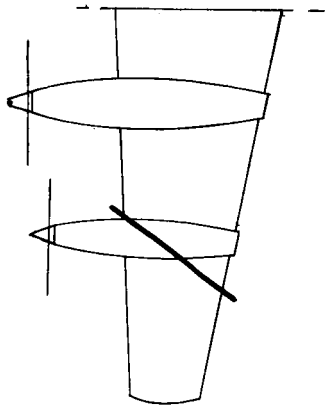

f = 11.1

Wing bending

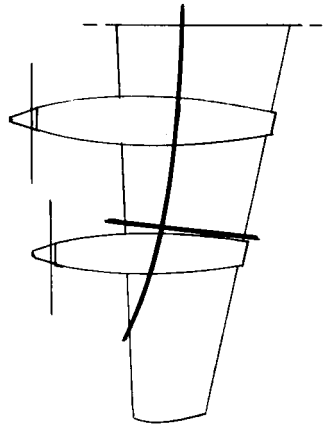

f = 15.6

Wing bending with outboard nacelles yaw; empennage roll

Antisymmetric modes

(b) Rolling-flight fuel configuration.

Figure 19.- Continued.

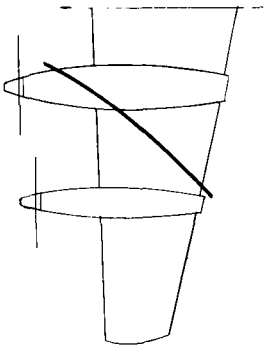

f = 7.1

Wing bending

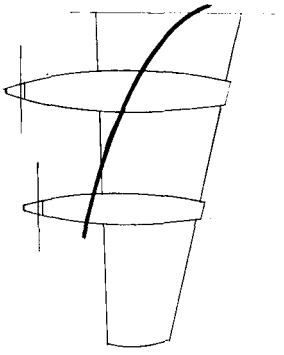

f = 11.2

Wing torsion

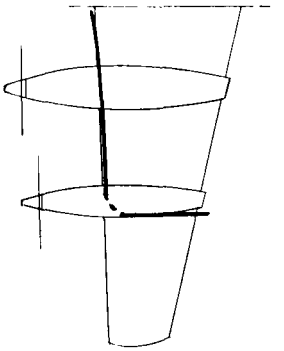

f = 18.4

Wing bending with horizontal-stabilizer bending; outboard nacelle yaw; inboard nacelle pitch

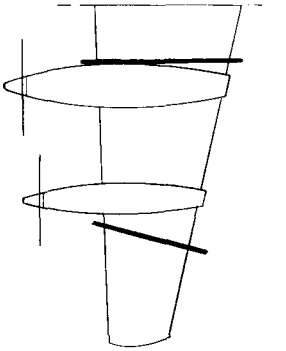

f = 27.3

2nd wing bending

Symmetric modes

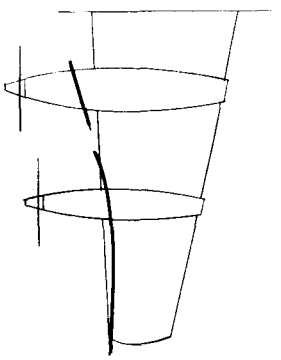

f = 9.6

Wing torsion with fuselage and empennage roll

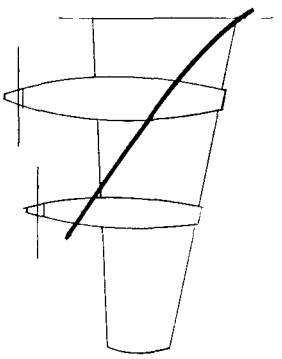

f = 12.5

Wing bending

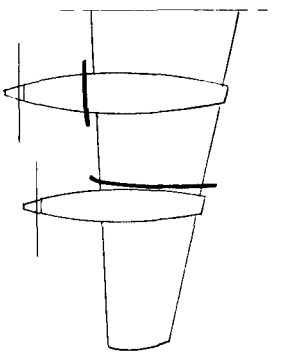

f = 15.9

Wing bending

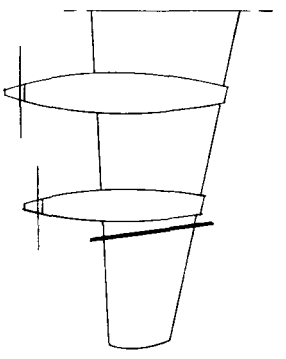

f = 21.6

Wing bending with empennage motion

Antisymmetric modes

(c) Diving-flight fuel configuration.

Figure 19.- Continued.

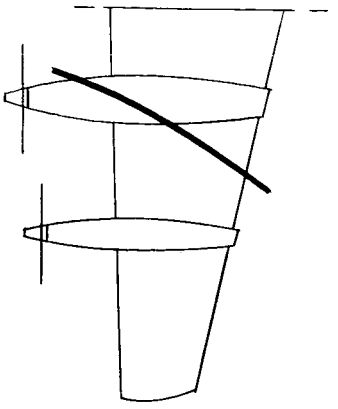

f = 7.1

Wing Bending

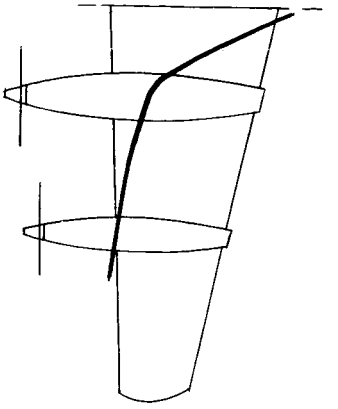

f = 10.4

Wing torsion

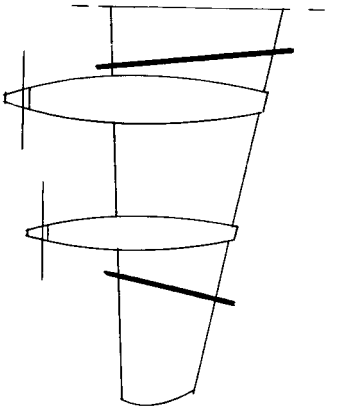

f = 26.0

2nd wing bending

Symmetric modes

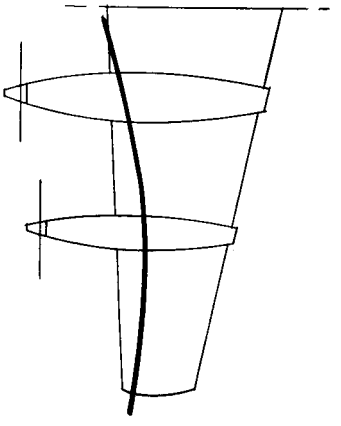

f = 9.1

Wing torsion

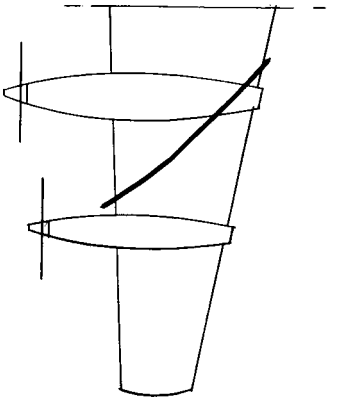

f = 12.4

Wing bending with fuselage lateral bending and torsion

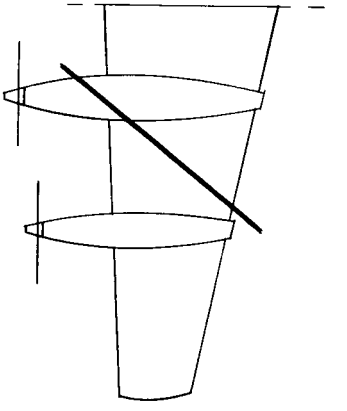

f = 21.3

Wing bending with horizontal-stabilizer bending

Antisymmetric modes

(d) Climbing-flight fuel configuration.

Figure 19.- Concluded.

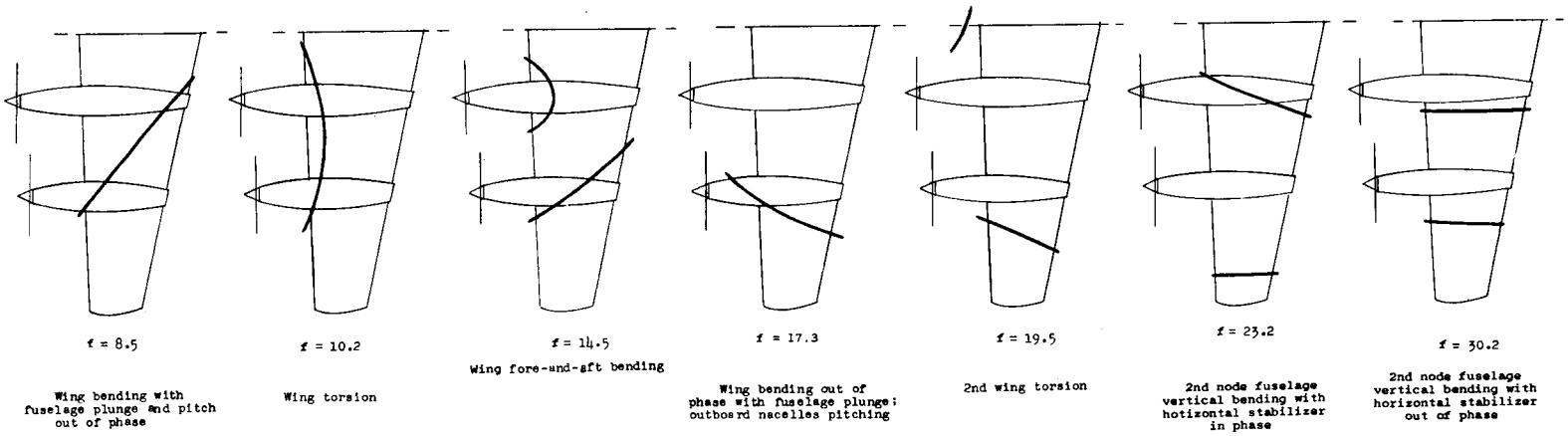

Figure 20.- Mode shapes and frequencies of model with 100-percent fuel load.

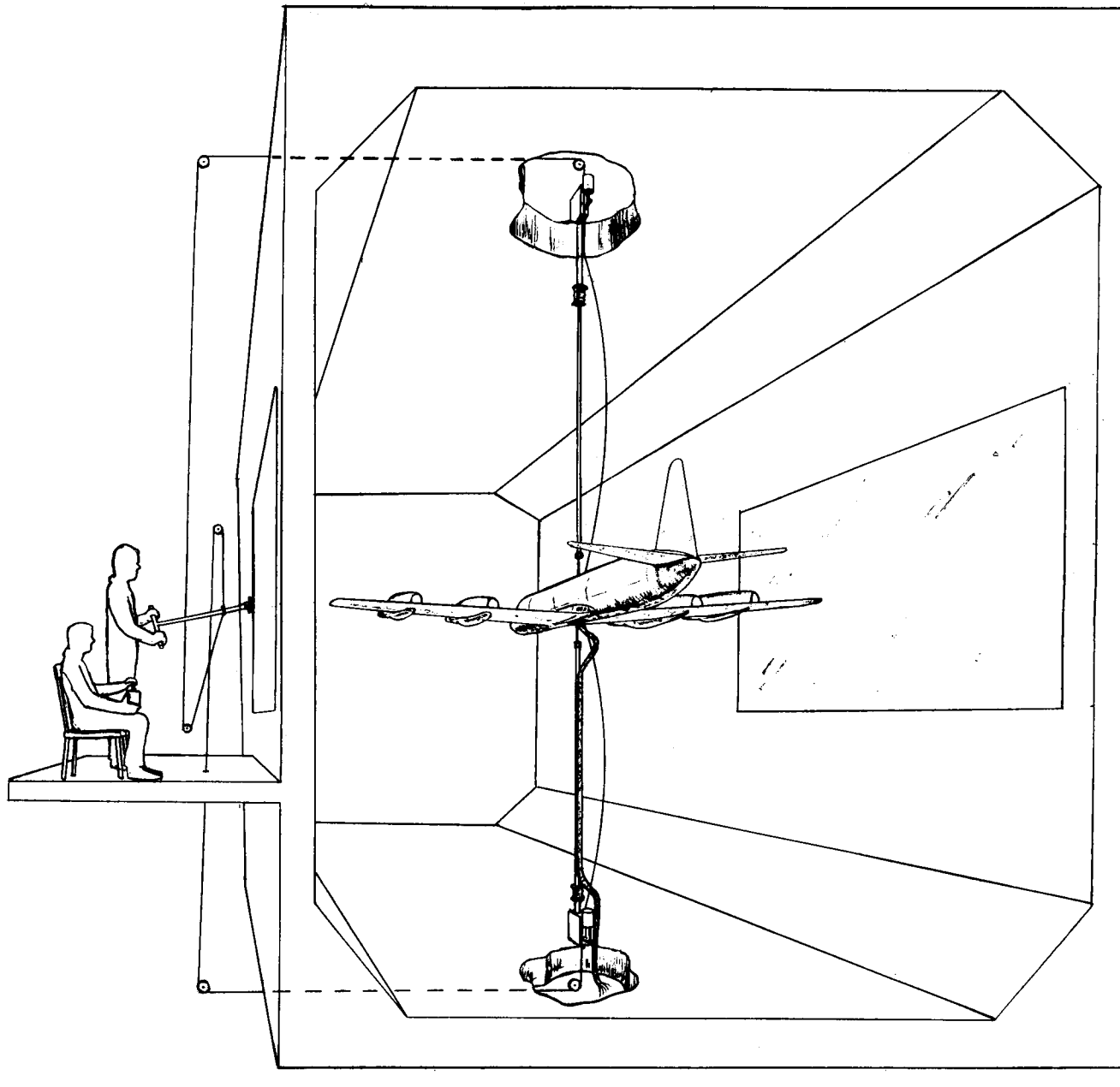

Figure 21.- Schematic diagram of model mounted in test section showing mounting system and model operators.

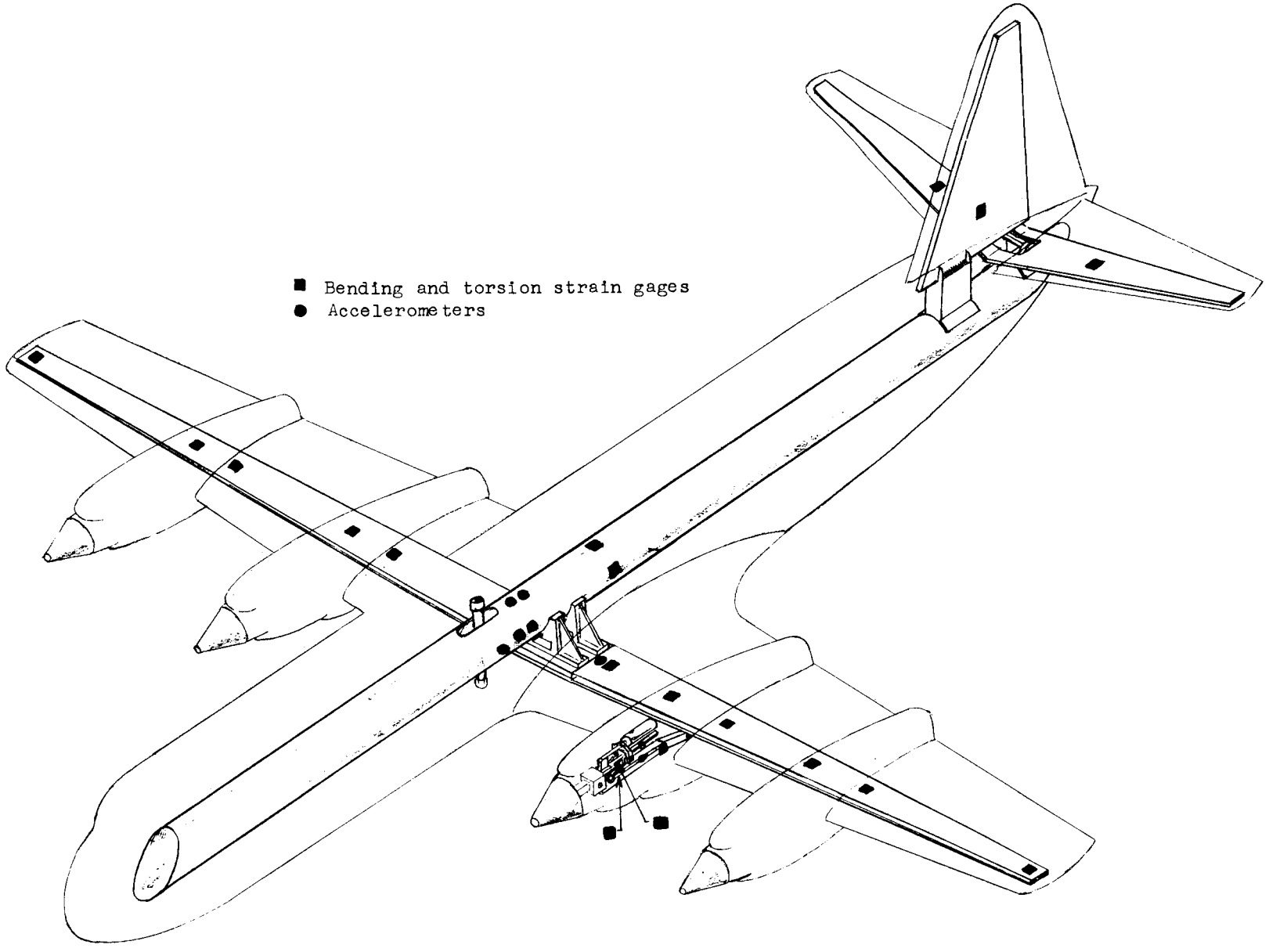

Figure 22.- Model showing structural members and locations of accelerometers and strain gages.

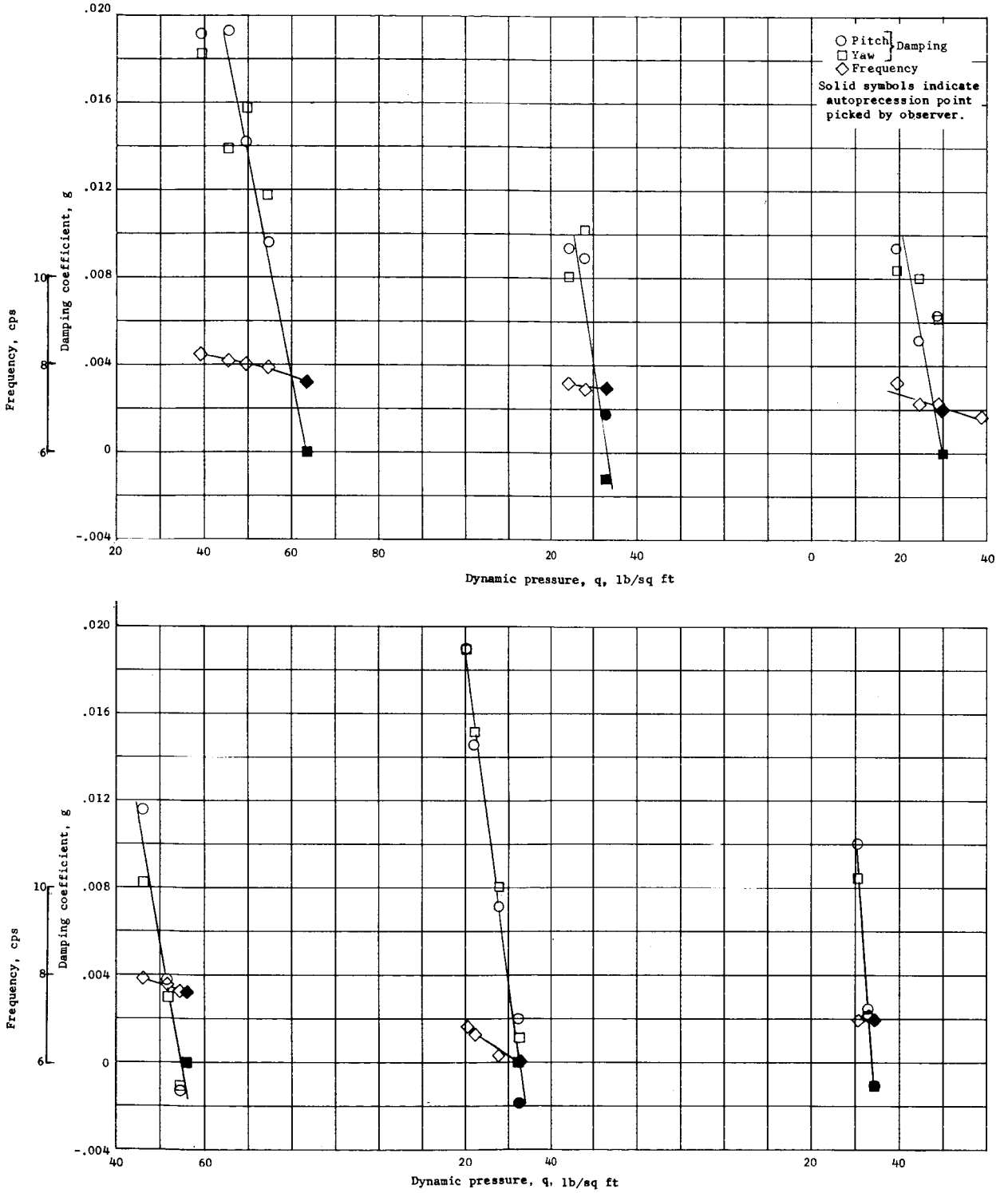

Figure 23.- Variation of precession frequency and damping with dynamic pressure for several typical configurations.

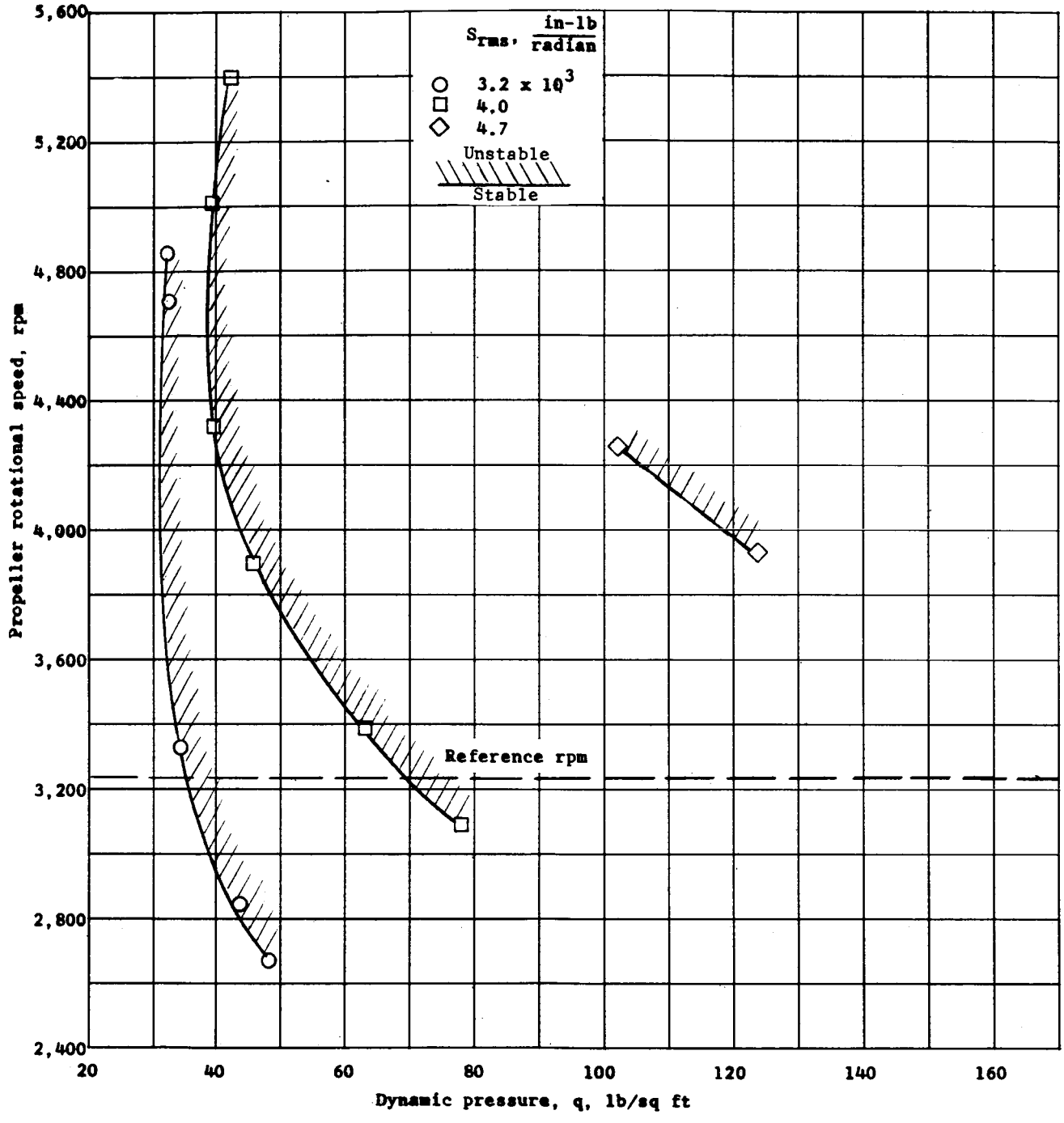

Figure 24.- Effect of root-mean-square stiffness on autoprecession boundary of power plant 4. $g \approx 0.014$; $S_\theta/S_\psi = 1.0$. (Other power plants have reference root-mean-square stiffness and $g \approx 0.04$.) Simulated 64-percent, level-flight fuel loading.

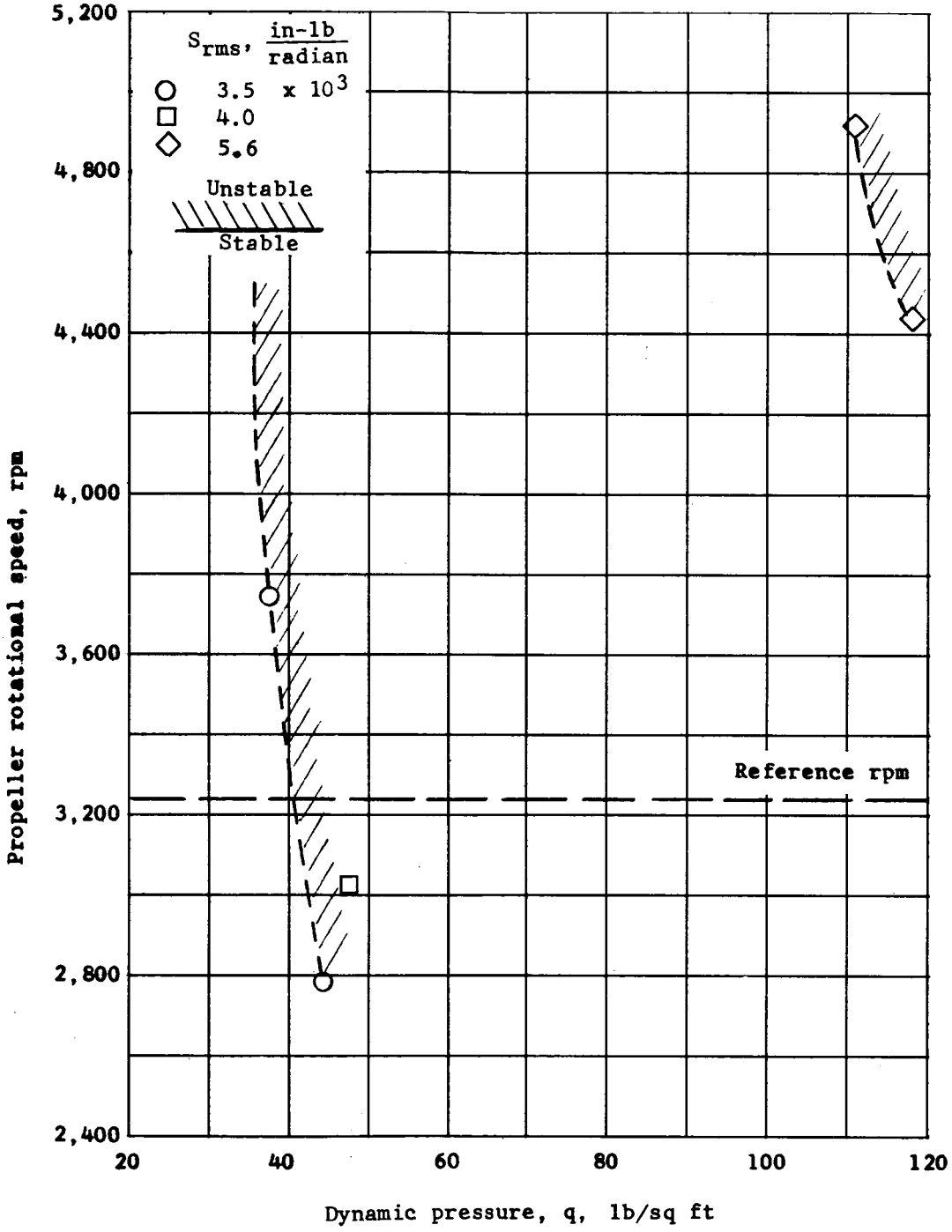

Figure 25.- Effect of root-mean-square stiffness on autoprecession boundary of power plant 4. $g \approx 0.014$; $S_\theta/S_\psi = 1.5$. (Other power plants have reference root-mean-square stiffness and $g \approx 0.04$.) Simulated 64-percent, level-flight fuel loading.

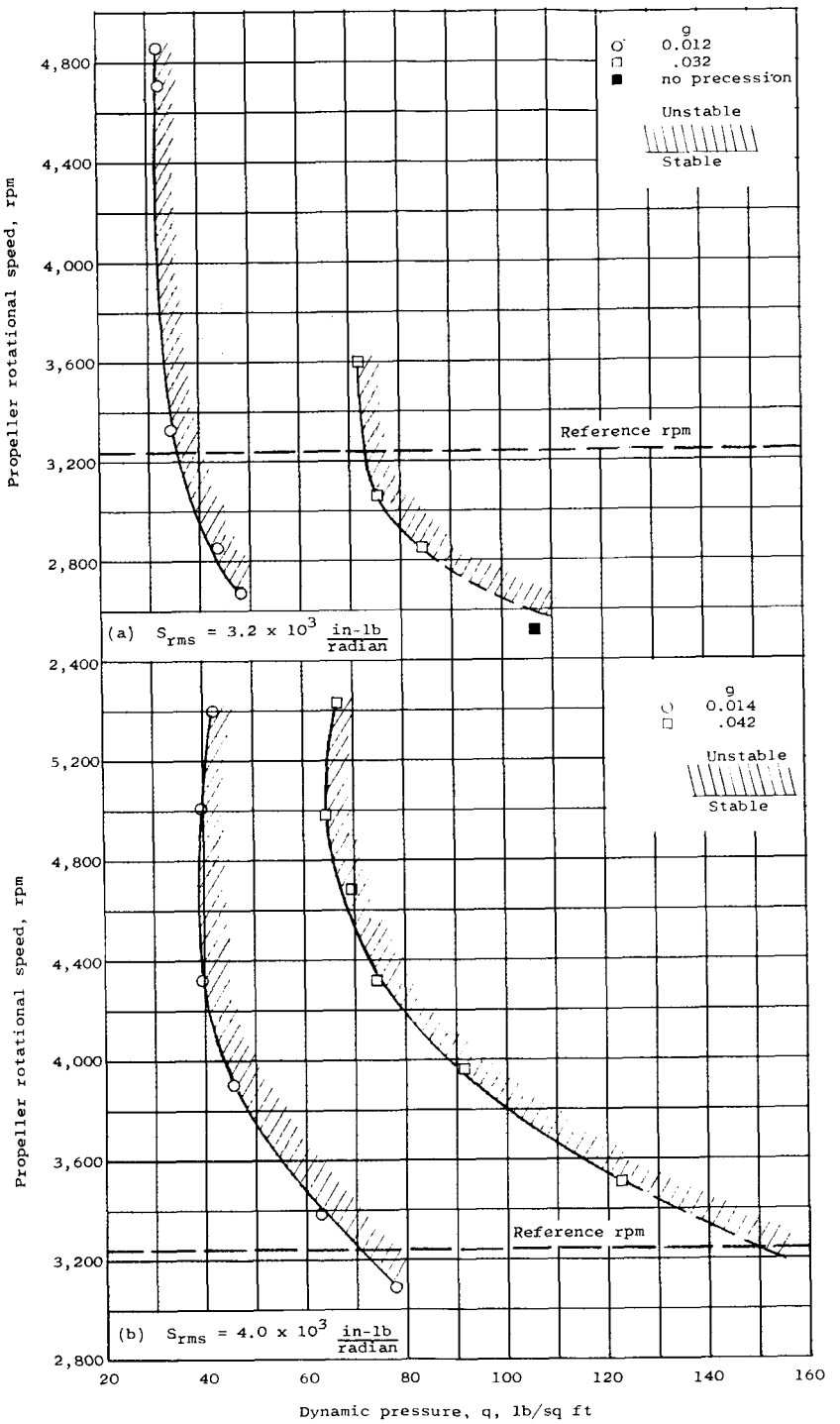

Figure 26.- Effect of structural damping coefficient on autoprecession boundary for power plant 4. $S_\theta/S_\psi = 1.0$. (Other power plants have reference root-mean-square stiffness and $g \approx 0.04$.) Simulated 64-percent, level-flight fuel loading.

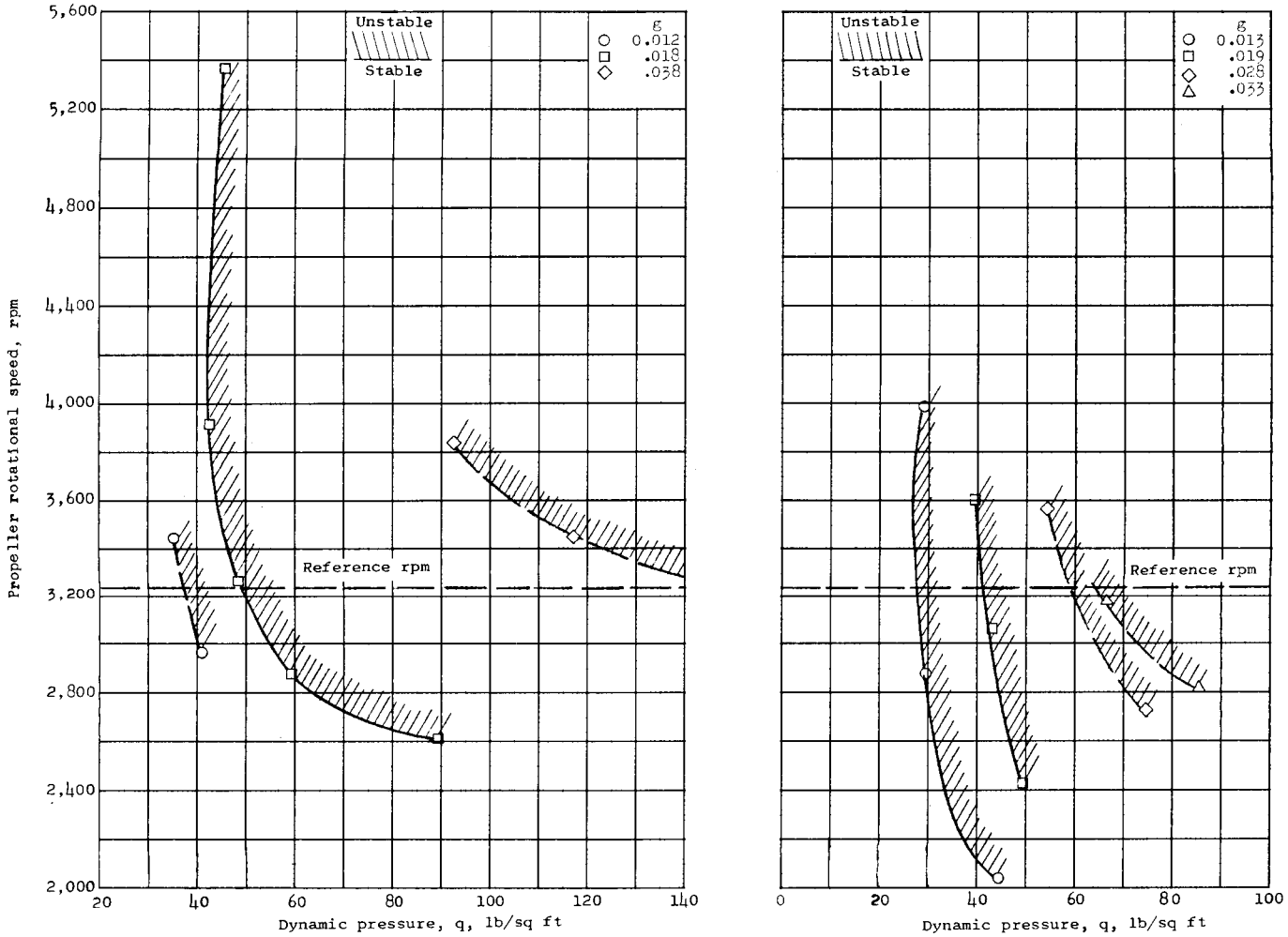

(a) $S_\theta/S_\psi = 0.55$.

(b) $S_\theta/S_\psi = 1.81$.

Figure 27.- Effect of structural damping coefficient on autoprecession boundary for power plant 4 at a root-mean-square stiffness of $3.6 \times 10^3 \frac{\text{in-lb}}{\text{radian}}$. (Other power plants have reference root-mean-square stiffness and $g \approx 0.04$.) Simulated 64-percent, level-flight fuel loading.

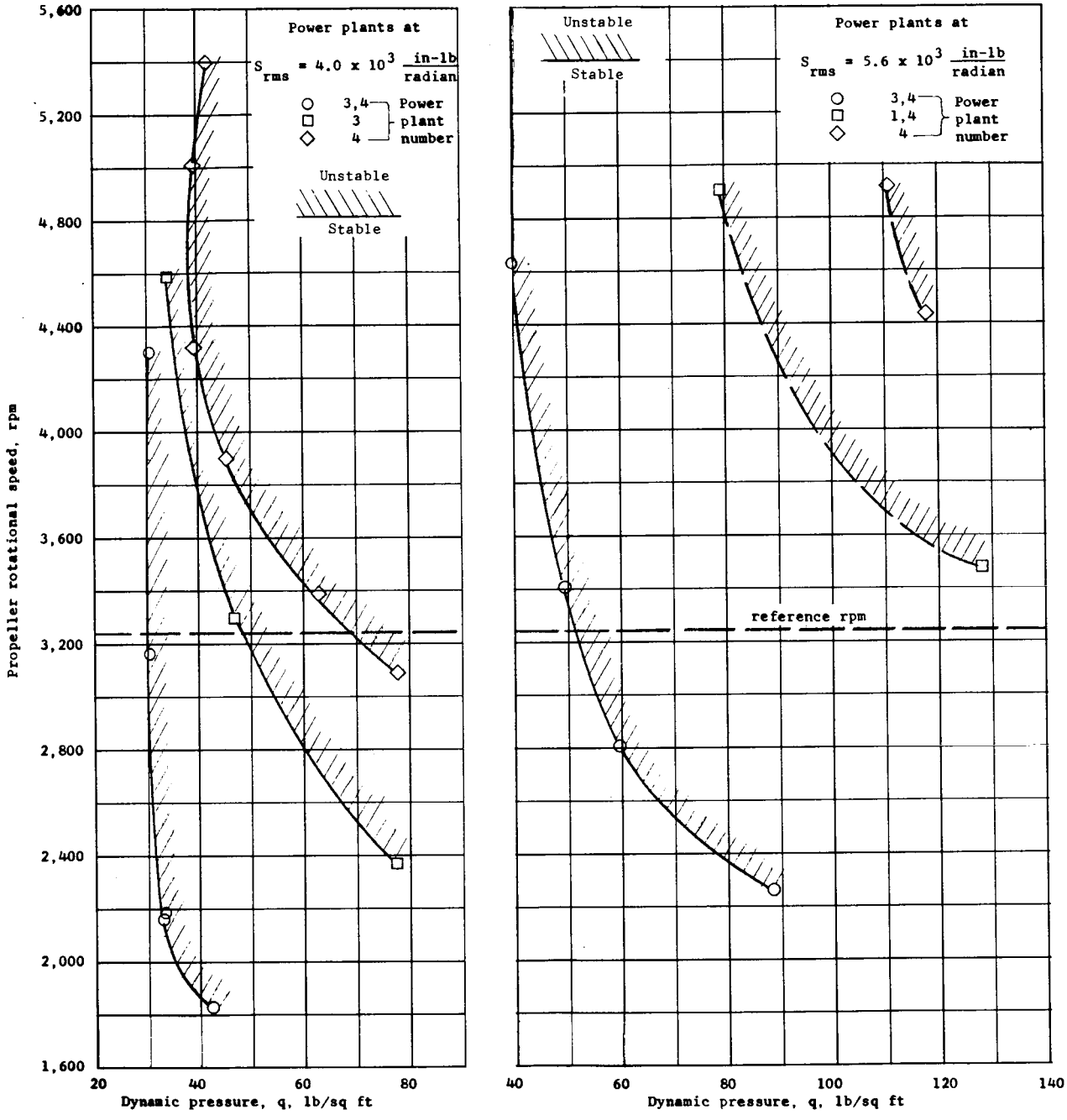

(a) S_θ/S_ψ = 1.0.

(b) S_θ/S_ψ = 1.5.

Figure 28.- Autoprecession boundaries for various power plants with reduced stiffnesses and low damping. $g \approx 0.014$. (Other power plants have reference root-mean-square stiffness and $g \approx 0.04$.) Simulated 64-percent, level-flight fuel loading.

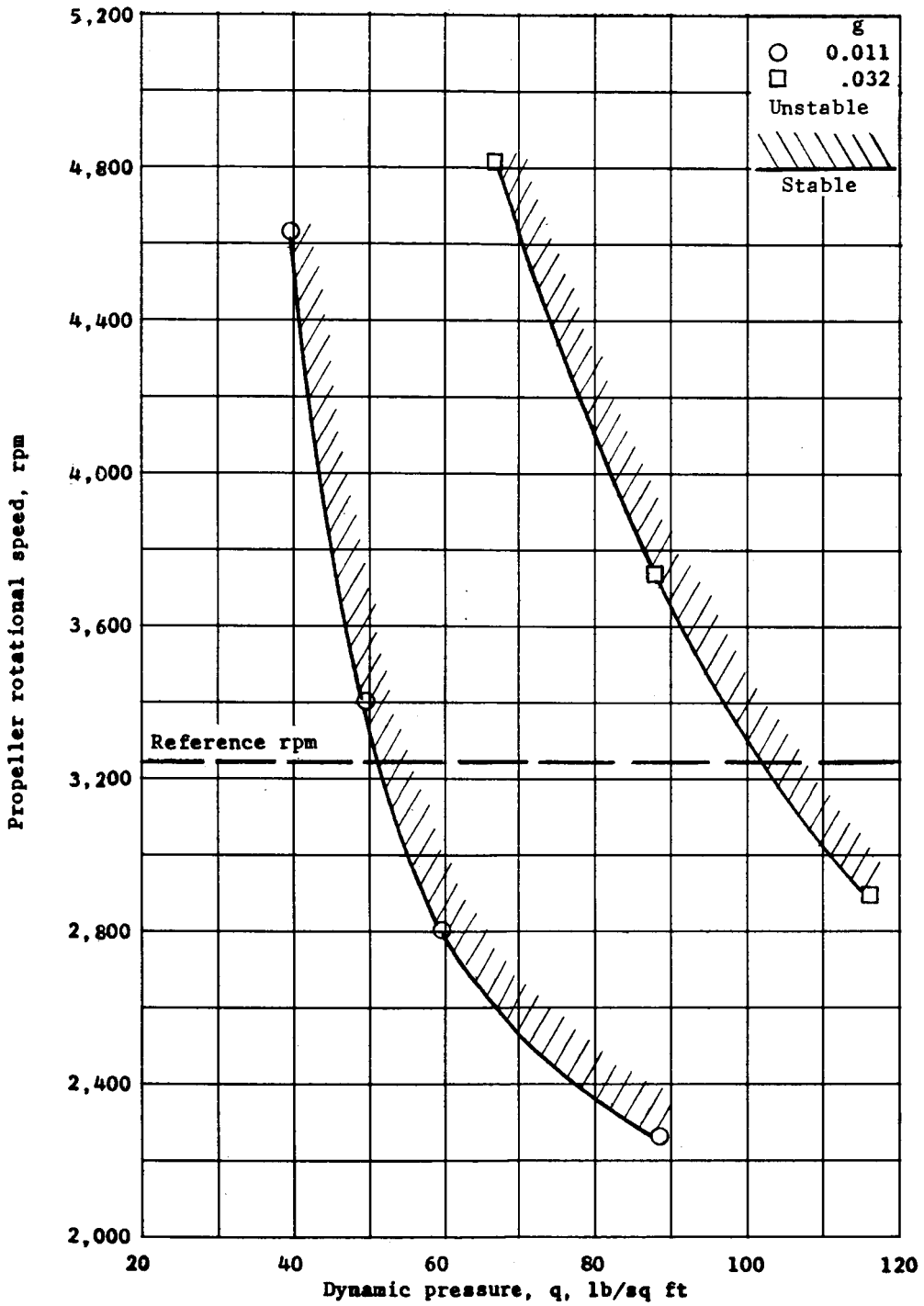

Figure 29.- Effect of structural damping coefficient on autoprecession boundary for power plants 3 and 4 at reduced stiffness. $S_{rms} = 5.6 \times 10^3 \frac{\text{in-lb}}{\text{radian}}$; $S_\theta/S_\psi = 1.5$. (Other power plants have reference root-mean-square stiffness and $g \approx 0.04$.) Simulated 64-percent, level-flight fuel loading.

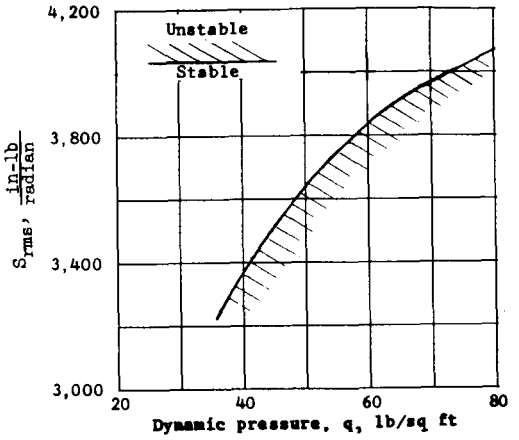

Figure 30.- Variation of dynamic pressure for autoprecession at standard propeller rotational speed with root-mean-square stiffness of power plant 4. $g \approx 0.014$; $S_\theta / S_\psi = 1.0$. (Other power plants have reference root-mean-square stiffness and $g \approx 0.40$.) Simulated 64-percent, level-flight fuel loading.

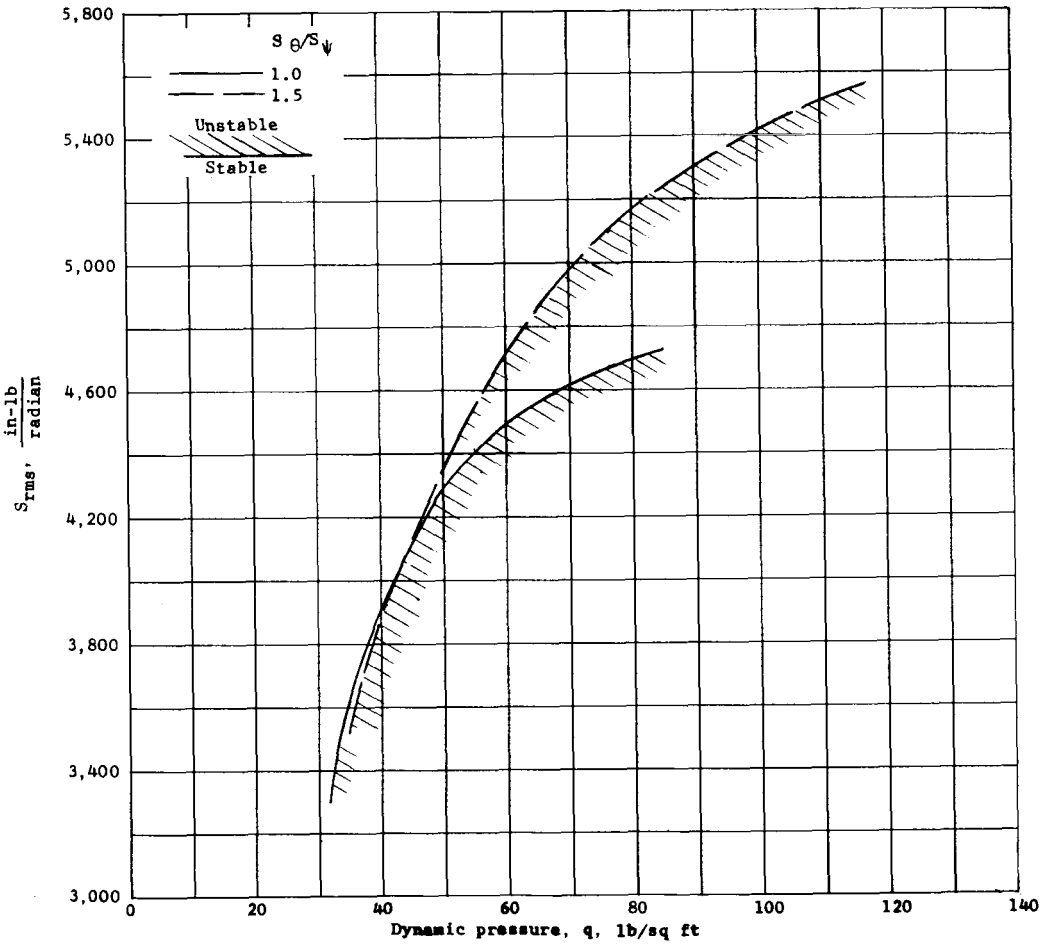

Figure 31.- Effect of stiffness ratio on variation of dynamic pressure for autoprecession at 140-percent reference propeller rotational speed with root-mean-square stiffness of power plant 4. $g \approx 0.014$. (Other power plants have reference root-mean-square stiffness and $g \approx 0.40$.) Simulated 64-percent, level-flight fuel loading.

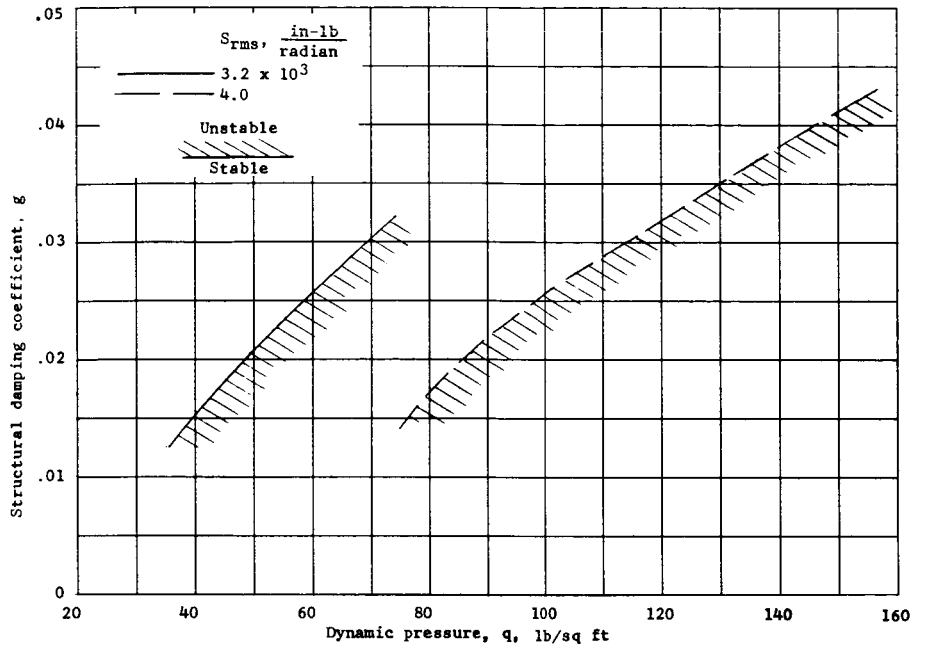

(a) $S_\theta / S_\psi = 1.0$.

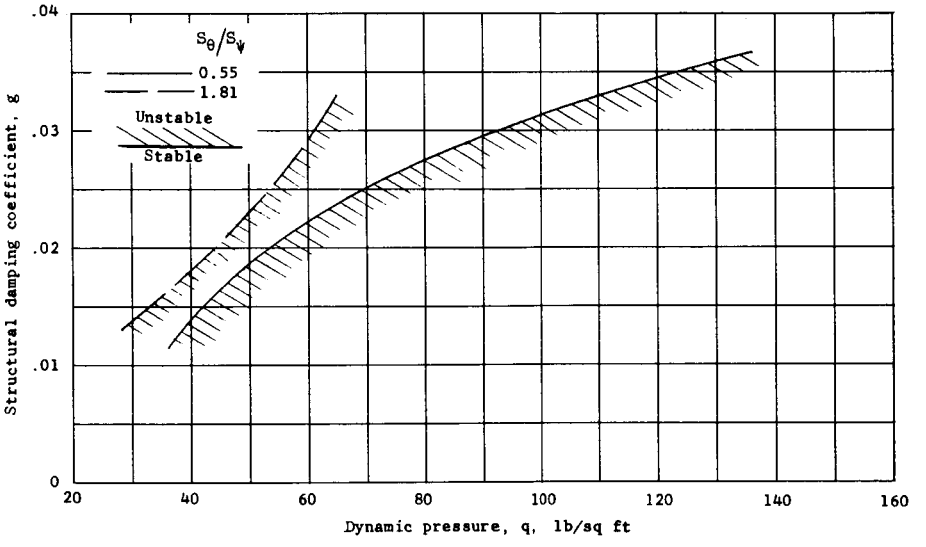

(b) $S_{rms} = 3.6 \times 10^3 \frac{in\text{-}lb}{radian}$.

Figure 32.- Variation of dynamic pressure for autoprecession at reference propeller rotational speed with structural damping coefficient for various root-mean-square stiffnesses and stiffness ratios of power plant 4. (Other power plants have reference root-mean-square stiffness and $g \approx 0.04$.) Simulated 64-percent, level-flight fuel loading.

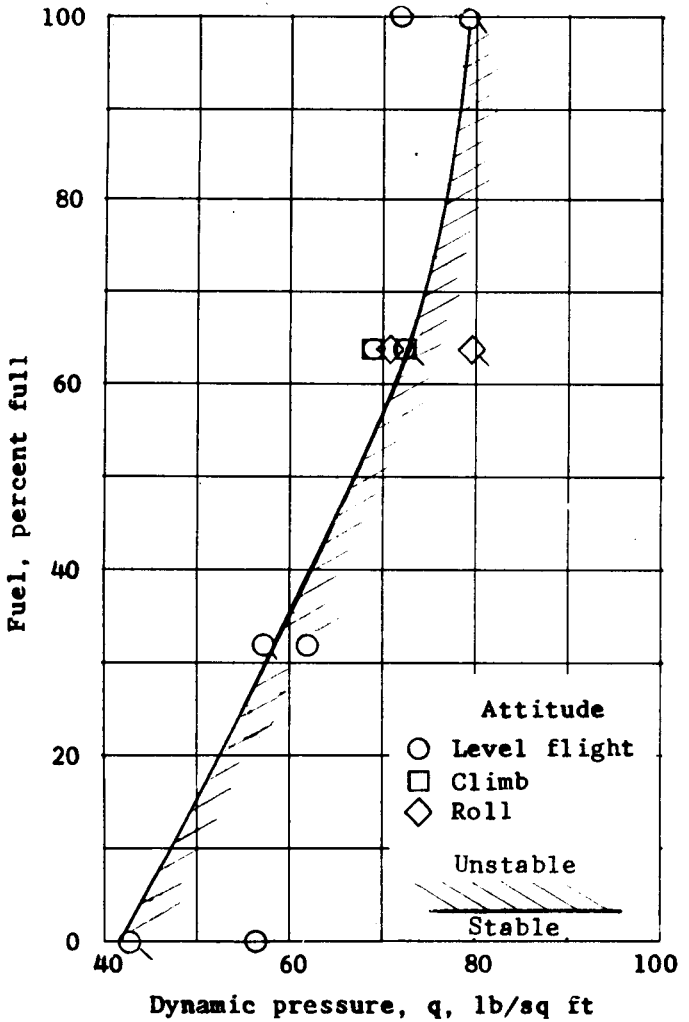

Figure 33.- Variation of dynamic pressure for autoprecession of power plant 4 with fuel load. Symbols with tails indicate data points adjusted to reference propeller rotational speed. $S_{rms} = 4.1 \times 10^3$; $S_\theta / S_\psi = 1.0$; $g \approx 0.014$. (Other power plants have reference root-mean-square stiffness and $g \approx 0.04$.)

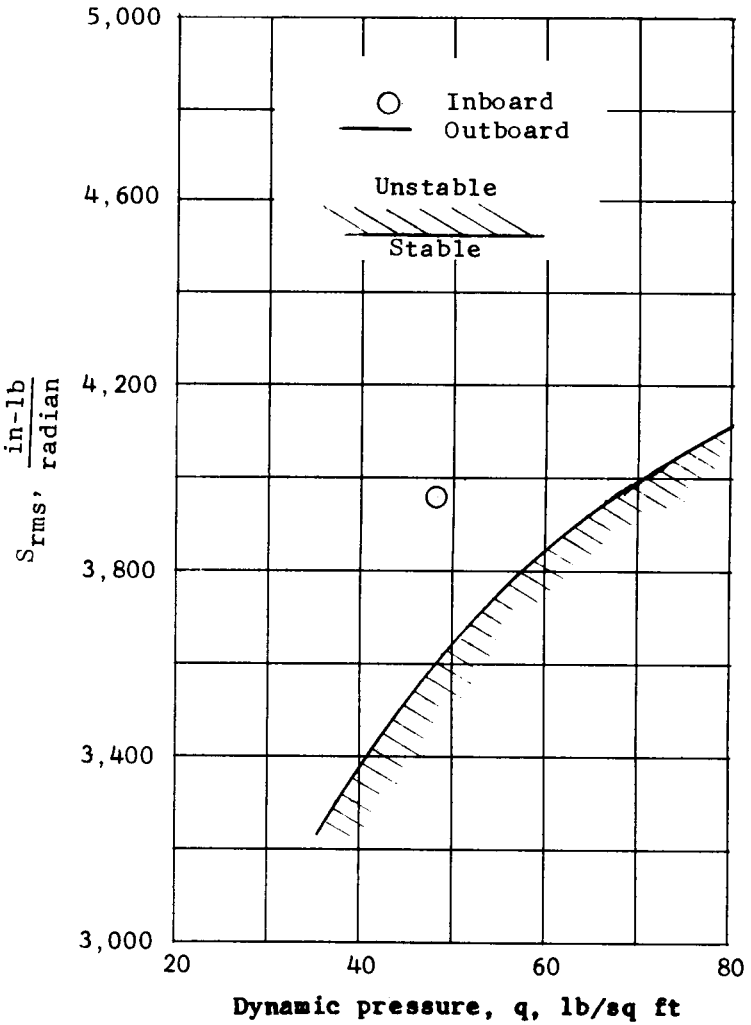

Figure 34.- Effect of power-plant location on autoprecession boundary. Reference propeller rotational speed with reduced stiffness and low damping in an outboard power plant and in an inboard power plant. $S_\theta / S_\psi = 1.0$. (Other power plants have reference root-mean-square stiffness and $g \approx 0.04$.)

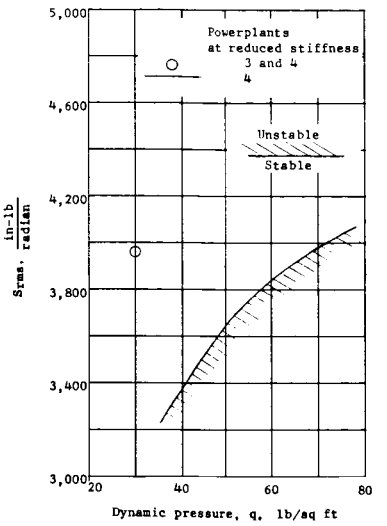

(a) Reference propeller rotational speed; $S_\theta/S_\psi = 1.0$.

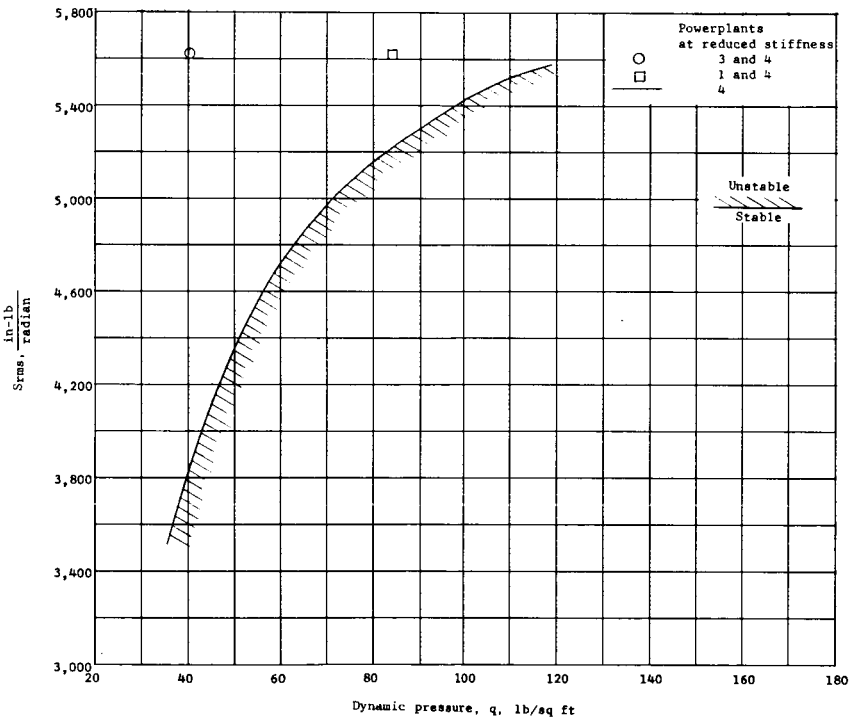

(b) 140-percent reference propeller rotational speed; $S_\theta/S_\psi = 1.5$.

Figure 35.- Effect of reduced stiffness in a single outboard power plant, an inboard-outboard power-plant combination, and two outboard power plants on autoprecession boundary. $g \approx 0.014$. (Other power plants have reference root-mean-square stiffness and $g \approx 0.04$.)

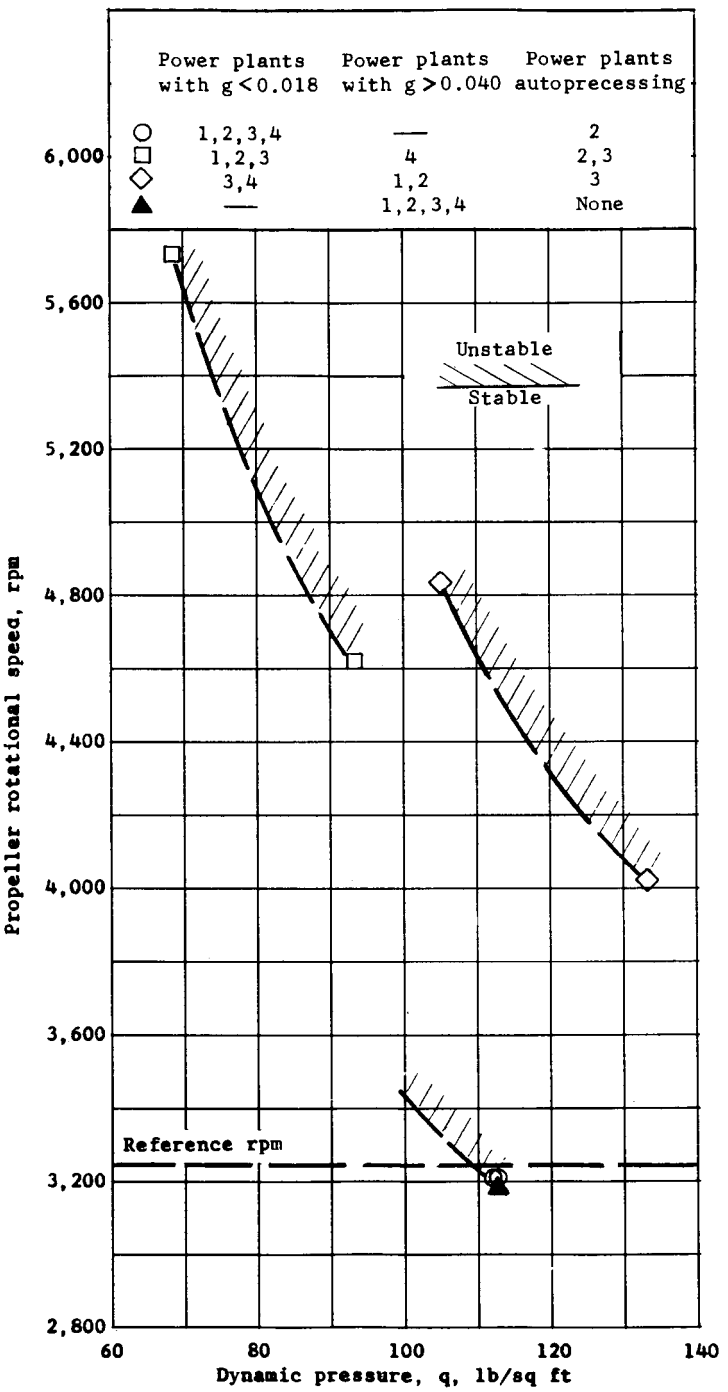

Figure 36.- Variation of dynamic pressure for autoprecession with propeller rotational speed for various power-plant damping configurations. $S_{rms} = 7.9 \times 10^3 \frac{\text{in-lb}}{\text{radian}}$; $S_\theta/S_\psi = 1.5$. Simulated 64-percent, level-flight fuel loading.

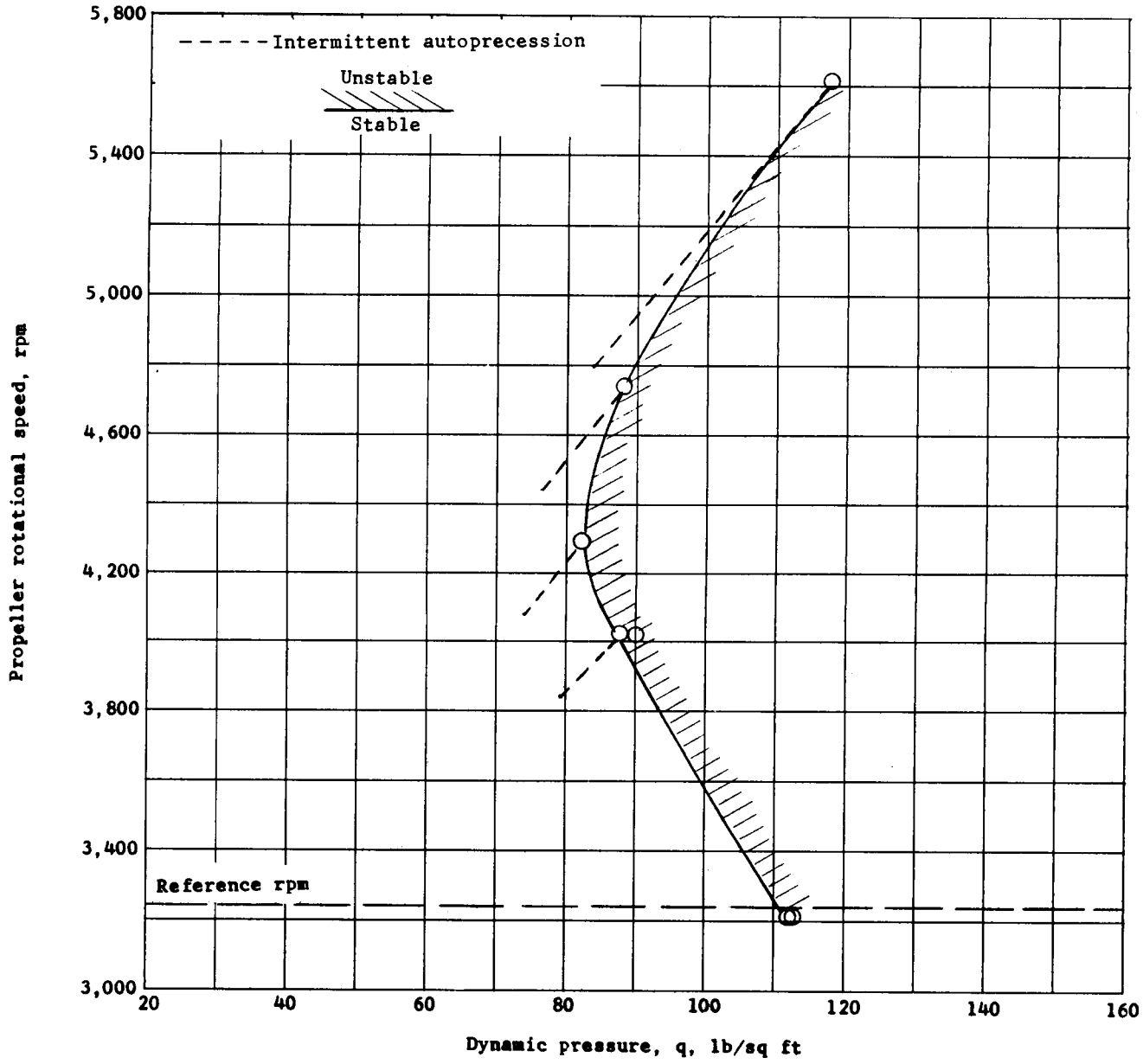

Figure 37.- Variation of dynamic pressure for autoprecession with propeller rotational speed for a single inboard propeller overspeeding. (All other propellers near reference rotational speed.) $S_{rms} = 7.9 \times 10^3 \frac{\text{in-lb}}{\text{radian}}$; $g \approx 0.014$; $S_\theta / S_\psi = 1.5$. Simulated 64-percent, level-flight fuel loading.

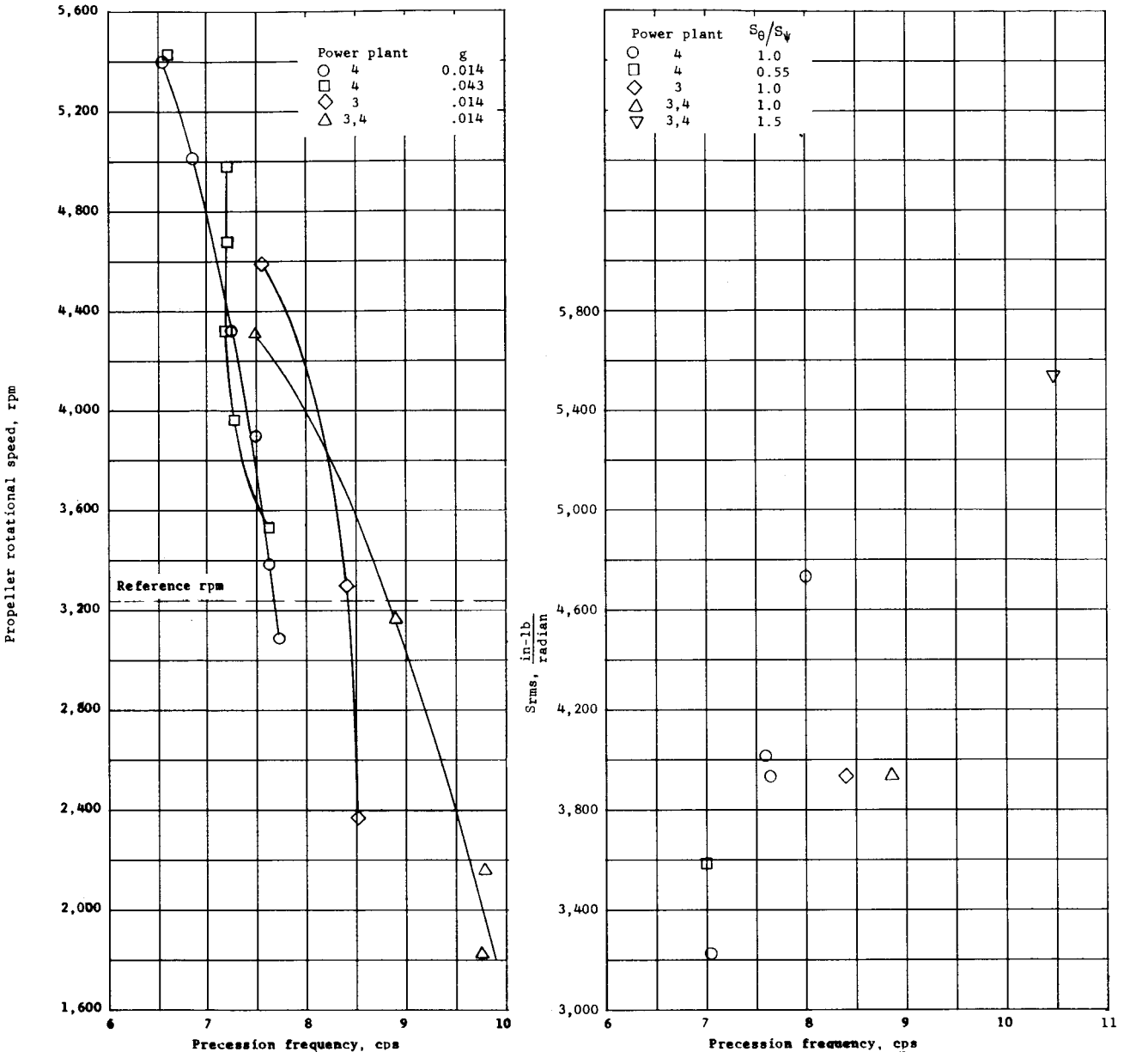

(a) Variation of autoprecession frequency with propeller rotational speed. $S_{rms} = 4.0 \times 10^3 \frac{in\text{-}lb}{radian}$; $S_\theta/S_\psi = 1.0$.

(b) Variation of autoprecession frequency with root-mean-square stiffness. Reference propeller rotational speed.

Figure 38.- Variations of autoprecession frequency with propeller rotational speed and root-mean-square stiffnesses for various power-plant combinations. (Other power plants have reference root-mean-square stiffness and $g \approx 0.04$.) Simulated 64-percent, level-flight fuel loading.

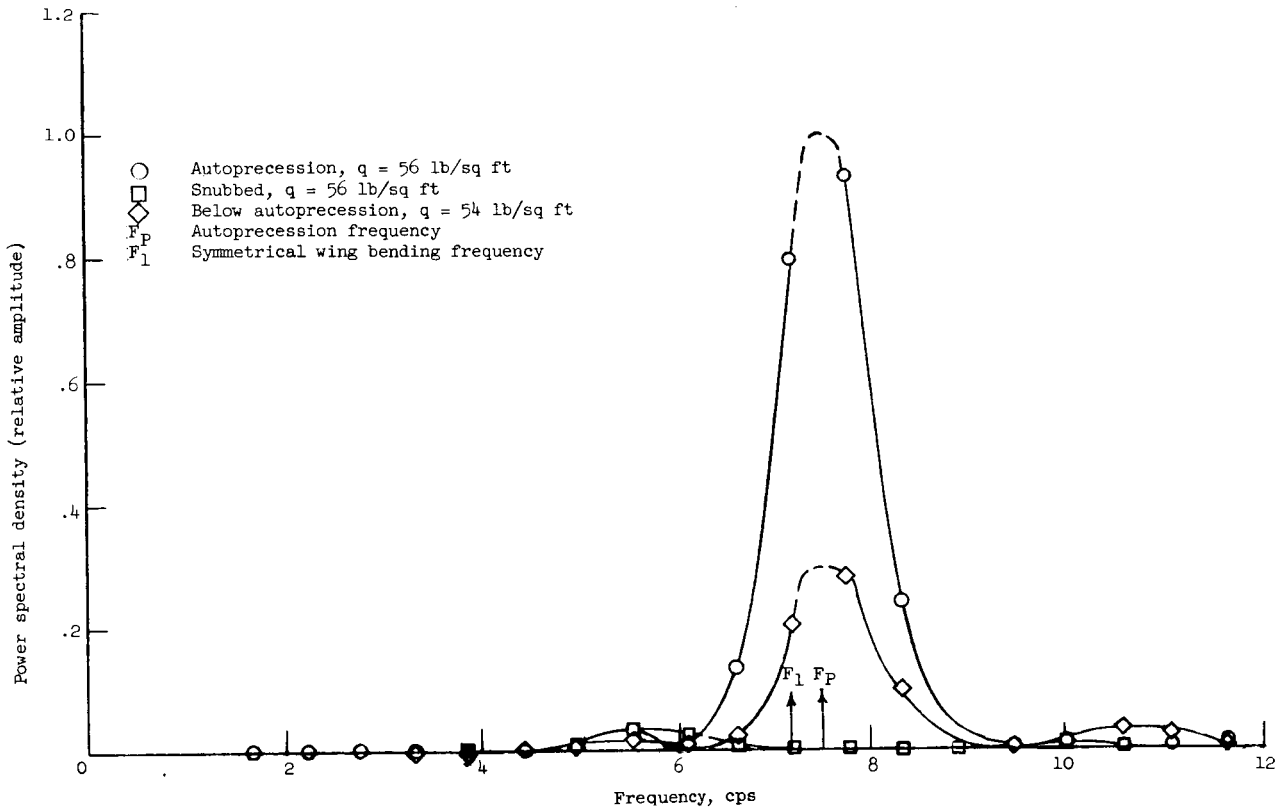

(a) Power-spectral-density analysis of wing torsion response.

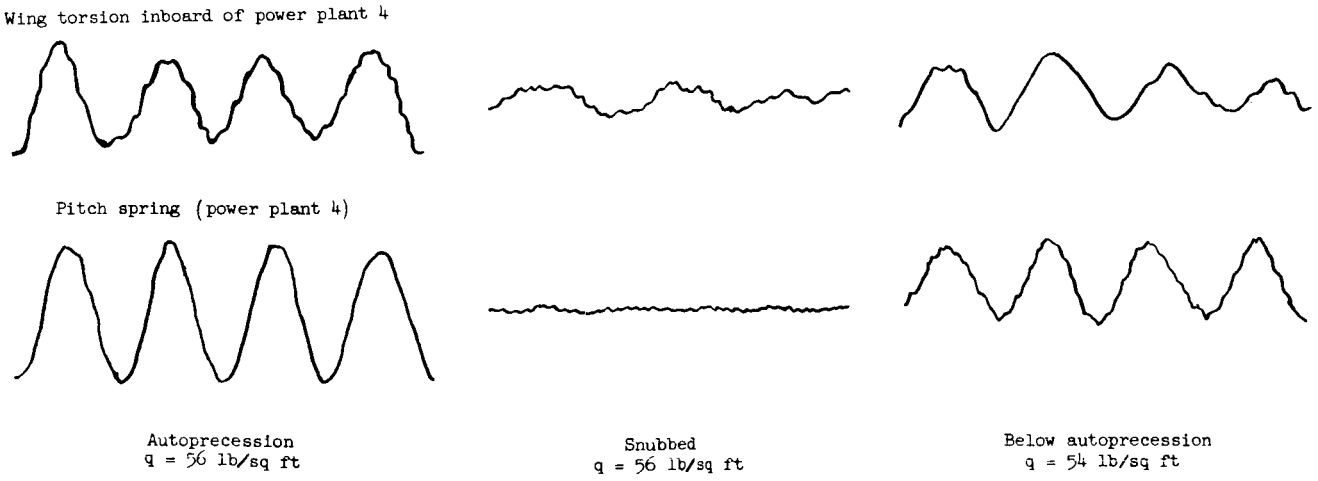

(b) Strain-gage response.

Figure 39.- Wing and power-plant response to autoprecession.